

# **Substrate multiplexed protein engineering facilitates promiscuous biocatalytic synthesis**

Allwin D. McDonald<sup>1,2</sup>, Peyton M. Higgins<sup>1,2</sup>, Andrew R. Buller<sup>1,\*</sup>

<sup>1</sup>*Department of Chemistry, University of Wisconsin–Madison, 1101 University Avenue, Madison, Wisconsin 53706, United States*

<sup>2</sup>*These authors contributed equally to this work*

\* To whom correspondence should be addressed: [arbuller@wisc.edu](mailto:arbuller@wisc.edu)

## **Supporting Information**

## **Table of Contents**

### **General experimental methods**

**Cloning and expression of *RgnTDC* site-saturation libraries**

**Screening of *RgnTDC* site-saturation libraries**

**Cloning of *PfTrpB* globally random mutagenesis libraries**

**Cloning of *PfTrpB* H275X site-saturation library**

**Screening of *PfTrpB* libraries**

**Expression of *RgnTDC* and *PfTrpB* variants**

**Turnover analysis of *RgnTDC* variants**

**[PLP] vs. activity for *RgnTDC* variants**

***RgnTDC* substrate multiplexed timecourse reaction**

**Michaelis-Menten analysis of *RgnTDC* variants**

**Single substrate activity analysis of *PfTrpB* variants**

**Michaelis-Menten analysis of *PfTrpB* variants**

**UV-Vis spectroscopy of *PfTrpB* variants**

**Protein crystallography of *PfTrpB*-H275E**

### **Supplemental Figures**

### **Supplemental Tables**

### **Supplemental Discussion**

**Introduction to substrate competition kinetics behind SUMS**

**Guide to optimization of substrate multiplexed screening (SUMS) method**

### **Synthetic Methods**

**Tryptophan analog biosynthesis and purification**

**Cascade synthesis and isolation of tryptamines**

**NMR spectra**

### **Supporting References**

## General experimental methods

Chemicals and reagents were purchased from commercial suppliers (Sigma-Aldrich, VWR, Chem-Impex International, Alfa Aesar) and used without further purification. *E. coli* (BL21 (DE3)) cells were used for protein expression. An Eppendorf E-porator (2500 V) was used for transformations. New Brunswick I26R, 120 V/60 Hz shakers (Eppendorf) were used for cell growth. Cell disruption via sonication was performed with a Sonic Dismembrator 550 (Fisher Scientific) sonicator. Optical density measurements were collected on a UV-2600 Shimadzu spectrophotometer (Shimadzu). UPLC-MS data were collected on an Acquity UHPLC with an Acquity QDA MS detector (Waters). Column separations were performed on an Isolera One Flash Purification system (Biotage). NMR data were collected on a Bruker 500 MHz spectrometer. High resolution mass data were collected with a Q Extractive Plus Orbitrap (NIH 1S10OD020022-1) instrument with the samples ionized by ESI. Kinetic data were fit with PRISM 8 Graphpad software.

### Cloning and expression of *RgnTDC* site-saturation libraries

A codon-optimized copy of the *Ruminococcus gnavus* tryptophan decarboxylase (*RgnTDC*) gene with a C-terminal His-tag was previously purchased<sup>1</sup> as a gBlock from Integrated DNA Technologies. This DNA fragment was inserted into a pET22b vector via Gibson assembly.<sup>2</sup> BL21 *E. coli* cells were subsequently transformed with the resulting cyclized DNA product *via* electroporation. After 30 min of recovery in Luria-Burtani (LB) media at 37 °C, cells were plated onto LB plates with 100 µg/mL ampicillin (AMP) and incubated overnight. Single colonies were used to inoculate 5 mL TB + 100 µg/mL AMP and grown overnight at 37 °C. pET22b-*RgnTDC* plasmid was purified via the Zymo Research Plasmid Prep kit and eluted in 20 µL sterile Milli-Q H<sub>2</sub>O. Plasmids were stored at -20 °C.

Based on a previously reported model of an *RgnTDC*-Trp complex (PDB ID: 4OBV),<sup>1,3</sup> active site residues in the *RgnTDC* active site were chosen for mutagenesis. The sites were: Phe98, Val99, His120, Leu126, Leu336, Leu339, Trp349, Leu355, and Thr356 (Fig S5). Primers were purchased from Integrated DNA Technologies. For each site of mutation, three primers encoding the degenerate codons NDT, VHG, and TGG at the codon of interest were mixed in a 12:9:1 ratio, respectively.<sup>4</sup>

Each gene library was amplified first as two separate fragments and then combined via polymerase chain assembly (PCA)<sup>5</sup> to form full-length *RgnTDC* gene mutagenized at the site of interest. The corresponding genes were then inserted into a pET22b vector as described above and then transformed into BL21(DE3) *E. coli* cells and plated on LB + 100 µg/mL AMP agar plates.

Individual colonies were picked and used to inoculate wells containing 600  $\mu$ l TB + 100  $\mu$ g/mL AMP in a 96-well plate. One column of the plate was used as an internal control with five wild-type colonies, one sterile control, and two non-*RgnTDC* pET22b negative controls. Plates were grown at 37 °C for 16 h at 200 RPMs. 20  $\mu$ l of this starter culture plate was used to inoculate 630  $\mu$ l TB + 100  $\mu$ g/mL AMP. These expression plates were grown at 37 °C for 3 h until OD<sub>600</sub> ~ 1.0. Plates were then placed on ice for 1 h. Expression was induced by addition of 50  $\mu$ l TB + 100  $\mu$ g/mL AMP + 14 mM IPTG + 7 mM indole. Plates were then grown at 23 °C for 16 h at 200 RPM and subsequently spun down at 4000  $xg$  for 15 min and the supernatant discarded. Plates containing cell pellets were stored at -20 °C.

### Screening of *RgnTDC* site-saturation libraries

Cell pellets were thawed and then resuspended in lysis buffer: 50 mM potassium phosphate buffer (pH = 8.0), 1 mg/mL Hen Egg White Lysozyme (GoldBio), 0.2 mg/mL DNaseI (GoldBio), 1 mM MgCl<sub>2</sub>, and 300  $\mu$ M pyridoxal 5'-phosphate (PLP). A volume of 600  $\mu$ L lysis buffer per well was used. After 45 min of shaking at 37 °C, the resulting lysate was then spun down at 4000  $xg$  to pellet cell debris. Then, 180  $\mu$ L of the resulting supernatant was added to 20  $\mu$ L of a substrate mixture in a separate reaction plate. Final substrate concentrations are as follows: **W349X 5-substituted-Trp screen**: 2 mM each of 5-methoxytryptophan, 5-ethoxytryptophan, 2-methyl-5-methoxytryptophan, 5-carboxamidotryptophan, and 5-acetyltryptophan; **W349X single-substrate screen**: 2 mM 5-methoxytryptophan; **active-site site-saturation mutagenesis screens**: 2 mM each of 2-methyltryptophan, 4-bromotryptophan, 5-methoxytryptophan, and 6-chlorotryptophan; 0.2 mM 7-iodotryptophan and 0.2 mM tryptophan. Reactions were incubated at 37 °C for 4 h, quenched via addition of 150  $\mu$ L 1:1 acetonitrile:1 M HCl, and centrifuged at 4000  $xg$  for 10 min. 200  $\mu$ L of the quenched reaction mixture supernatant was filtered into a 96-well plate for UPLC-MS analysis. Data were collected on an Acquity UHPLC with an Acquity QDA MS detector (Waters) using an Intradia Amino Acid column (Imtakt). Tryptamine product  $m/z$  ion counts were used to quantify product formation from the tryptophan reaction mixture from corresponding standard curves (Fig S15).

### Cloning of *PfTrpB* globally random mutagenesis libraries

The plasmid encoding an engineered  $\beta$ -subunit of tryptophan synthase from *Pyrococcus furiosus*, *PfTrpB*<sup>2B9</sup> (2B9), was obtained from the Arnold lab.<sup>6</sup> The mutations in this variant were previously shown to confer kinetic and spectroscopic properties that mimic native allosteric activation by the  $\alpha$ -subunit of tryptophan synthase.<sup>7</sup> The 2B9-encoding plasmid was used as a template for global random mutagenesis to prepare error-prone libraries. PCR amplification of the 2B9 gene was conducted with the addition of MnCl<sub>2</sub> (100 or 150  $\mu$ M) to induce mutagenesis. The amplified products were purified by gel electrophoresis and extracted from the gel using a Zymoclean Gel DNA Recovery Kit. The resulting gene libraries were inserted into a pET22(b)+ plasmid via Gibson

assembly<sup>2</sup> and transformed into *E. coli* BL21(DE3) cells via electroporation. Cells were recovered in TB media for 30 minutes at 37 °C and 220 RPM. Cells were plated onto LB + 100 µg/mL AMP agar plates and incubated overnight at 37 °C.

### **Cloning of *PfTrpB* H275X site-saturation library**

To construct a site-saturation mutagenesis library at the H275 site, three primers with the degenerate codons NDT, VHG, and TGG were purchased from IDT and mixed in a 12:9:1 ratio.<sup>4</sup> The 2B9 gene was amplified with this primer mixture, resulting in two gene fragments, which were combined via PCA to generate a full-length gene.<sup>5</sup> The gene was purified by gel electrophoresis and extracted using a Zymoclean Gel DNA Recovery Kit. The resulting gene library was inserted into a pET22(b)+ plasmid via Gibson assembly and transformed into *E. coli* BL21(DE3) cells via electroporation. Cells were recovered in TB media for 30 minutes at 37 °C and 220 RPM. Cells were plated onto LB + 100 µg/mL AMP agar plates and incubated at 37 °C overnight.

### **Screening of *PfTrpB* libraries**

Individual colonies were picked and used to inoculate wells containing 600 µl TB + 100 µg/mL AMP in a 96-well plate. One column of the plate was used as an internal control with five parent (2B9) colonies, one sterile control, and two non-*PfTrpB* pET22b negative controls. Plates were grown at 37 °C for 16 h at 200 RPM. Expression cultures in a fresh 96-deep well plate containing TB + 100 µg/mL AMP (630 µL) were inoculated using starter culture (20 µL) and grown at 37 °C and 180 RPM until cultures reached an OD<sub>600</sub> of at least 0.6 (approximately 3 hours). Expression cultures were chilled on ice for 30 minutes then inoculated with IPTG (1 mM final concentration). Expression plates were incubated at 23 °C for 16 h at 180 RPM then centrifuged at 4000 xg for 15 min and the supernatant discarded. Cell pellets were stored at -20 °C until lysed.

Cell pellets were thawed and then resuspended in lysis buffer: 50 mM potassium phosphate buffer (pH = 8.0), 1 mg/mL Hen Egg White Lysozyme (GoldBio), 0.2 mg/mL DNaseI (GoldBio), 1 mM MgCl<sub>2</sub>, and 300 µM pyridoxal 5'-phosphate (PLP). A volume of 300 µL lysis buffer per well was used. Cells were lysed for 1 h at 37 °C then heat treated at 75 °C for 15 min. After cooling on ice, lysate was spun down at 4000 xg at 4 °C for 20 min.

A 96-well plate was loaded with 20 µL substrate mixture (final concentration of 5 mM each 2-methylindole, 4-cyanoindole, 5-methoxyindole, 6-hydroxyindole, and indoline, plus 2.5 mM 7-chloroindole). All indole stocks were prepared in DMSO. For globally random mutagenesis library plate A, potassium phosphate buffer (50 mM, pH = 8.0, 160 µL) containing L-serine (5 mM final concentration) was added, followed by heat-treated lysate (20 µL). For subsequent plates, lysate volume was increased to 50 µL and buffer volume reduced to 130 µL. Reactions were set up such that the DMSO cosolvent comprised 10% of the final reaction volume (200 µL). Reactions were run at room

temperature (25 °C) for 2.5 h and were quenched with 200 µL acetonitrile containing 0.1 M HCl and 1 mM tryptamine (as internal standard). Plates were spun down at 4000 xg at 4°C for 20 min. A 200 µL aliquot of each quenched reaction was filtered into a 96-well plate for analysis by UPLC-MS. Product formation was quantified by integration of peaks on single ion retention (SIR) channels corresponding to each expected product, normalized against the tryptamine internal standard.

### **Expression of *RgnTDC* and *PfTrpB* variants**

Cells from wells containing putatively activated *RgnTDC* or *PfTrpB* variants were inoculated into 5 mL TB + AMP and grown for 16 h at 37 °C. Each variant strain culture was used to inoculate 500 mL TB + AMP, which was subsequently grown at 37 °C for 3 h, or until OD<sub>600</sub> ~ 1.5. Cultures were chilled on ice for 30 min, and then induced with 1 mM IPTG. Cells expressing *RgnTDC* were additionally supplemented with 0.5 mM indole, as this was found to boost cell growth. Cultures expressed for 16 h at 23 °C. The next morning, cells were pelleted via centrifugation at 4000 xg for 15 min. Supernatants were bleached and discarded and pellets were weighed and stored at -20 °C until lysis.

To purify enzyme variants, cell pellets were thawed at room temperature and then resuspended in lysis buffer: 50 mM potassium phosphate buffer (pH = 8.0), 1 mg/mL Hen Egg White Lysozyme (GoldBio), 0.2 mg/mL DNaseI (GoldBio), 1 mM MgCl<sub>2</sub>, and 300 µM pyridoxal 5'-phosphate (PLP). A volume of 4 mL of lysis buffer per gram of wet cell pellet was used. After 30 min of shaking at 37 °C, *RgnTDC* lysis suspensions were disrupted using sonication (5 min; 0.8 s on, 0.2 s off at a power setting of 5). *PfTrpB* lysis suspensions were heat treated at 75 °C for 15 min as an alternative to sonication. The resulting lysate was spun down at 75,000 xg to pellet cell debris. Ni/NTA beads (GoldBio) were added to the supernatant and incubated on ice for 30 to 60 min prior to purification by Ni-affinity chromatography. The column was washed with 3 column volumes of wash buffer A (20 mM imidazole, 50 mM potassium phosphate buffer (pH = 8.0)) and with 2 column volumes of wash buffer B (40 mM imidazole, 50 mM potassium phosphate buffer (pH = 8.0); *PfTrpB* variants only), and the proteins were eluted with an elution buffer (250 mM imidazole, 50 mM potassium phosphate buffer (pH = 8.0)). Elution of the desired protein product was monitored by the disappearance of its bright yellow color (resulting from the PLP cofactor) from the column. The protein product was dialyzed to < 1 µM imidazole, dripped into liquid nitrogen to flash freeze, and stored at -80 °C. The concentration of protein was determined by Bradford assay upon thawing. Generally, this procedure yielded 50 – 200 mg per L culture for *RgnTDC* variants and 200 – 500 mg per L culture for *PfTrpB* variants.

### **Turnover analysis of *RgnTDC* variants**

*RgnTDC* variants were thawed on ice from storage at -80 °C and then centrifuged at 15,000 xg for 5 min to pellet aggregated protein. The supernatant was then diluted between

1:1 and 1:100 in 50 mM potassium phosphate buffer (pH = 8.0) (depending on enzyme concentration). Reactions were run in plastic 96-well plates with 10 mM Trp analog, either 33 nM or 1  $\mu$ M TDC variant, and 1000 equivalents PLP relative to TDC with a total volume of 100  $\mu$ L in 50 mM potassium phosphate buffer (pH = 8.0). Reactions were incubated for 16 h at 37 °C. Reactions were quenched with 200  $\mu$ L acetonitrile and further diluted with 100  $\mu$ L H<sub>2</sub>O. Quenched reactions were centrifuged at 15,000  $xg$  for 10 min prior to analysis by UPLC-MS. Enzymatic activity was quantified by integrating the substrate and product UV absorbance peaks at 280 nm. Reactions were run in triplicate, with replicate reactions run on different days with freshly thawed enzyme (Fig 2g).

### **[PLP] vs. activity for *RgnTDC* variants**

*RgnTDC* variants were thawed and prepared as described above. 10 mM 6-chlorotryptophan was added to a solution with varying molar equivalents of PLP relative to TDC (500 nM, 5  $\mu$ M, 50  $\mu$ M, or 500  $\mu$ M). TDC was added such that the final concentration was 50 nM and the solution was diluted up to 100  $\mu$ L with 50 mM potassium phosphate buffer (pH = 8.0). Reactions were incubated for 16 h at 37 °C. Reactions were quenched with 200  $\mu$ L acetonitrile and diluted with 100  $\mu$ L H<sub>2</sub>O. Quenched reactions were centrifuged at 15,000  $xg$  for 10 min prior to UPLC-MS injection of the supernatant. Enzymatic activity was quantified by integrating the substrate and product UV absorbance peaks at 280 nm. Reactions were run in duplicate, with replicate reactions run on separate days with freshly thawed enzyme (Fig S22).

### ***RgnTDC* substrate multiplexed timecourse reaction**

*RgnTDC* variants were thawed and prepared as described above. Reaction conditions included 0.25  $\mu$ M *RgnTDC*, 2.5  $\mu$ M PLP, and one of two sets of substrate mixes: 2.5 mM tryptophan, 2-methyltryptophan, 4-bromotryptophan, and 6-chlorotryptophan; or 0.25 mM tryptophan and 6-chlorotryptophan, 2.5 mM 2-methyltryptophan and 4-bromo-tryptophan. Reactions were filled to 100  $\mu$ L with 50 mM potassium phosphate pH = 8.0. Reactions were conducted in triplicate and incubated for 4 h at 37 °C. Reactions timepoints were taken by quenching 10  $\mu$ L of the reaction solution in 190  $\mu$ L of acetonitrile, followed by dilution with 200  $\mu$ L H<sub>2</sub>O. Quenched reactions were centrifuged at 15,000  $xg$  for 10 min prior to UPLC-MS injection of the supernatant. Product abundance was quantified via single-ion retention and fit to product standard curves (Fig S16).

### **Michaelis-Menten analysis of *RgnTDC* variants**

*RgnTDC* variants were thawed on ice from storage at -80 °C and then centrifuged at 15,000  $xg$  for 5 min to pellet aggregated protein. The supernatant was then diluted between 1:1 and 1:100 in 50 mM potassium phosphate buffer (pH = 8.0), depending on enzyme concentration. Reaction conditions used 0.1 – 20 mM tryptophan analog with 10 equivalents of PLP cofactor relative to TDC in 1.7 mL Eppendorf tubes with a total volume of 100  $\mu$ L in 50 mM potassium phosphate buffer (pH = 8.0). The enzyme and substrate solutions were equilibrated to 37 °C prior to mixing. Final enzyme concentrations were 0.1 – 5  $\mu$ M. At various time points after addition of *RgnTDC*, 20  $\mu$ L aliquots of the reaction solution were quenched

in 180  $\mu\text{L}$  acetonitrile and diluted with 200  $\mu\text{L}$   $\text{H}_2\text{O}$ . Quenched reactions were centrifuged at 15,000  $\times g$  for 10 min prior to UPLC-MS injection of the supernatant. Enzymatic activity was quantified by integrating the substrate and product UV absorbance peaks at 280 nm. All replicate reactions were run on different days with fresh enzyme. Initial velocity slopes were fit using the revised Michaelis-Menten equation as described by Johnson 2019.<sup>8</sup>

### Single substrate activity analysis of *PfTrpB* variants

*PfTrpB* variants were thawed on ice from storage at  $-80\text{ }^\circ\text{C}$  and then centrifuged at 15,000  $\times g$  for 5 min to pellet aggregated protein. Each variant was diluted in 50 mM potassium phosphate buffer (pH = 8.0) to a concentration of 40  $\mu\text{M}$ . Single substrate reactions were prepared in duplicate for each *PfTrpB* variant on a 96-well plate. Reaction conditions included 10 mM indole analog, 30 mM Ser, 2  $\mu\text{M}$  *PfTrpB* (5000 max TON), and 10% DMSO in 100 mM potassium phosphate buffer (pH = 8.0). Reactions were run at  $37\text{ }^\circ\text{C}$  for 1 h. Reaction aliquots (75  $\mu\text{L}$ ) were quenched with 75  $\mu\text{L}$  acetonitrile + 0.1 M HCl + 1 mM tryptamine (as internal standard) and diluted with an additional 150  $\mu\text{L}$  1:1 acetonitrile: $\text{H}_2\text{O}$ . Quenched reactions were centrifuged at 15,000  $\times g$  for 10 min then filtered into a 96-well plate for UPLC-MS analysis. Product formation was quantified by integration of peaks on single ion retention (SIR) channels corresponding to each expected product, normalized against the tryptamine internal standard.

### Michaelis-Menten analysis of *PfTrpB* variants

*PfTrpB* variants were thawed on ice from storage at  $-80\text{ }^\circ\text{C}$  and then centrifuged at 15,000  $\times g$  for 5 min to pellet aggregated protein. The supernatant was diluted in 100 – 200 mM potassium phosphate buffer (pH = 8.0) to obtain sufficiently dilute concentrations for initial velocity kinetic measurements.

**Indole:** Rate of formation of Trp from indole and Ser was measured at 290 nm, as described previously.<sup>9</sup> *PfTrpB* variants (0.34 – 1.57  $\mu\text{M}$  final concentration) in 200 mM potassium phosphate buffer (pH = 8.0) were pre-incubated in quartz cuvettes at  $37\text{ }^\circ\text{C}$ . Indole (3 – 400  $\mu\text{M}$  final concentration) was added, followed by Ser (2.5 mM for 2B9 and H275E, 25 mM for H275R). Indole stocks were prepared using DMSO, such that the final reaction volume (400  $\mu\text{L}$ ) was comprised of 5% DMSO. Cuvettes were inverted to mix, and absorbance at 290 nm was collected for 2 min. All replicate reactions were run on two different days with fresh enzyme. Initial velocity slopes were calculated and fit using the revised Michaelis-Menten equation as described by Johnson 2019.<sup>8</sup>

**Indoline:** Formation of 2,3-dihydroisotryptophan (DIT) from indoline and Ser was measured by integration of UPLC peaks at 254 nm. A calibration curve was used to convert integration of the UPLC peak to a concentration of DIT (Fig S37). Reaction conditions included 1 – 50 mM indoline, 10 mM Ser, 1 – 2  $\mu\text{M}$  *PfTrpB*, and 5% DMSO in 100 mM potassium phosphate buffer (pH = 8.0) in 1.7 mL epi-tubes. The enzyme and substrate solutions were equilibrated to  $37\text{ }^\circ\text{C}$  prior to mixing. Reaction aliquots (50  $\mu\text{L}$ ) were quenched in acetonitrile (125  $\mu\text{L}$ ) at various time points (5 – 60 min) and diluted with 75  $\mu\text{L}$  water (1:5

dilution factor). Quenched samples were centrifuged (15,000 *xg*, 5 min) and analyzed by UPLC-MS. All replicate reactions were run on three different days with fresh enzyme. Initial velocity slopes were calculated and fit using the revised Michaelis-Menten equation as described by Johnson 2019.<sup>8</sup>

### **UV-Vis spectroscopy of *PfTrpB* variants**

*PfTrpB* variants were thawed on ice from storage at -80 °C and then centrifuged at 15,000 *xg* for 5 min to pellet aggregated protein. The supernatant was diluted in 200 mM potassium phosphate buffer (pH = 8.0) to obtain a final concentration of 300 μM. A baseline spectrum (600-250 nm, 1 nm interval, fast scan) was collected on 200 mM potassium phosphate buffer (284 μL, pH = 8.0) at 25 °C. *PfTrpB* (20 μL) was added to the cuvette for a final concentration of 20 μM enzyme and an enzyme-only spectrum was collected. To study Ser binding and rate of the shunt pathway, Ser (12.5 μL, 20 mM final concentration) was added, and the cuvette was inverted to mix. Spectra were collected every 10 minutes for 12 scans (110 minutes total) to track pyruvate formation (320 nm) over time. To study Trp binding, Trp was titrated into a sample of 20 μM *PfTrpB* and a spectrum was collected at each concentration (0-1200 μM).

### **Protein crystallography of *PfTrpB*-H275E**

Crystals of the H275E *PfTrpB*<sup>2B9</sup> variant were grown in sitting drops against a 1-mL reservoir containing 13-21% PEG3350 and 0.1 M Na HEPES buffer (pH = 7.85), with mother liquor containing 2 μL of H275E (8.0 or 15 mg/mL) and 2 μL of well solution. Crystals grew over the course of several days and were stable in the dark over several weeks. Trp- and 4-Cl-Trp-bound crystals were prepared by addition of solid Trp or 4-Cl-Trp (approx. 1 mg) to pre-formed crystals. Crystals were cryoprotected by dredging through Fomblin-Y then through Paratone-N and flash frozen in liquid N<sub>2</sub>. Data were collected remotely at the Argonne National Laboratory Advanced Photon Source on either beamline 21ID-D (PDB ID: 7RNQ) or beamline 23ID-B (PDB ID: 7RNP, 7ROF). Data were integrated and scaled using XDS and AIMLESS.<sup>10,11</sup> Structures were solved by molecular replacement with PHASER, using CCP4.<sup>12,13</sup> Search models for each structure were comprised of a single monomer of a previously solved *PfTrpB*<sup>2B9</sup> structure, where the H275 site was deleted, ligands and waters were removed, and the remaining model was subjected to geometric refinement in Refmac5. PDB ID: 6AM7 was used as the search model for the unbound H275E structure, and PDB ID: 6AM8 was used as the search model for the Trp- and 4-Cl-Trp-bound structures. Model building was performed in Coot and refinement was conducted using Refmac5. The TLS motion server was used to calculate TLS operators; we selected 10 operators for each chain in the asymmetric unit.<sup>14</sup> The MolProbity server was used to evaluate the structure prior to final refinement.<sup>14,15</sup> Crystallographic and refinement statistics are reported in Table S3.

## Supplemental Figures

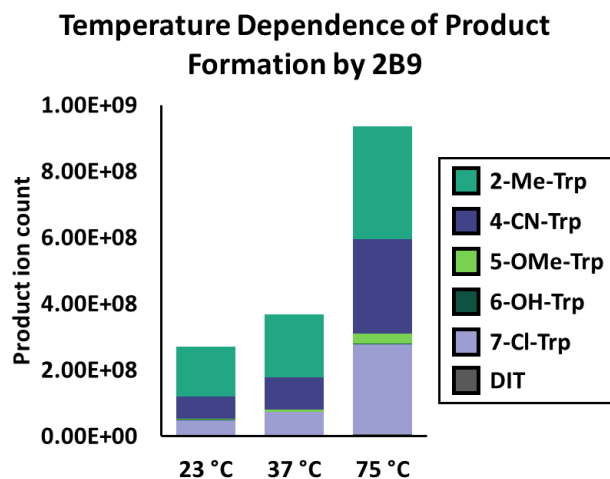


**Figure S1.** The activity of 2B9 is temperature dependent. Improved activity at moderate temperatures was a selective pressure used for engineering of 2B9. Reactions were run with a multiplexed substrate panel, 5 mM Ser, and 6.8  $\mu\text{M}$  2B9 in 100 mM  $\text{KPi}$  buffer (pH = 8.0) and quenched after 10 minutes. Substrate panel: 5 mM each of 2-Me-indole, 5-OMe-indole, 6-OH-indole, and indoline and 2.5 mM each of 4-F-indole and 7-Cl-indole.

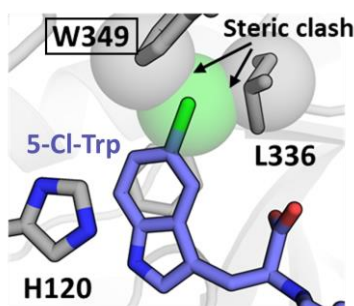


**Figure S2.** RgnTDC active-site model of 5-chlorotryptophan, modelled from PDB ID: 4OBV.<sup>3</sup> The potential steric interaction of the 5-chloro-substituent with the W349 and L336 residues is highlighted. Figure adapted from McDonald et al. 2019.<sup>1</sup>

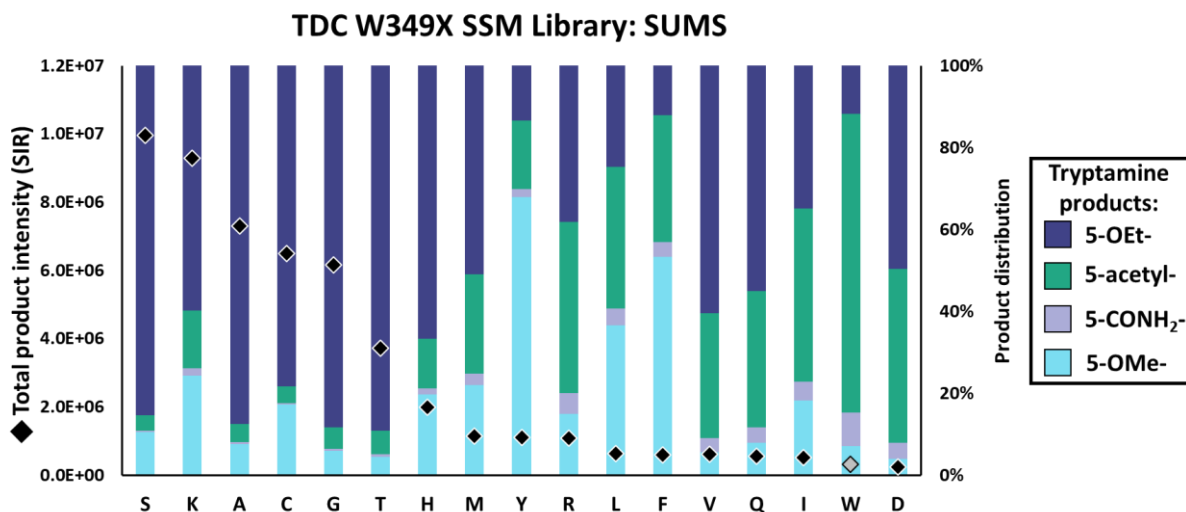


**Figure S3.** Results from substrate-multiplexed screening (SUMS) of the W349 site-saturation mutagenesis (SSM) library with various 5-substituted tryptophan analogs. Colored bars represent relative amounts of each product formed, and black diamonds indicate total intensity of single ion retention (SIR) from each product's unique m/z. The wild-type sequence is denoted by a grey diamond. Relative product amounts and SIR intensity were averaged from all wells with the given sequence. 2-methyl-5-methoxytryptophan was also included as a potential substrate, but no product was observed.

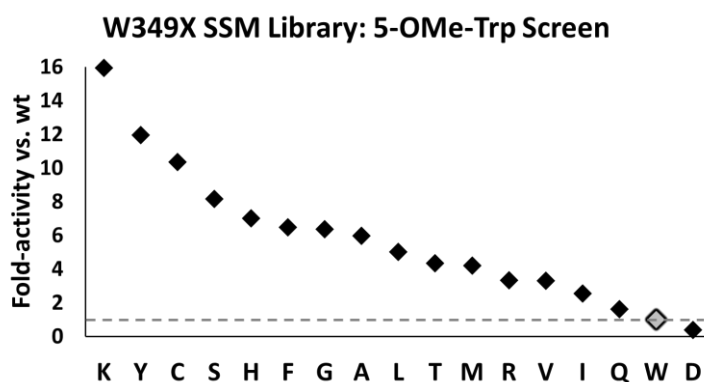


**Figure S4.** Single-substrate screen of the W349 site-saturation mutagenesis library with 5-methoxytryptophan. Fold-activities were determined relative to wild-type (wt) *RgnTDC* wells from absorbance at 280 nm. Depicted fold-activities represent averaged fold-activities relative to wt activity for all wells with the above given sequence.

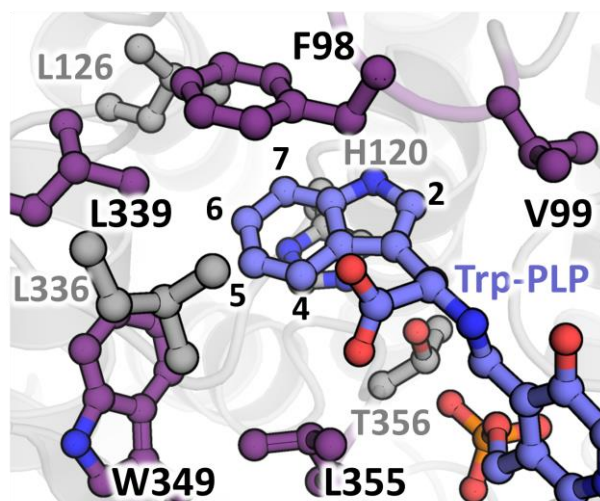


**Figure S5.** Active-site model of *RgnTDC* (built from PDB ID: 4OBV)<sup>3</sup> with residues highlighted in purple at which mutations were found that significantly altered promiscuity or improved activity). Mutations at residues highlighted in gray were found to not significantly alter promiscuity (H120, L126) or resulted in catalytically feeble enzymes (L336, T356).

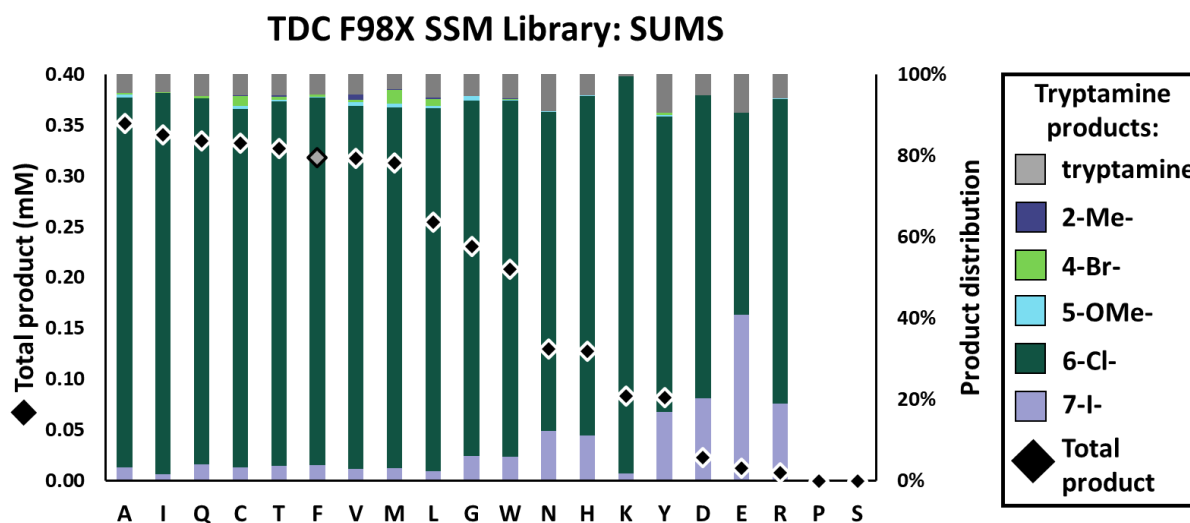


**Figure S6.** Retention of function (ROF) curve from substrate-multiplexed screening (SUMS) of the F98 site-saturation mutagenesis library. Colored bars represent relative amounts of each product formed, and diamonds represent mM total product produced, as determined by single-ion retention standard curves. The wild-type sequence is denoted by a grey diamond. Relative product amounts and mM total product were averaged from all wells with the given sequence. (No proline or serine mutations were sequenced from this library).

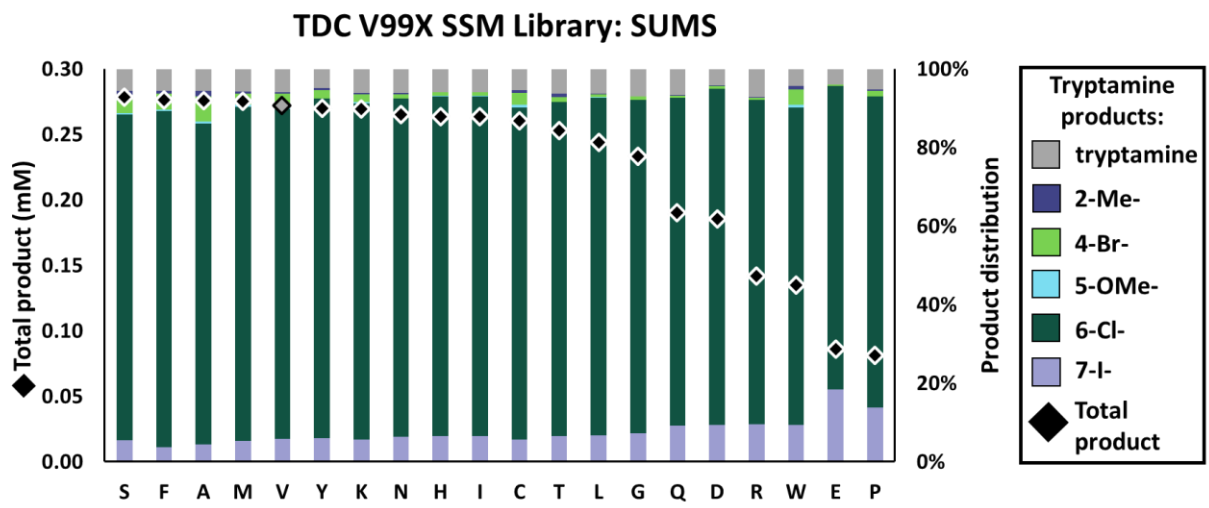


**Figure S7.** Retention of function (ROF) curve from substrate-multiplexed screening (SUMS) of the V99 site-saturation mutagenesis library. Colored bars represent relative amounts of each product formed, and diamonds represent mM total product produced, as determined by single-ion retention standard curves. The wild-type sequence is denoted by a grey diamond. Relative product amounts and mM total product were averaged from all wells with the given sequence.

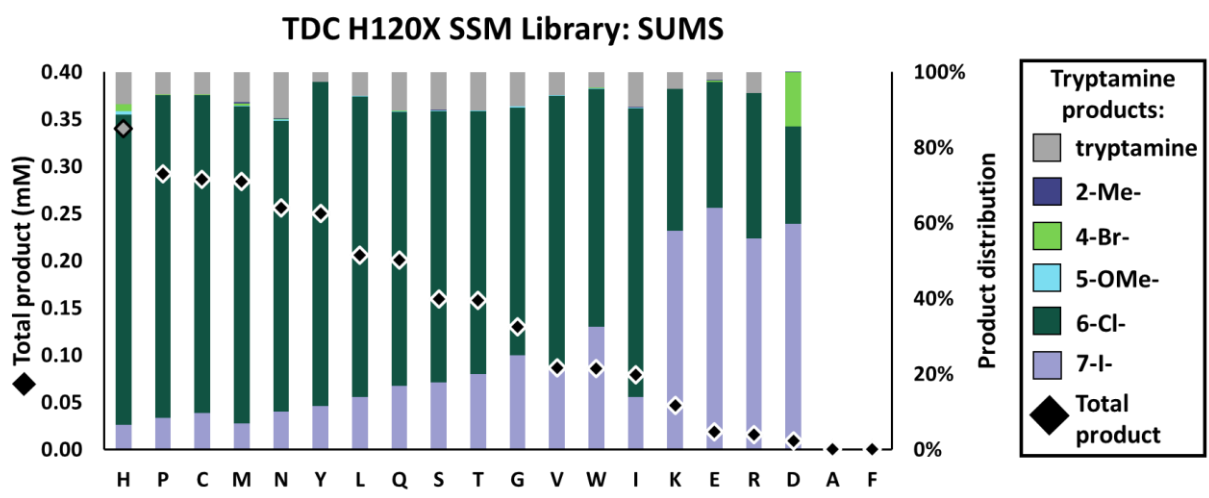


**Figure S8.** Retention of function (ROF) curve from substrate-multiplexed screening (SUMS) of the H120 site-saturation mutagenesis library. Colored bars represent relative amounts of each product formed, and diamonds represent mM total product produced, as determined by single-ion retention standard curves. The wild-type sequence is denoted by a grey diamond. Relative product amounts and mM total product were averaged from all wells with the given sequence. (No alanine or phenylalanine mutations were sequenced from the library).

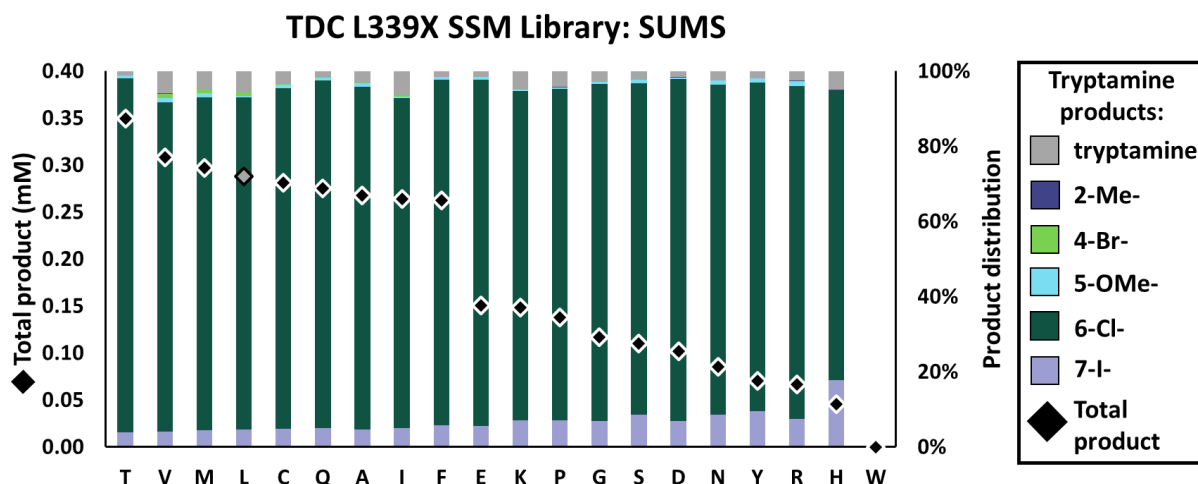


**Figure S9.** Retention of function (ROF) curve from substrate-multiplexed screening (SUMS) of the L339 site-saturation mutagenesis library. Colored bars represent relative amounts of each product formed, and diamonds represent mM total product produced, as determined by single-ion retention standard curves. The wild-type sequence is denoted by a grey diamond. Relative product amounts and mM total product were averaged from all wells with the given sequence. (No tryptophan mutations were sequenced from the library).

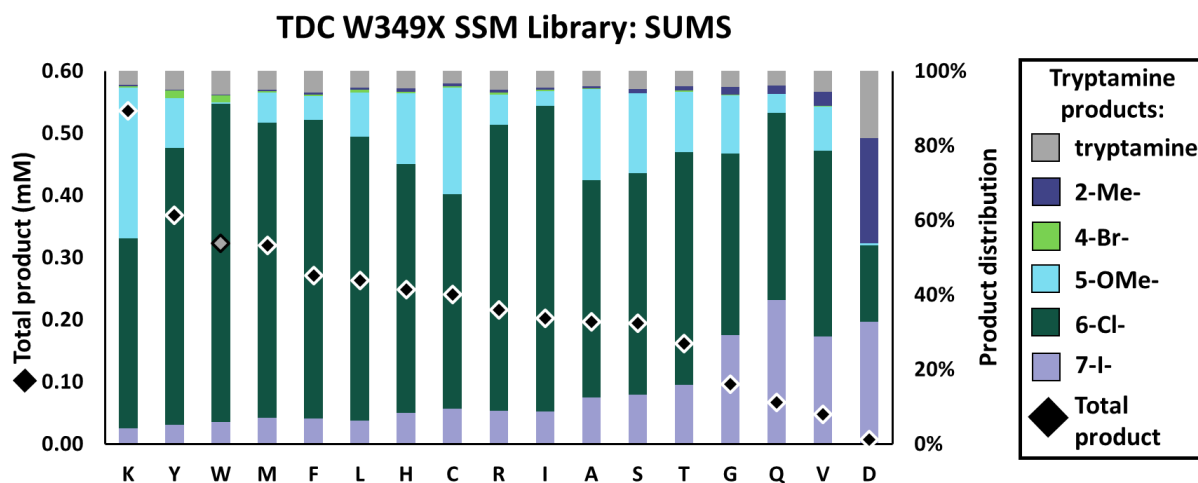


**Figure S10.** Retention of function (ROF) curve from substrate-multiplexed screening (SUMS) of the W349 site-saturation mutagenesis library. Colored bars represent relative amounts of each product formed, and diamonds represent mM total product produced, as determined by single-ion retention standard curves. The wild-type sequence is denoted by a grey diamond. Relative product amounts and mM total product were averaged from all wells with the given sequence.

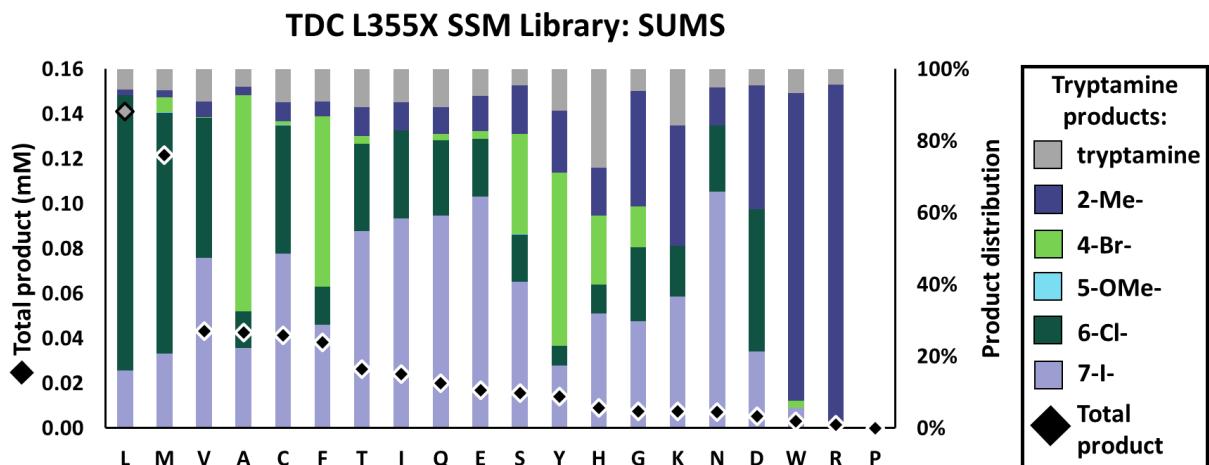


**Figure S11.** Retention of function (ROF) curve from substrate-multiplexed screening (SUMS) of the L355 site-saturation mutagenesis library. Colored bars represent relative amounts of each product formed, and diamonds represent mM total product produced, as determined by single-ion retention standard curves. The wild-type sequence is denoted by a grey diamond. Relative product amounts and mM total product were averaged from all wells with the given sequence. (No proline mutations were sequenced from the library).

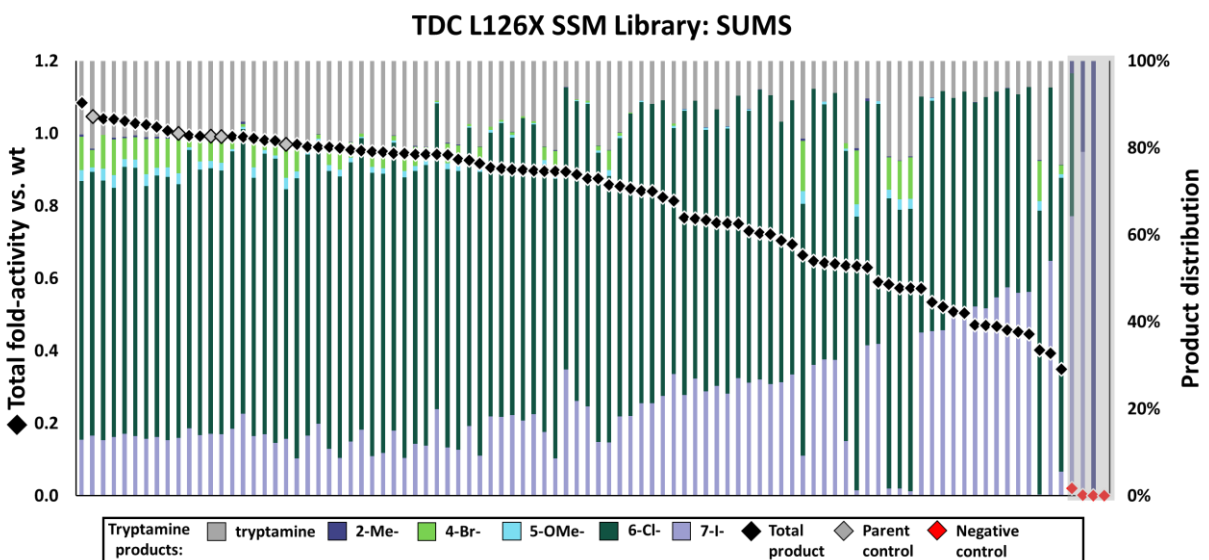


**Figure S12.** Retention of function (ROF) curve from substrate-multiplexed screening (SUMS) of the L126 site-saturation mutagenesis library. Colored bars represent relative amounts of each product formed, and diamonds represent mM total product produced, as determined by single-ion retention standard curves. Wild-type sequences are denoted by grey diamonds, while negative controls are shown as red diamonds. Greyed-out section indicates wells where the quality of signal-to-noise was too low and the relative product distributions are dominated by noise and therefore no longer indicative of enzyme promiscuity.

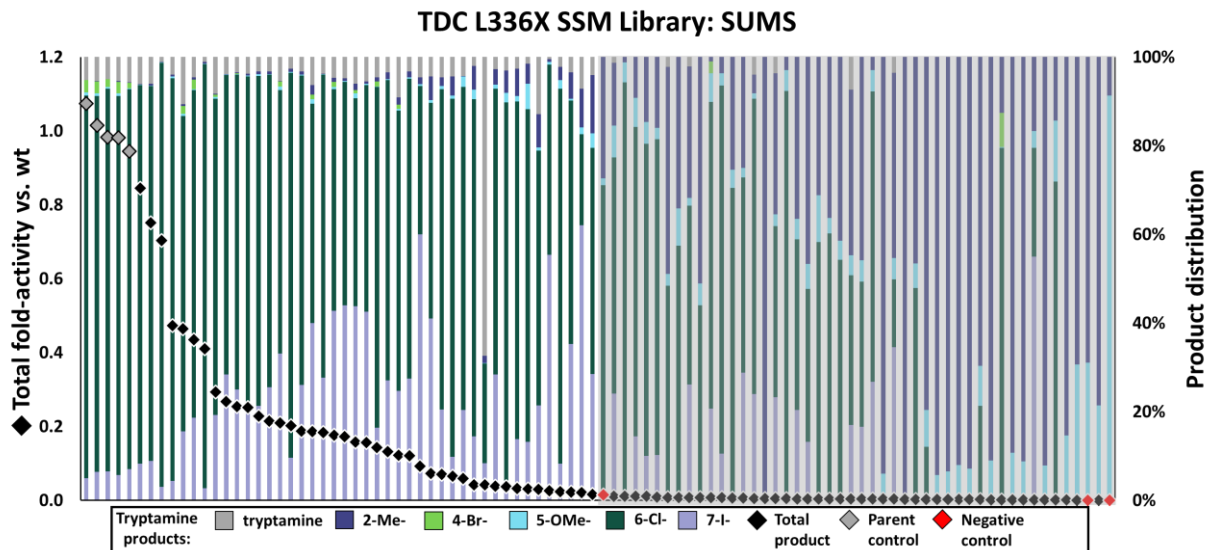


**Figure S13.** Retention of function (ROF) curve from substrate-multiplexed screening (SUMS) of the L336 site-saturation mutagenesis library. Colored bars represent relative amounts of each product formed, and diamonds represent mM total product produced, as determined by single-ion retention standard curves. Wild-type sequences are denoted by grey diamonds, while negative controls are shown as red diamonds. Greyed-out section indicates wells where the quality of signal-to-noise was too low and the relative product distributions are dominated by noise and therefore no longer indicative of enzyme promiscuity.

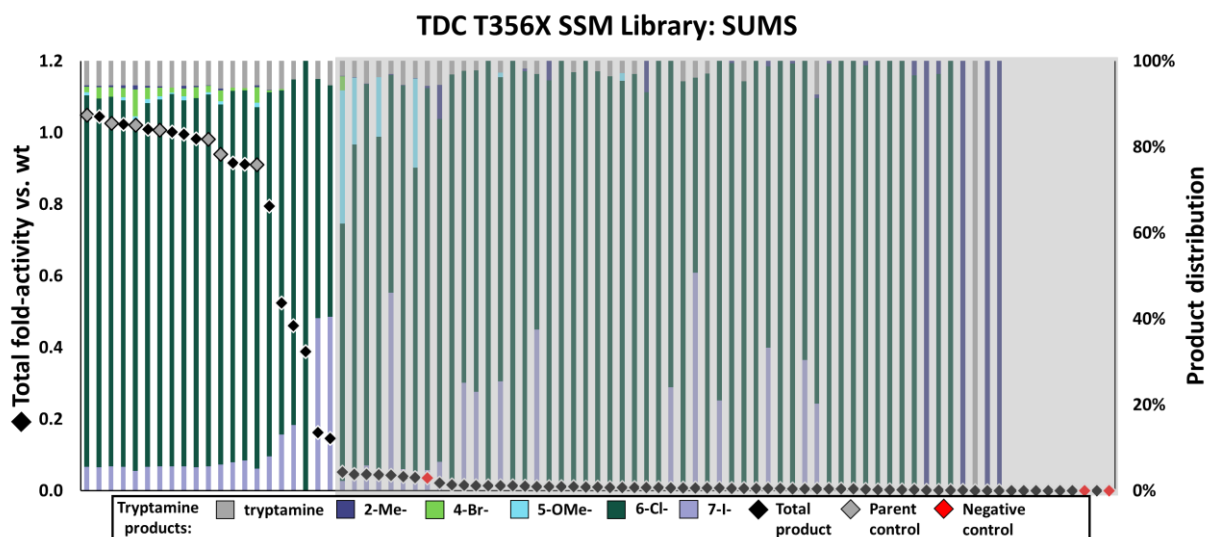


**Figure S14.** Retention of function (ROF) curve from substrate-multiplexed screening (SUMS) of the T356 site-saturation mutagenesis library. Colored bars represent relative amounts of each product formed, and diamonds represent mM total product produced, as determined by single-ion retention standard curves. Wild-type sequences are denoted by grey diamonds, while negative controls are shown as red diamonds. Greyed-out section indicates wells where the quality of signal-to-noise was too low and the relative product distributions are dominated by noise and therefore no longer indicative of enzyme promiscuity.

Tryptamine standard curves for *RgnTDC* SSM library product quantification

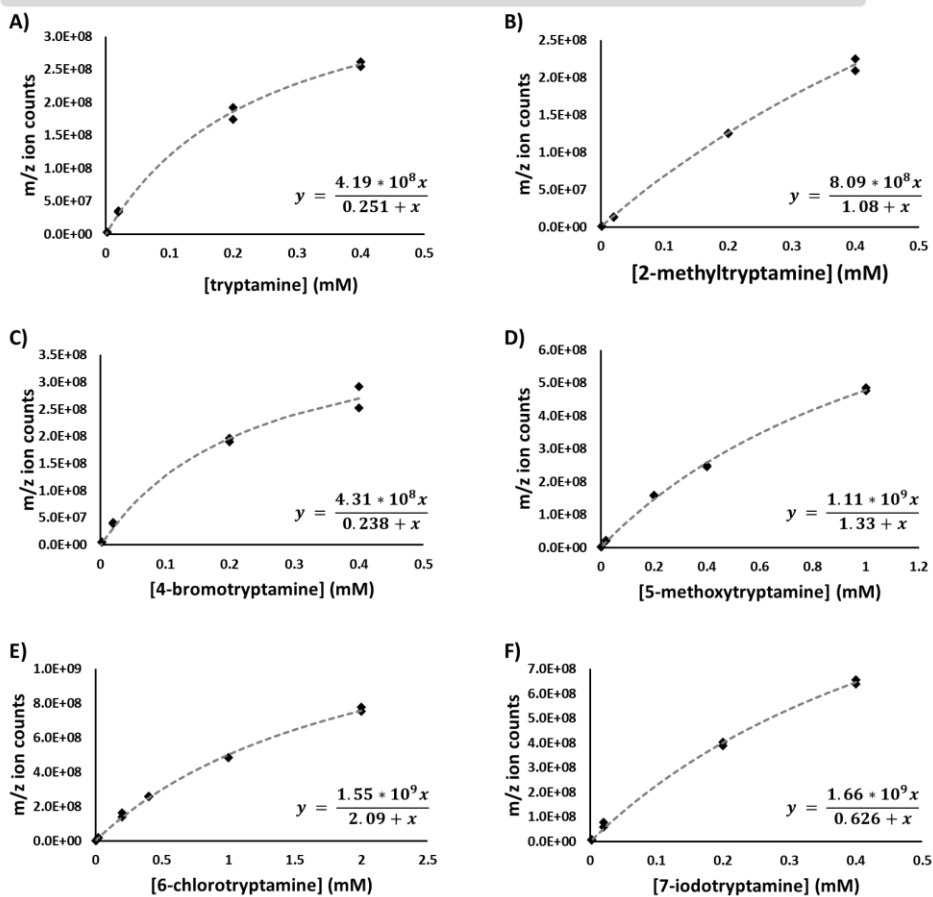


**Figure S15.** Tryptamine standard curves for analysis of product abundance in *RgnTDC* SSM libraries.

Tryptamine standard curves for *RgnTDC* substrate multiplexed timecourse product quantification

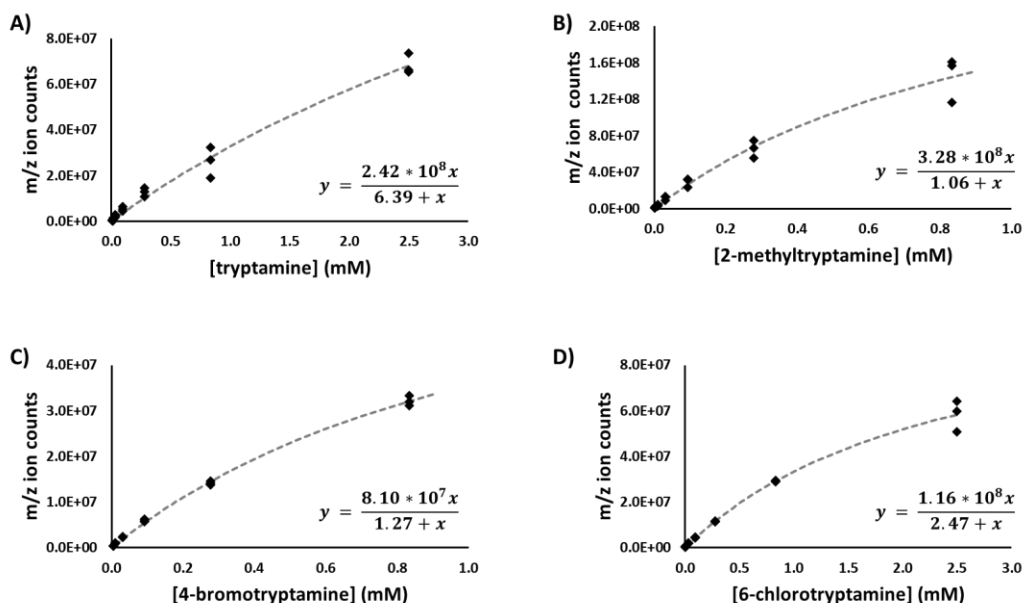


**Figure S16.** Tryptamine standard curves for analysis of product abundance in the *RgnTDC* substrate multiplexed timecourse reactions.

wild-type *RgnTDC* kinetics

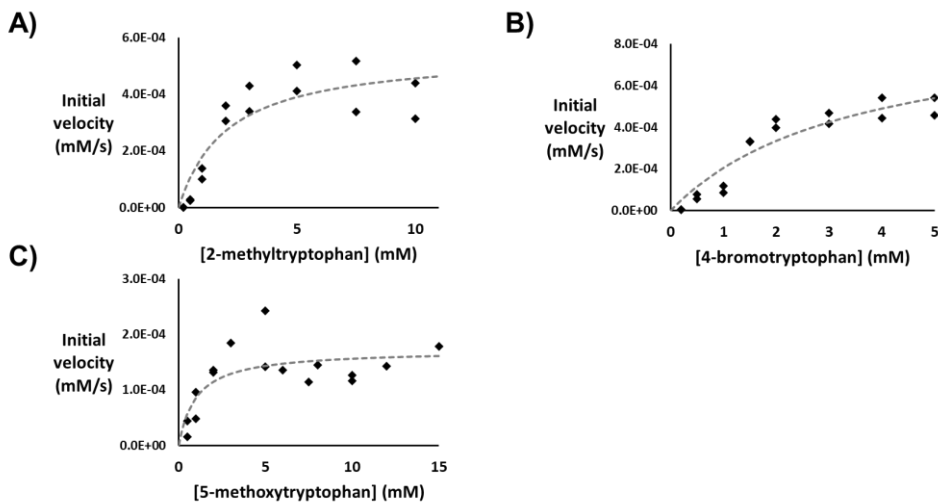


**Figure S17.** Michaelis-Menten curves for wild-type *RgnTDC* with 2-methyltryptophan, 4-bromotryptophan, and 5-methoxytryptophan. Relative enzyme concentration used are as follows: **A)** 10  $\mu$ M *RgnTDC*, **B)** 2.5  $\mu$ M *RgnTDC*, **C)** 10  $\mu$ M *RgnTDC*.

### F98V *RgnTDC* kinetics

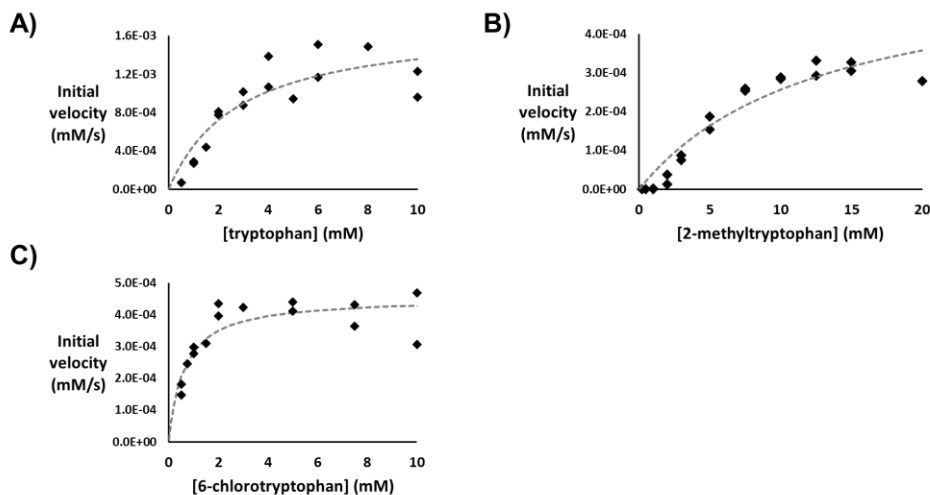


**Figure S18.** Michaelis-Menten curves for F98V *RgnTDC* with tryptophan, 2-methyltryptophan, and 6-chlorotryptophan. Relative enzyme concentration used are as follows: **A)** 0.2  $\mu\text{M}$  *RgnTDC*, **B)** 14  $\mu\text{M}$  *RgnTDC*, **C)** 0.5  $\mu\text{M}$  *RgnTDC*.

### W349K *RgnTDC* kinetics

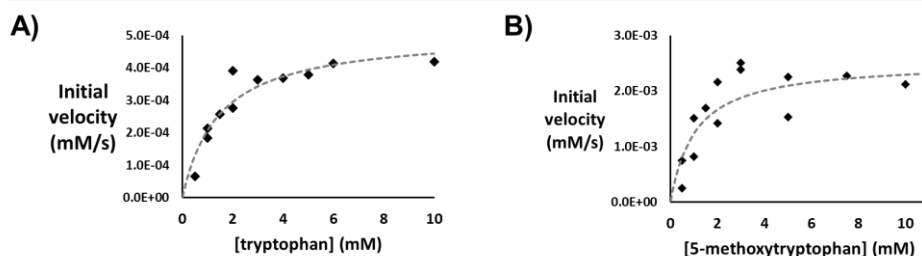


**Figure S19.** Michaelis-Menten curves for W349K *RgnTDC* with tryptophan and 5-methoxytryptophan. Relative enzyme concentration used are as follows: **A)** 0.5  $\mu\text{M}$  *RgnTDC*, **B)** 10  $\mu\text{M}$  *RgnTDC*.

### L355A *RgnTDC* kinetics

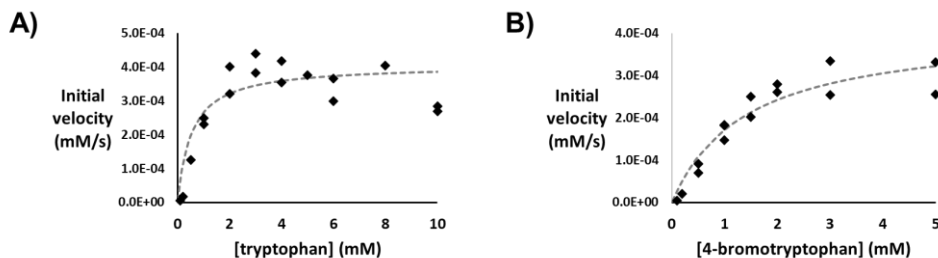


**Figure S20.** Michaelis-Menten curves for L355A *RgnTDC* with tryptophan and 4-bromotryptophan. Relative enzyme concentration used are as follows: **A)** 3  $\mu\text{M}$  *RgnTDC*, **B)** 0.5  $\mu\text{M}$  *RgnTDC*.

L355F *RgnTDC* kinetics

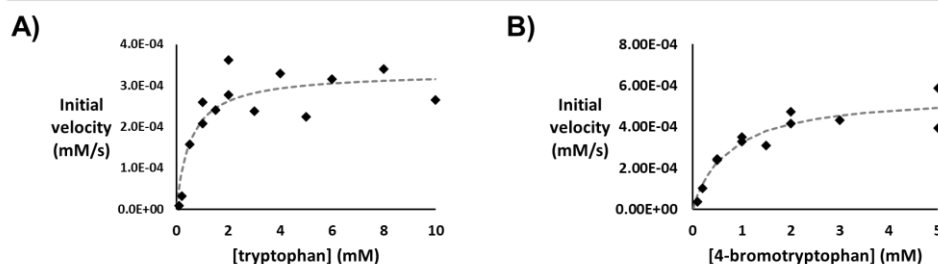


**Figure S21.** Michaelis-Menten curves for L355F *RgnTDC* with tryptophan and 4-bromotryptophan. Relative enzyme concentration used are as follows: **A)** 0.1  $\mu\text{M}$  *RgnTDC*, **B)** 0.5  $\mu\text{M}$  *RgnTDC*.

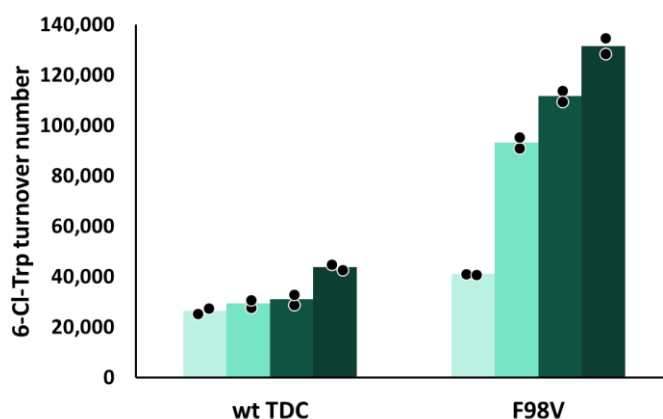


**Figure S22.** Comparison of effect of additional pyridoxal phosphate (PLP) on conversion of 6-chlorotryptophan (6-Cl-Trp) to 6-chlorotryptamine. Amount of PLP shown is relative to the *RgnTDC* concentration of 50 nM. Reactions were conducted in duplicate. F98V *RgnTDC* showed a higher dependence on PLP than wild-type (wt) *RgnTDC*, potentially indicating weaker cofactor binding.

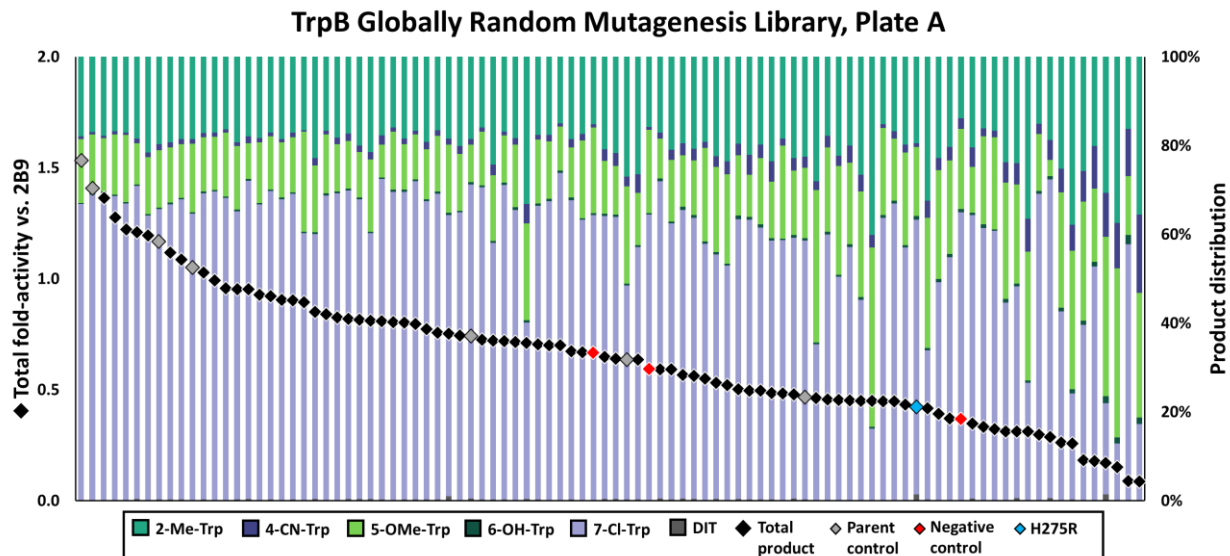


**Figure S23.** SUMS results for plate A of the *PflTrpB* globally random mutagenesis library, with 2B9 as the parent enzyme. Colored bars represent relative amounts of each product formed, and diamonds represent total product formed, based on ion count integrations of single-ion retention (SIR) channels. Parent (2B9) controls are denoted by grey diamonds, while negative controls are shown as red diamonds. Substrate panel: 5 mM each of 2-Me-indole, 4-CN-indole, 5-OMe-indole, 6-OH-indole, and indoline; and 2.5 mM 7-Cl-indole. The signal-to noise ratio throughout plate A was generally poor, but variant H275R was identified in this screen and subsequently validated in both substrate-multiplexed and single-substrate reactions.

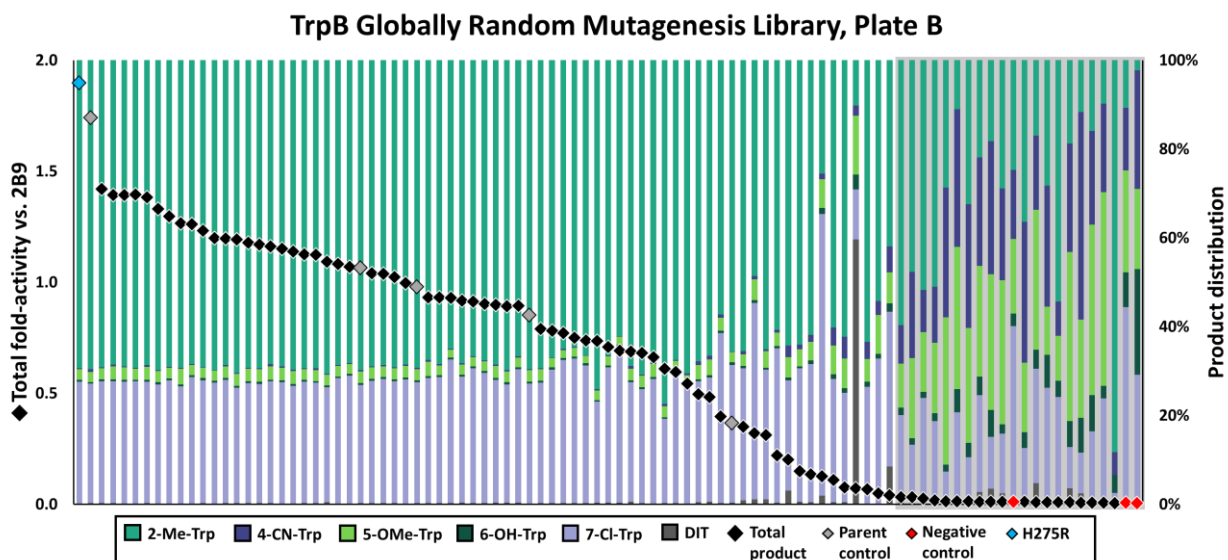


**Figure S24.** SUMS results for plate B of the *PfTrpB* globally random mutagenesis library, with 2B9 as the parent enzyme. Colored bars represent relative amounts of each product formed, and diamonds represent total product formed, based on ion count integrations of single-ion retention (SIR) channels. Parent (2B9) controls are denoted by grey diamonds, while negative controls are shown as red diamonds. Substrate panel: 5 mM each of 2-Me-indole, 4-CN-indole, 5-OMe-indole, 6-OH-indole, and indoline; and 2.5 mM 7-Cl-indole. Greyed-out section indicates wells where the quality of signal-to-noise was too low and the relative product distributions are dominated by noise and therefore no longer indicative of enzyme promiscuity.

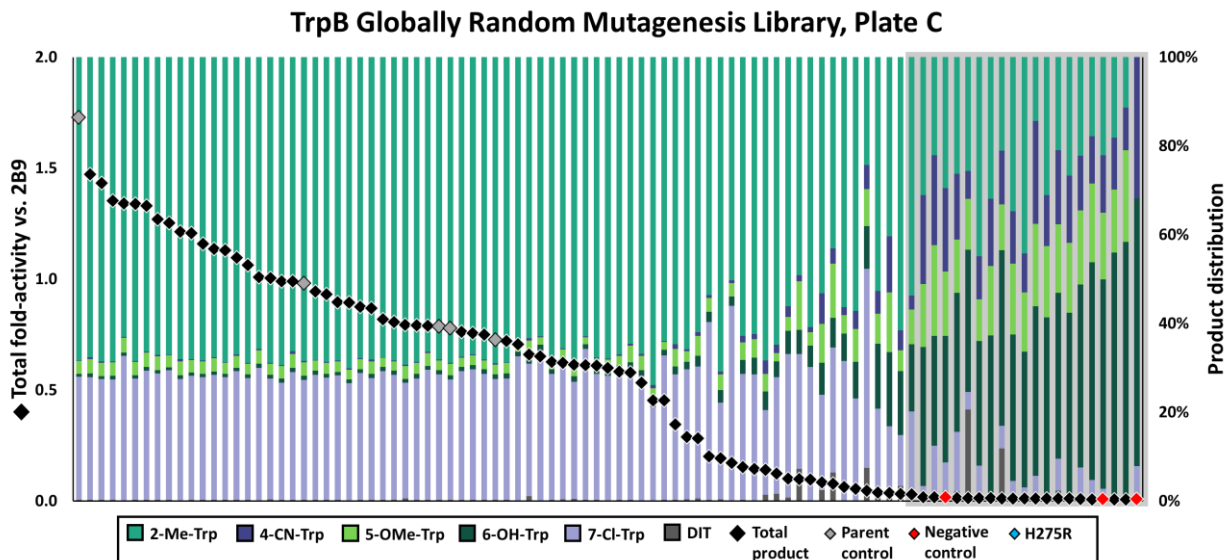


**Figure S25.** SUMS results for plate B of the *PTrpB* globally random mutagenesis library, with 2B9 as the parent enzyme. Colored bars represent relative amounts of each product formed, and diamonds represent total product formed, based on ion count integrations of single-ion retention (SIR) channels. Parent (2B9) controls are denoted by grey diamonds, while negative controls are shown as red diamonds. Substrate panel: 5 mM each of 2-Me-indole, 4-CN-indole, 5-OMe-indole, 6-OH-indole, and indoline; and 2.5 mM 7-Cl-indole. Greyed-out section indicates wells where the quality of signal-to-noise was too low and the relative product distributions are dominated by noise and therefore no longer indicative of enzyme promiscuity.

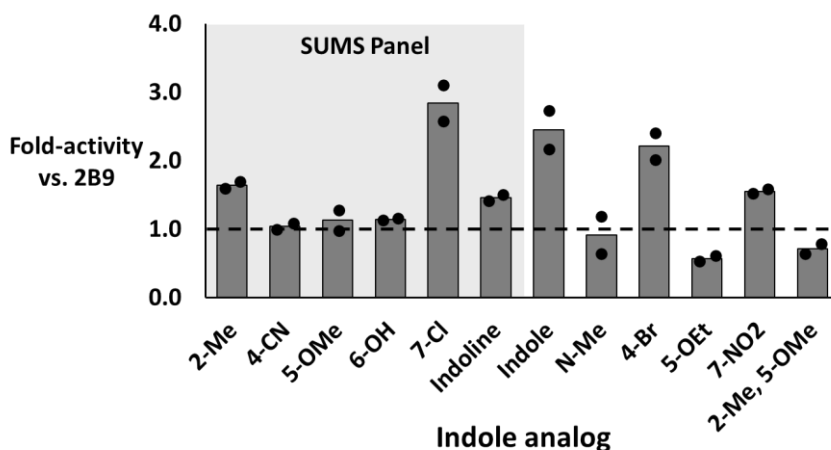


**Figure S26.** Activity of I102T in single-substrate reactions, relative to 2B9 (black dashed line). Reactions consisted of 10 mM indole substrate, 30 mM Ser, and 2  $\mu$ M *PTrpB* in 100 mM potassium phosphate buffer (pH = 8.0) and 10% DMSO. Reactions were run in duplicate at 37  $^{\circ}$ C.

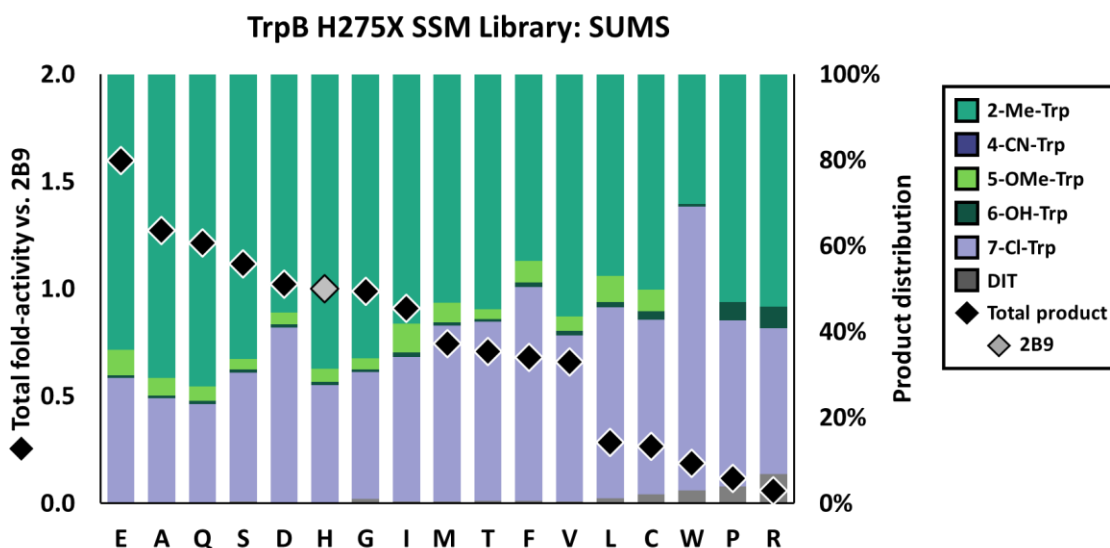


**Figure S27.** SUMS results for the *PfTrpB* H275X site-saturation mutagenesis library. Colored bars represent relative amounts of each product formed, and diamonds represent total product formed, based on ion count integrations of single-ion retention (SIR) channels. The parent (2B9) sequence is denoted by a grey diamond. Substrate panel: 5 mM each of 2-Me-indole, 4-CN-indole, 5-OMe-indole, 6-OH-indole, and indoline, and 2.5 mM 7-Cl-indole. No 4-CN-Trp product was detected. No lysine, asparagine, or tyrosine mutations were sequenced from this library plate.

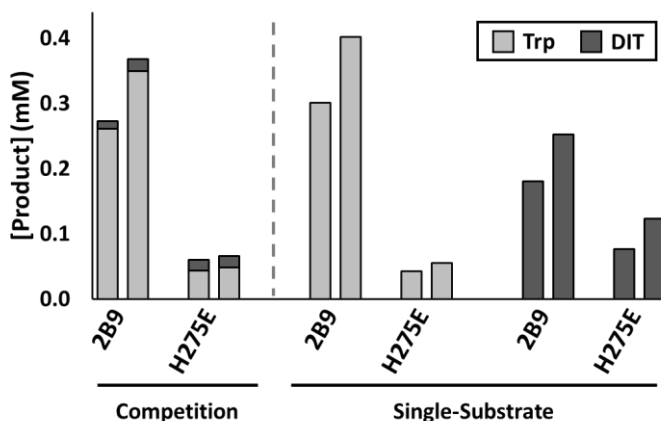


**Figure S28.** Comparison of Trp and DIT production under competition and single-substrate reaction conditions, using purified 2B9 and H275R enzymes. Reactions consisted of 1.5 mM indole and/or 15 mM indoline, 30 mM Ser, and 5  $\mu$ M *PfTrpB* in 100 mM potassium phosphate buffer (pH = 8.0) and 10% DMSO at 37  $^{\circ}$ C.

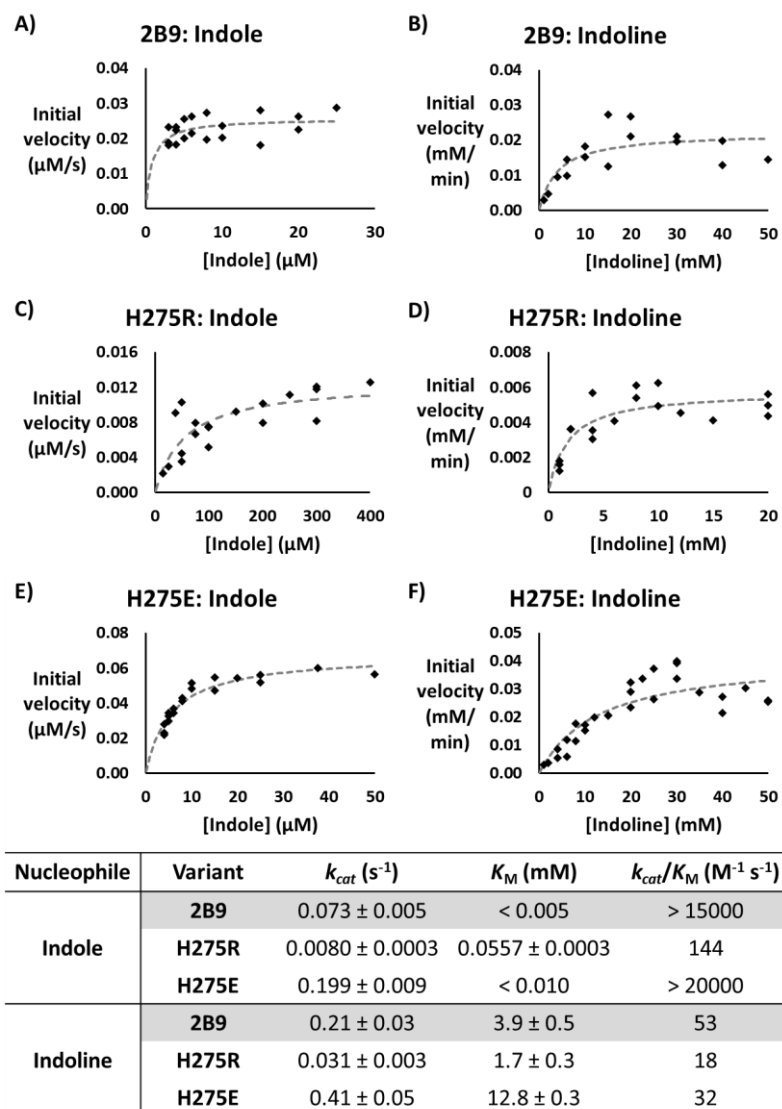


**Figure S29.** Michaelis-Menten curves for 2B9 (A, B), H275R (C, D), and H275E (E, F) with indole or indoline. Enzyme concentrations used are as follows: **A)** 0.35  $\mu$ M, **B)** 1.76  $\mu$ M, **C)** 1.57  $\mu$ M, **D)** 3.13  $\mu$ M, **E)** 0.34  $\mu$ M, and **F)** 1.70  $\mu$ M. See SI methods for additional experimental details.

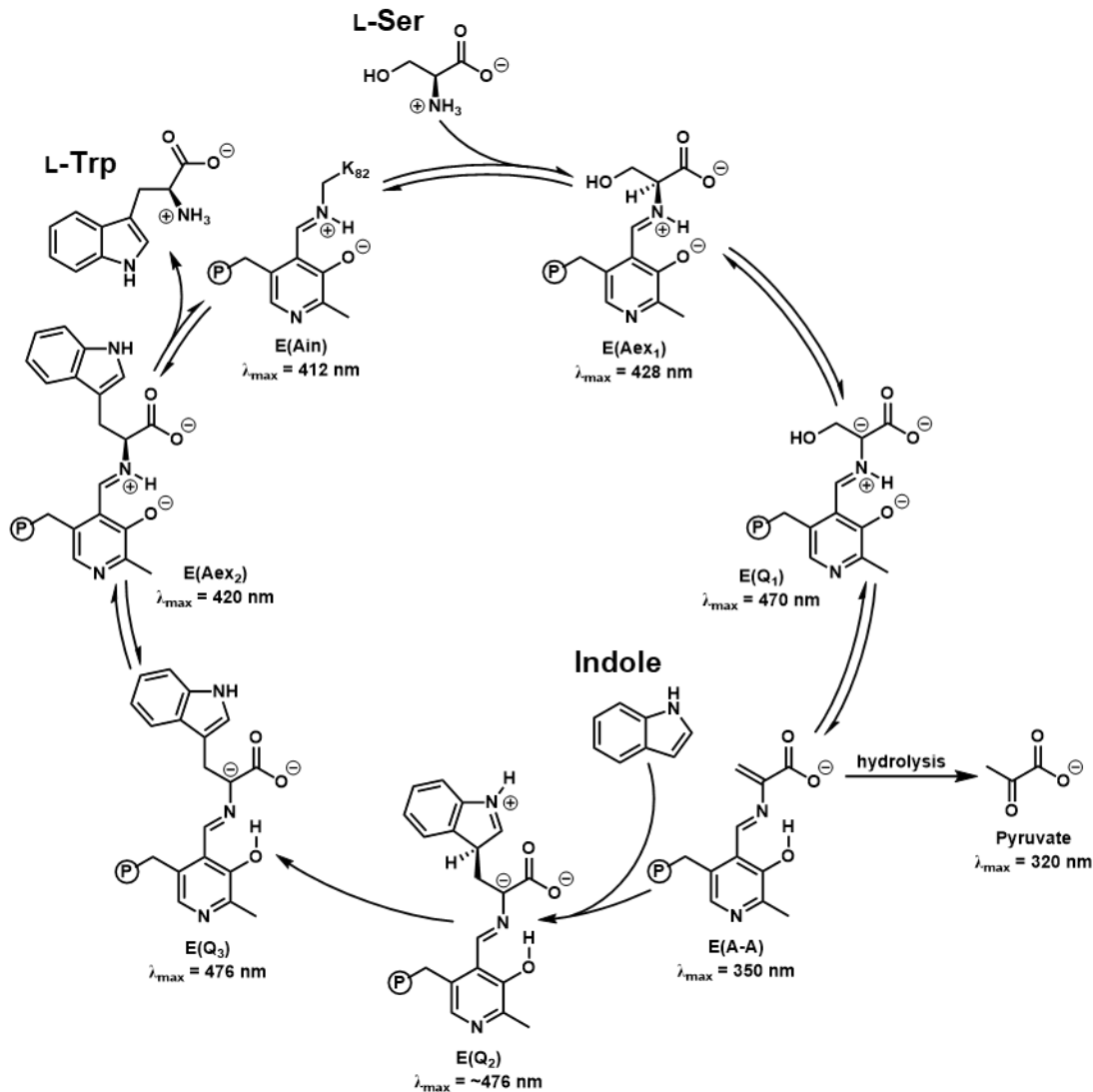


**Figure S30.** Mechanism of the native reaction catalyzed by *PflTrpB*. PLP-bound intermediates are labeled with names and  $\lambda_{\text{max}}$  values (from Buller et al.),<sup>7</sup> which enable analysis by UV-vis spectroscopy. The reactive amino-acrylate intermediate (E(A-A)) can be degraded by a hydrolysis shunt pathway that forms pyruvate.

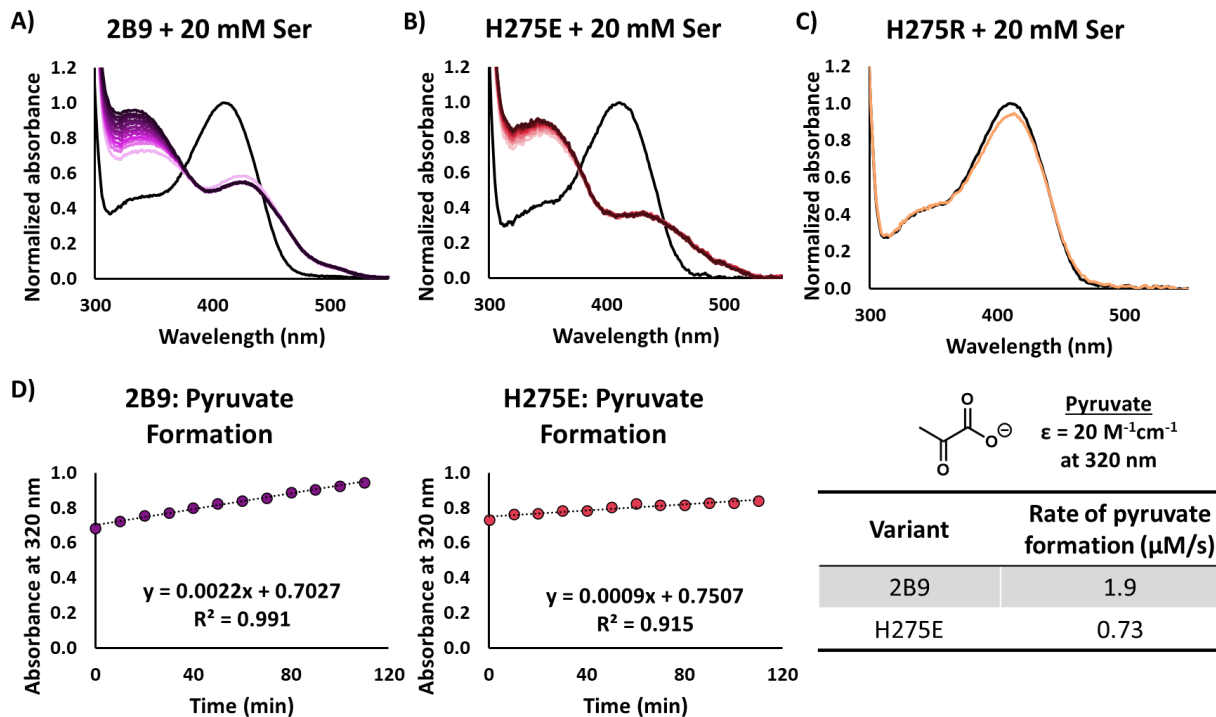


**Figure S31.** UV-vis spectral changes upon addition of L-serine (Ser) to *Pf*TrpB variants. Enzyme only (20  $\mu\text{M}$ ) spectra are shown in black. **A)** For 2B9, addition of 20 mM Ser leads to formation of both external aldimine (428 nm) and amino-acrylate (350 nm) intermediates. Over time (light to dark traces), the amino-acrylate is hydrolyzed to form pyruvate (320 nm) via a shunt reaction. **B)** For H275E, addition of 20 mM Ser leads to formation of primarily amino-acrylate (350 nm). Over time (light to dark traces), the amino-acrylate intermediate is relatively stable compared to 2B9. **C)** For H275R, addition of 20 mM Ser results in only minimal formation of external aldimine (428 nm), orange trace. **D)** Comparison of rate of formation of pyruvate by 2B9 (left) and H275E (right)

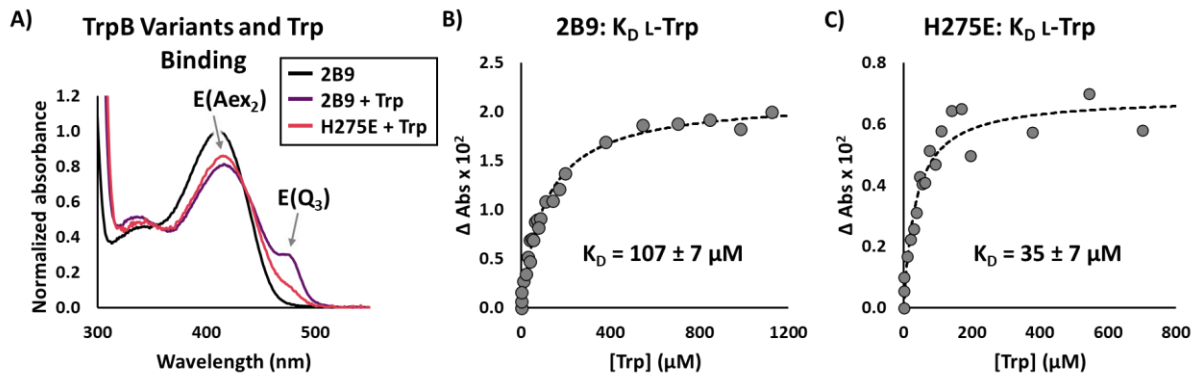


**Figure S32.** Determination of  $K_D$  of L-Trp with 2B9 and H275E. **A)** A representative enzyme only (20  $\mu\text{M}$ ) spectrum is shown in black. Addition of 1 mM Trp to 2B9 (purple trace) results in formation of both external aldimine (420 nm) and quinonoid (476 nm) intermediates. Addition of 1 mM Trp to H275E (pink trace) results primarily in formation of an external aldimine Trp adduct. **B, C)** Absorbance at 475 nm, corresponding to a Trp quinonoid intermediate, was used to determine  $K_D$  with Trp. Trp was titrated into a solution of 20  $\mu\text{M}$  enzyme, and resulting changes in absorbance were fit to a single-site binding model.

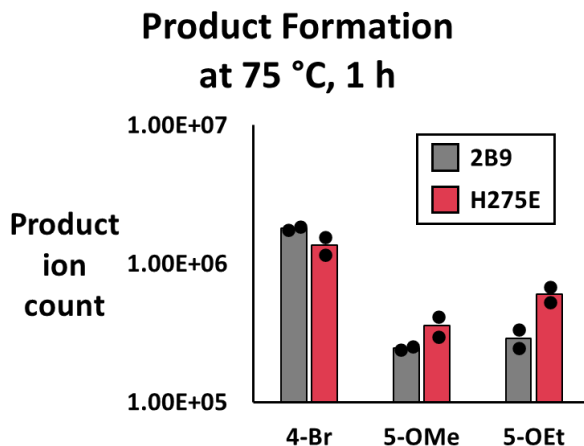


**Figure S33.** The increased activity of H275E is generally maintained at 75 °C. Enzyme activity is reported based on ion count integrations of single-ion retention (SIR) channels (log scale). Reactions consisted of 10 mM indole substrate, 30 mM Ser, and 1  $\mu\text{M}$  *Pf*TrpB in 100 mM potassium phosphate buffer (pH = 8.0) and 10% DMSO. Reactions were run in duplicate.

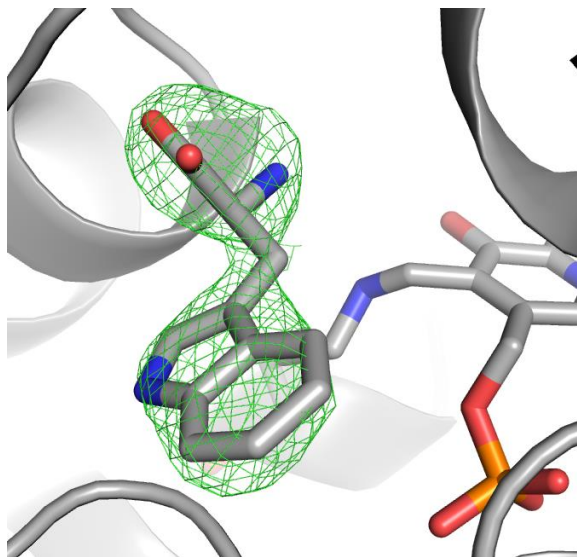


**Figure S34.** Trp binding non-covalently to H275E, Fo-Fc omit map contoured at  $3\sigma$ . PDB ID: 7ROF.

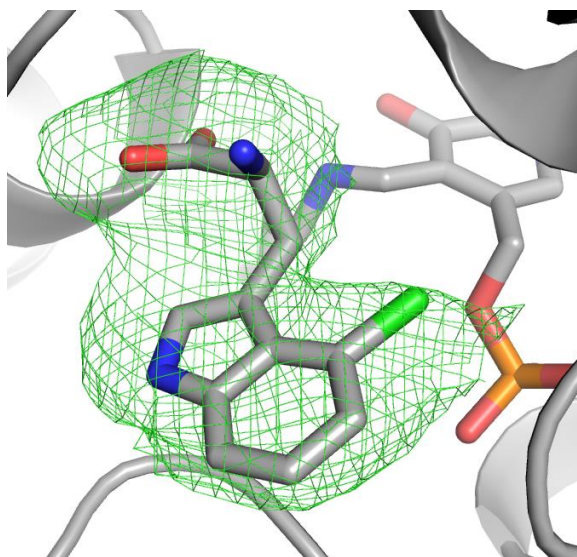


**Figure S35.** 4-Cl-Trp binding non-covalently to H275E, Fo-Fc omit map contoured at  $2\sigma$ . PDB ID: 7RNP.

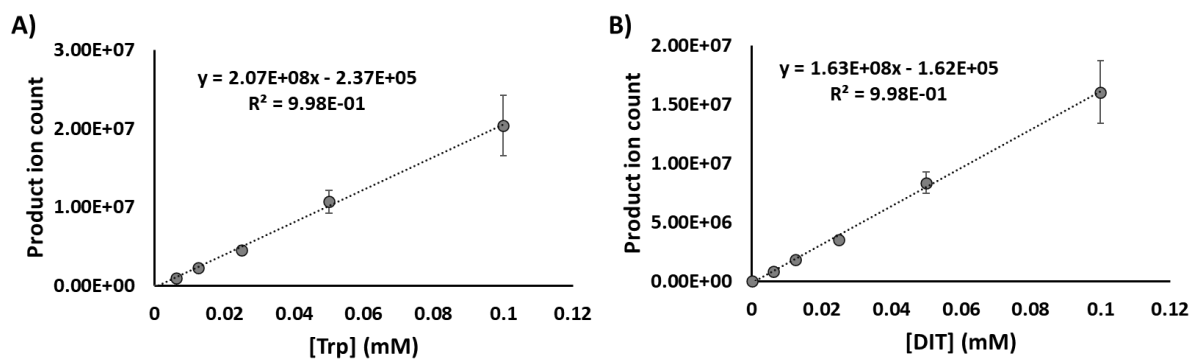


**Figure S36.** Calibration curves for quantification of L-tryptophan (Trp, **A**) and 2,3-dihydroisotryptophan (DIT, **B**) in multiplexed and single-substrate reactions (See Fig 4c).

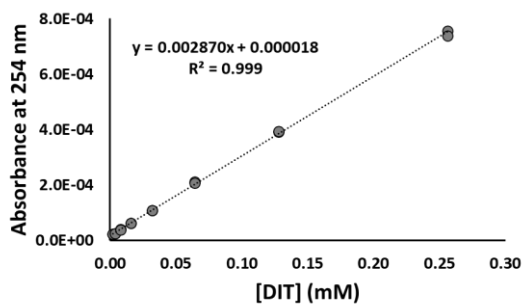


**Figure S37.** Calibration curve for quantification of 2,3-dihydroisotryptophan (DIT) to measure Michaelis-Menten parameters for conversion of indoline to DIT by *PfTrpB* variants.

## Supplemental Tables

**Table S1. *Rgn*TDC variant Michaelis-Menten kinetic data**

Substrate	Variant	$k_{\text{cat}}$ ( $\text{s}^{-1}$ )	$K_{\text{M}}$ (mM)	$k_{\text{cat}}/K_{\text{M}}$ ( $\text{M}^{-1} \text{s}^{-1}$ )
Trp	wt TDC	11 ± 1	1.6 ± 0.4	6900
	F98V	8.7 ± 1.4	2.8 ± 0.3	3100
	W349K	1.0 ± 0.1	1.4 ± 0.2	700
	L355A	0.14 ± 0.01	0.53 ± 0.45	260
	L355F	3.3 ± 0.3	0.54 ± 0.36	6200
2-Me-Trp	wt TDC	0.055 ± 0.008	2.0 ± 0.4	27
	F98V	0.042 ± 0.009	13 ± 0.3	3.3
4-Br-Trp	wt TDC	0.37 ± 0.08	3.4 ± 0.3	110
	L355A	0.82 ± 0.1	1.4 ± 0.2	590
	L355F	1.1 ± 0.1	0.7 ± 0.2	1600
5-OMe-Trp	wt TDC	0.017 ± 0.002	0.99 ± 0.48	17
	W349K	0.25 ± 0.03	1.1 ± 0.3	240
6-Cl-Trp	wt TDC	0.52 ± 0.02	0.14 ± 0.03	3700
	F98V	0.91 ± 0.06	0.60 ± 0.2	1500

**Table S2. *Rgn*TDC variant total turnover number with different substrates**

	<b>wt TDC</b>	<b>F98V</b>	<b>W349K</b>	<b>L355A</b>	<b>L355M</b>
<b>Trp</b>	<b>90,000 ± 21,000</b>	<b>210,000 ± 30,000</b>	<b>21,000 ± 3,000</b>	<b>3,000 ± 2,000</b>	<b>82,000 ± 19,000</b>
<b>7-I-Trp</b>	<b>250,000 ± 60,000</b>	<b>56,000 ± 11,000</b>	<b>19,000 ± 4,000</b>	<b>8,000 ± 900</b>	<b>160,000 ± 50,000</b>
<b>6-Cl-Trp</b>	<b>35,000 ± 9,000</b>	<b>120,000 ± 30,000</b>	<b>13,000 ± 4,000</b>	<b>1,000 ± 200</b>	<b>41,000 ± 14,000</b>
<b>6-NO<sub>2</sub>-Trp</b>	<b>10,000 ± 3,000</b>	<b>55,000 ± 15,000</b>	<b>18,000 ± 6,000</b>	<b>300 ± 100</b>	<b>14,000 ± 6,000</b>
<b>5-OMe-Trp</b>	<b>220 ± 20</b>	<b>160 ± 20</b>	<b>6,000 ± 300</b>	<b>60 ± 10</b>	<b>240 ± 20</b>
<b>5-OEt-Trp</b>	<b>90 ± 70</b>	<b>90 ± 10</b>	<b>7,000 ± 100</b>	<b>30 ± 5</b>	<b>90 ± 90</b>
<b>4-Br-Trp</b>	<b>2,200 ± 600</b>	<b>400 ± 300</b>	<b>100 ± 70</b>	<b>10,000 ± 2,000</b>	<b>20,000 ± 10,000</b>
<b>2-Me-Trp</b>	<b>1,000 ± 100</b>	<b>2,500 ± 700</b>	<b>7 ± 0</b>	<b>1,000 ± 100</b>	<b>1,000 ± 240</b>

**Table S3. X-Ray crystallographic data collection and refinement statistics**

PDB ID	7RNQ	7ROF	7RNP
Protein	<i>N</i> -His- <i>Pf</i> TrpB <sup>2B9</sup> -H275E	<i>N</i> -His- <i>Pf</i> TrpB <sup>2B9</sup> -H275E	<i>N</i> -His- <i>Pf</i> TrpB <sup>2B9</sup> -H275E
Ligand	None	Trp	4-Cl-Trp
<b>Data Collection</b>			
Space group	P2 <sub>1</sub> 2 <sub>1</sub> 2 <sub>1</sub>	P2 <sub>1</sub> 2 <sub>1</sub> 2 <sub>1</sub>	P2 <sub>1</sub> 2 <sub>1</sub> 2 <sub>1</sub>
Cell dimensions (Å)	a,b,c = 57.0, 82.7, 322.6	a,b,c = 57.4, 82.7, 322.3	a,b,c = 56.2, 81.2, 321.0
Cell angles	$\alpha = \beta = \gamma = 90^\circ$	$\alpha = \beta = \gamma = 90^\circ$	$\alpha = \beta = \gamma = 90^\circ$
Wavelength (Å)	0.97618	1.033167	1.033167
Beamline	21ID-D	23ID-B	23ID-B
Resolution (Å)	40 – 2.1	40 – 2.39	40 – 2.25
Last bin (Å)	(2.14 – 2.10)	(2.45 – 2.39)	(2.30 – 2.25)
No. observations	1,199,094 (54,391)	823,988 (62,539)	935,385 (63,013)
Completeness (%)	99.5 (93.6)	99.5 (99.5)	98.8 (98.7)
R <sub>pim</sub>	0.065 (0.684)	0.058 (1.548)	0.046 (0.825)
CC(1/2)	0.995 (0.818)	0.998 (0.488)	0.998 (0.703)
I/σI	11.7 (1.5)	8.4 (0.8)	8.8 (1.1)
Redundancy	13.4 (12.7)	13.4 (14.1)	13.4 (14.4)
<b>Refinement</b>			
Total no. of reflections	85150	58486	66413
Total no. of atoms	11732	11153	11224
TLS operators	40	40	40
Final bin (Å)	(2.16 – 2.10)	(2.45 – 2.39)	(2.31 – 2.25)
R <sub>work</sub> (%)	21.4 (32.0)	22.7 (39.4)	22.7 (38.1)
R <sub>free</sub> (%)	24.8 (36.2)	27.1 (39.7)	26.7 (39.8)
Average B factor (Å <sup>2</sup> )	45.6	72.4	63.8
Ramachandran plot Favored, %	97.6	96.4	96.7
Allowed, %	99.7	99.8	99.7
Outliers, %	0.3	0.2	0.3

Values in parenthesis are for the highest resolution shell.  $R_{\text{merge}} = \sum |I_0 - I| / \sum I_0$ , where  $I_0$  is the intensity of an individual reflection, and  $I$  is the mean intensity for multiply recorded reflections.  $R_{\text{work}} = \sum ||F_o - F_c|| / F_o$ , where  $F_o$  is an observed amplitude and  $F_c$  a calculated amplitude.  $R_{\text{free}}$  is the same statistic calculated with a 5% subset of the data that was excluded from refinement.

## Supplemental Discussion

### Introduction to substrate competition kinetics behind SUMS

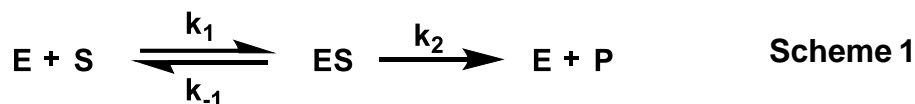
We provide here a brief discussion on the underlying kinetics for multiplexed reactions as an initial guide for understanding substrate competition kinetics in the context of SUMS for protein engineering of single-substrate activity. We note that Stanišić et al. 2019 provide an excellent discussion on substrate competition kinetics.<sup>16</sup> We also found Chou and Talalay 1977, Cornish-Bowden 1984, and Andrews 2016 to be particularly useful references.<sup>17-19</sup> While detailed understanding of substrate competition kinetics is not required to implement SUMS, we contend that considering substrate competition's impact on screening results will aid attempts to engineer synthetically useful enzymes.

#### 1. Substrate competition kinetic background

Starting from the traditional Michaelis-Menten equation (Eq. 1):

$$v_0 = \frac{k_{cat} * [E_T] * [S]}{K_M + [S]}, \quad \text{Eq S1.}$$

we use the familiar definitions  $v_0$  = initial velocity,  $[E_T]$  = total enzyme concentration,  $[S]$  = concentration of substrate, and  $K_M$  = Michaelis-Menten constant. For a unimolecular, irreversible reaction (Scheme 1), if  $k_2 \ll k_1, k_{-1}$ , we can approximate  $k_{cat} = k_2$ .

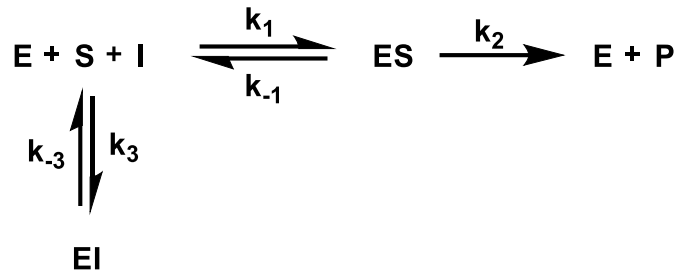


In this simplified model,  $K_M$  can be approximated as a function of the rate constants involved in the formation/breakdown of the ES complex:

$$K_M = \frac{k_{-1} + k_2}{k_1} \quad \text{Eq S2.}$$

In the case of single substrate reactions where  $[S] \gg K_M$ , the term  $k_{cat} * [E_T] = V_{max}$  becomes the main determinant in the rate of product formation. We show below that this familiar kinetic phenomenon no longer holds for reactions where multiple substrates are present.

We found it instructive to consider substrate competition through the lens of competitive inhibition. A competitive inhibitor decreases overall enzymatic activity by binding in the enzyme active site, decreasing the availability of enzyme active sites that can catalyze the given transformation on substrate S (Scheme 2).



**Scheme 2**

The impact of inhibitor *I* with an inhibition constant *K<sub>I</sub>* on the rate of an enzymatic reaction can be calculated as:

$$v_0 = \frac{k_{cat} * [E_T] * [S]}{K_M \left(1 + \frac{[I]}{[K_I]}\right) + [S]}$$

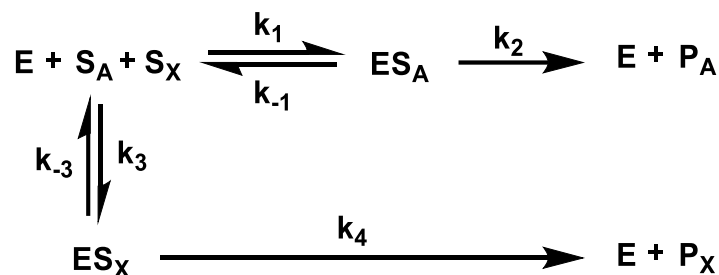
**Eq S3.**

where:

$$K_I = \frac{k_{-3}}{k_3}.$$

**Eq S4.**

In a multiplexed reaction, substrates will mutually inhibit each another by competing for active site binding in a fashion analogous to competitive inhibition. Given the simple model below of *S<sub>A</sub>* and *S<sub>X</sub>* competing to form products *P<sub>A</sub>* and *P<sub>X</sub>* (Scheme 3), respectively, the additional rate constant *k<sub>4</sub>* for the formation of *P<sub>X</sub>* is the only distinction between this model and the previous competitive inhibition model (Scheme 2).



**Scheme 3**

*S<sub>X</sub>* becomes a classical competitive inhibitor when *k<sub>4</sub>* = 0, where *K<sub>MX</sub>* = *K<sub>I</sub>*. This means *K<sub>MX</sub>* can be defined as the Michaelis-Menten constant for a given *S<sub>X</sub>* and describes the inhibition of *S<sub>X</sub>* on *S<sub>A</sub>*, as shown in Equation S5.

$$v_{A0} = \frac{k_{catA} * [E_T] * [S_A]}{K_{MA} \left(1 + \frac{[S_X]}{[K_{MX}]}\right) + [S_A]}$$

**Eq S5.**

Therefore, for any given number of additional substrates, the initial velocity of formation of *P<sub>A</sub>* can be described as:

$$v_{A0} = \frac{k_{catA} * [E_T] * [S_A]}{K_{MA} \left( 1 + \frac{[S_B]}{[K_{MB}]} + \dots + \frac{[S_Z]}{[K_{MZ}]} \right) + [S_A]} \quad \text{Eq S6.}$$

where the sum of the ratios of  $[S_X]$  and  $K_{MX}$  models the present substrate competition and inhibition in a substrate multiplexed reaction. Therefore, even when  $[S_X] \gg K_{MX}$  for all substrates, substrate  $K_M$ 's still have a significant impact on relative product distribution.

## 2. Supporting data for substrate competition kinetic model

Many synthetic applications of enzymes use single-substrate conditions. In the context of single-substrate reactions with high substrate concentrations,  $k_{cat}$  is an excellent predictor of relative activity, as measured by observed total turnover numbers for different chlorinated tryptophan analogs (Fig S38A, data from reference<sup>1</sup>). Catalytic efficiency,  $k_{cat}/K_M$ , is a less useful predictor of single-substrate activity (Fig S38B).

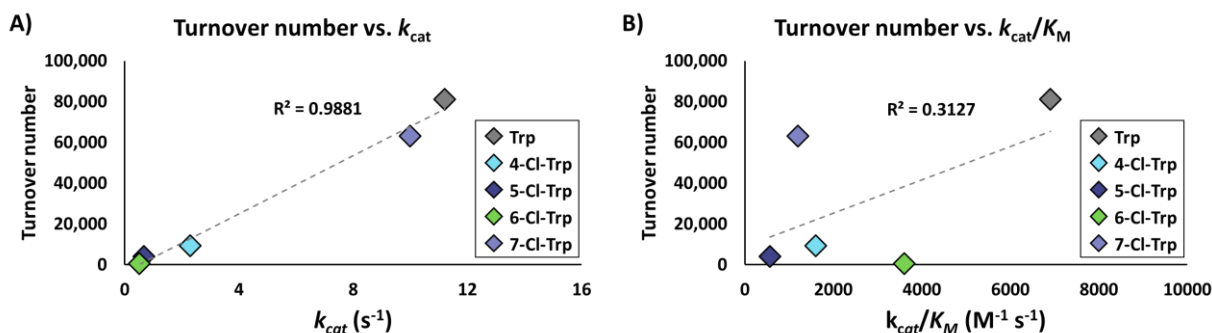


**Figure S38.** Comparison of single-substrate activity correlation with **A)**  $k_{cat}$  or **B)**  $k_{cat}/K_M$ . Turnover numbers and Michaelis-Menten parameters from McDonald et al. 2019.<sup>1</sup>

Conversely, in a reaction where substrates compete for an enzyme active site, the ratio of  $k_{cat}/K_M$  can be used to predict relative product abundance. From an example three-substrate multiplexed reaction of *RgnTDC*, we show that the relative ratios of the three products do not correlate well to the substrates' relative  $k_{cat}$ 's (Fig S39A) but correlate very well with substrate  $k_{cat}/K_M$ 's, as determined from single-substrate kinetic measurements (Fig S39B).

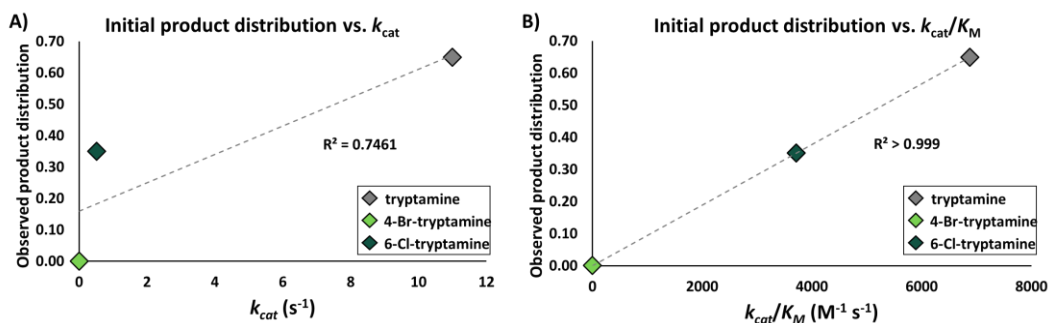


**Figure S39.** Observed product percentage from a multiplexed reaction correlated with **A)**  $k_{cat}$  or **B)**  $k_{cat}/K_M$ . (1  $\mu$ M *Rgn*TDC, 10  $\mu$ M pyridoxal phosphate, 5 mM each substrate: Trp, 6-Cl-Trp, 4-Br-Trp, 5 min @ 37 °C. Michaelis-Menten parameters from McDonald et al. 2019 and Table S1.<sup>1</sup>

### 3. Suppression of inhibition

During library screening, some variants may acquire mutations that increase the abundance of one or more products. Several distinct kinetic scenarios can provide this outcome. In the simplest case, the mutations may increase the  $k_{cat}$  with a substrate, leading to more product formed. Alternatively, mutations may leave  $k_{cat}$  minimally changed but selectively decrease the  $K_M$  with a substrate, making it a more effective competitive inhibitor in a multiplexed setting and leading to increased occupancy of the available active sites. Both kinetic changes provide a classically activated enzyme, where mutation increases the catalytic efficiency,  $k_{cat}/K_M$ .

However, there is an alternative scenario that may arise in substrate multiplexed settings where a product increases in abundance, but there is either no change or a *decrease* in the catalytic efficiency of the enzyme. This phenomenon arises when two (or more) substrates in competition react with significantly different catalytic efficiencies. As has been described above, the substrate with the higher catalytic efficiency will dominate the enzyme active site. If a mutation decreases the catalytic efficiency for both substrates but is much more deleterious with the originally preferred substrate, then the occupancy of the active site in competition will shift relative to the parent enzyme to favor the less-reactive substrate. *In effect, the ability of a ‘good’ substrate to inhibit reaction with ‘bad’ substrates is diminished.* Consequently, the amount of product formed from less-reactive substrates can actually increase, despite a decrease in the catalytic efficiency with which they are formed. We describe this phenomenon as activation through “suppression of inhibition.” Notably, the apparent increases in activity caused by suppression of inhibition do not translate to single substrate conditions. These changes are reproducible, and not an indication of wild errors or mysterious effects in the screening process.

To illustrate this subtle concept, we have generated a hypothetical scenario in Fig S40. The hypothetical parent enzyme strongly favors formation of product B in a multiplexed setting. For variant 1, the  $K_M$  for substrate B has increased 100-fold,

suppressing its ability to inhibit substrate A. Consequently, variant 1 produces far more product A than the parent enzyme in the multiplexed assay, as determined by the relative  $k_{cat}/K_M$  values for each substrate-enzyme pair. However, parent and variant 1 would form product A at the same rate in a single-substrate reaction, since both enzymes have the same  $k_{cat}$  and  $K_M$  for substrate A.

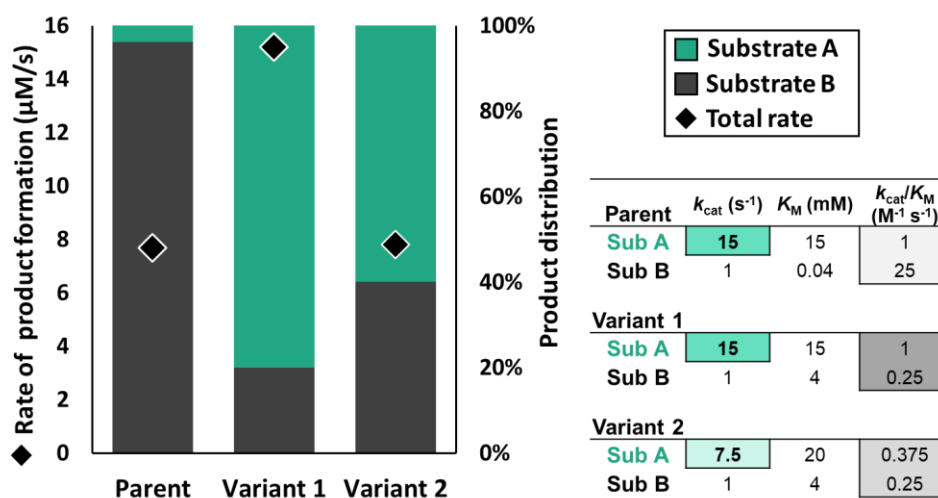


**Figure S40.** Simulation of suppression of inhibition for a parent enzyme and two hypothetical variants with given kinetic parameters (left). Simulation conditions were as follows: 3.3 mM each substrate and 7.5  $\mu$ M enzyme. Relative bar heights represent rates of initial product formation as calculated by Equation S6. Simulated kinetic parameters are shown in the table (right). Product ratios in competition are governed by the ratio of the substrates'  $k_{cat}/K_M$ , and relative activity in single-substrate reactions is determined by  $k_{cat}$ .

In the more sophisticated case of variant 2, the  $K_M$  for substrate B has again increased 100-fold, suppressing its ability to inhibit substrate A. Along with this change, we considered a decrease in  $k_{cat}$  and increase in  $K_M$  for substrate A. In the multiplexed assay, variant 2 will generate more product from substrate A. However, single-substrate reactions will reveal that variant 2 actually has *decreased* catalytic efficiency with substrate A relative to parent. At first glance, single-substrate and multiplexed results may appear to contradict one another, but we contend through the examples shown here that the suppression of inhibition phenotype can be rationalized using standard kinetic analysis.

We have not yet determined a simple means for predicting whether improvements in activity identified by SUMS are due to an increase in catalytic efficiency or merely suppression of inhibition. However, this scenario arises when screening on substrates that have significant differences in their relative reactivity. During the assay design phase of SUMS (detailed below), one can choose substrates with similar reactivity to limit the impact of the suppression of inhibition phenomenon. Regardless, validation of potential hits is a core step in protein engineering that can untangle details of the mutational impact.

For context, a similar validation step is also necessary when screening libraries using single substrates. In the case of both single-substrate and multiplexed assays, sometimes promising variants identified in screening do not validate as hits with improved catalytic activity.

While activation through suppression of inhibition may be undesirable in the short term, this information may still provide value. As we describe in the main text, such data indicate that a mutation is influencing the active site of the enzyme. This information can be leveraged for non-classical steps in directed evolution, targeting these residues for additional mutagenesis to potentially lead to truly activating mutations.

## Guide to optimization of substrate multiplexed screening (SUMS) method

We provide here a discussion on possible optimization routes for fine-tuning a substrate multiplexed screen. We acknowledge there are additional options for optimization but will highlight ones we felt had the greatest impact on our development of SUMS for protein engineering for single-substrate activity.

### 1. Choice of substrates

While there is no “right” or “wrong” panel of substrates, the substrates chosen for SUMS will directly impact the information gained from screening. This list is not intended to be comprehensive, and any substrate panels should be tested with parent enzyme to confirm that all desired products can be resolved as anticipated.

#### a. Number of substrates

Any number of substrates can be added to a multiplexed substrate mixture. We chose <10 substrates for the reported screens for simplicity and to ease interpretation of the data. Additional substrates may be considered according to the time constraints of the researcher, the degree of mutual substrate inhibition with the selected substrates, and any potential instrumental limitations.

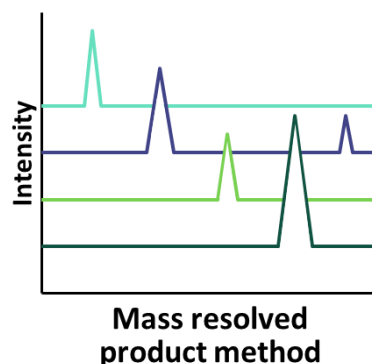


**Figure S41.** SUMS output example with five substrates at four unique masses.

b. *Substrate/product masses*

The implementation of SUMS described here leveraged MS-based peak integration to quantitate distinct products. Although chromatographic resolution of products of the same mass could work in a SUMS setting, we chose substrates that will yield products with unique m/z's (Fig S41).

c. *Relative substrate activity*

Since highly active substrates can inhibit the formation of products from less active substrates, the addition of both highly active and inactive substrates to a substrate mixture may decrease the amount of information obtained from a screen. *In principle, a SUMS setup will have maximum sensitivity when each of the substrates is a relatively poor substrate for the native enzyme, such that none is a good competitive inhibitor and there is a large potential dynamic range of improved activities.* However, differences in baseline activity do not prevent successful application of SUMS. Substrates with which the parent enzyme has no detectable activity can be added to the screening mixture to monitor for variants that gain new activity. The presence of more reactive substrates may obscure low levels of activity that arise, but modulation of relative substrate concentrations can account for differences in activities.

## 2. Screening time

For a single-substrate screen to be sensitive to improvements in activity, the parent enzyme must not reach full conversion of substrate to product. However, in a multiplexed screen, the reaction rate for different substrates may vary greatly. It is possible that some substrates may reach high or even full conversion while others may show only trace activity. One may thus choose conditions under which all desired products are observed, possibly resulting in full consumption of certain substrates. As reactions depart the initial velocity regime, the relative product ratios will shift away from the ratios of substrates'  $k_{cat}/K_M$  values, as shown in Fig S42A. We therefore describe the distribution of products as the *SUMS promiscuity profile* rather than a specificity profile, since relative rates of product formation are not necessarily assessed. In this way, the screen can identify variants that both retain existing activity and improve activity on poor substrates.

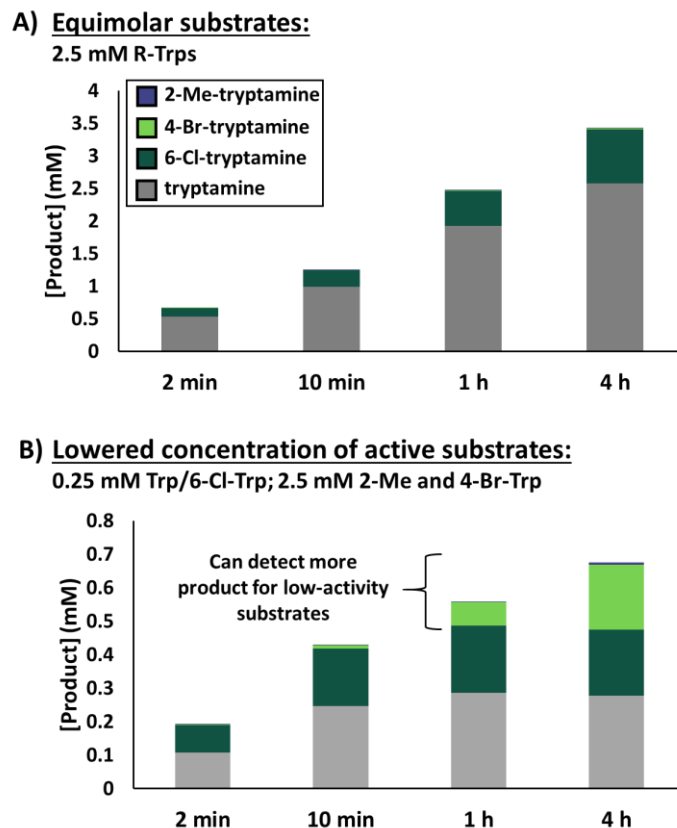


**Figure S42.** Timecourse of a substrate multiplexed reaction of wild-type *RgnTDC* with 2-methyltryptophan, 4-bromotryptophan, 6-chlorotryptophan, and tryptophan. Reactions run in triplicate, and graphed data indicates the average [product] between replicates. **A)** 2.5 mM each R-Trp, 0.25  $\mu$ M TDC **B)** 2.5 mM 2-Me-Trp and 4-Br-Trp, 0.25 mM Trp and 6-Cl-Trp, 0.25  $\mu$ M TDC.

### 3. Relative substrate concentrations

#### a. Unimolecular reactions

To help offset the impact of mutual substrate inhibition, the relative concentrations of the various substrates can be adjusted. As shown in Fig S42B, the inhibitory capacity of highly reactive substrates can be reduced by decreasing their concentration. Such an approach increases the abundance of poorer products (Fig S42B, ~10-fold increase in total product formed for 4-Br-Trp and 2-Me-Trp) while maintaining an activity threshold for the substrates with high baseline activity.

### b. Higher order reactions

For enzymes that catalyze bimolecular and higher order reactions, early timepoint product distributions can be 'captured' by limiting the stoichiometry of a non-multiplexed substrate (Knorrscheidt et al. 2021 describe such an approach with limiting concentrations of H<sub>2</sub>O<sub>2</sub> for their peroxygenase reactions.<sup>20</sup>) Due to the bimolecular nature of TrpB's reaction, a limiting amount of L-serine can be utilized to ensure that tryptophan production stalls with respect to indole consumption. In this way, reaction time and catalyst loading optimization is greatly simplified.

## Synthetic Methods: Tryptophan analog biosynthesis and purification

For each tryptophan analog, the corresponding indole derivative (~1 mmol) was added to a 100 mL pressure flask and dissolved in MeOH (5 mL). L-Serine (3 mmol) was added, and the resulting solution was diluted to just under 100 mL with 50 mM potassium phosphate buffer (pH = 8.0). PLP was added such that the final concentration was 300  $\mu$ M. Then, 2B9 was added at 0.1% mol catalyst relative to the indole analog. The solution was incubated at 75 °C for 16 h. Following UPLC-MS analysis of conversion, the solution was heat-treated at 90 °C for 30 min. Solutions were evaporated down to 10 mL, filtered, and run over C18 via flash chromatography with H<sub>2</sub>O/MeOH. Tryptophan products typically eluted between 10-35% MeOH. Product-containing fractions were combined and evaporated down to ~2-3 mL, where the solutions were transferred to pre-tared flasks, evaporated to dryness, resuspended in H<sub>2</sub>O, flash-frozen, and lyophilized for 24 – 48 h. Resulting powders were weighed and submitted for <sup>1</sup>H-NMR analysis, with final reported yields taking hydration states into account (*all tryptophan analog products were isolated as hydrates*).

### 2-methyltryptophan

2-methyltryptophan was isolated as an off-white powder (81.8 mg) in 94% yield. <sup>1</sup>H NMR (500 MHz, MeOD)  $\delta$  7.64 – 7.58 (m, 1H), 7.31 – 7.25 (m, 1H), 7.06 (td,  $J$  = 7.1, 1.4 Hz, 1H), 7.02 (td,  $J$  = 7.5, 1.3 Hz, 1H), 3.86 (dd,  $J$  = 9.9, 4.2 Hz, 1H), 3.52 – 3.46 (m, 1H), 3.08 (dd,  $J$  = 15.2, 10.0 Hz, 1H), 2.44 (s, 3H). Spectrum matched previously reported spectra.<sup>9</sup>

### 2-methyl-5-methoxytryptophan

2-methyl-5-methoxytryptophan was isolated as a tan powder (164 mg) in 66% yield. <sup>1</sup>H NMR (500 MHz, MeOD)  $\delta$  7.18 (d,  $J$  = 2.4 Hz, 1H), 7.15 (d,  $J$  = 8.6 Hz, 1H), 6.69 (dd,  $J$  = 8.7, 2.4 Hz, 1H), 3.85 (s, 3H), 3.76 (dd,  $J$  = 9.8, 4.2 Hz, 1H), 3.38 (dd,  $J$  = 15.0, 4.2 Hz, 1H), 2.97 (dd,  $J$  = 14.9, 9.8 Hz, 1H), 2.41 (s, 3H). <sup>13</sup>C NMR (126 MHz, MeOD)  $\delta$  174.08,

153.91, 134.36, 131.06, 128.63, 110.68, 110.27, 104.24, 99.64, 55.86, 54.99, 26.93, 10.18.

**MS/ESI** m/z for [M-H]<sup>-</sup>; C<sub>13</sub>H<sub>16</sub>N<sub>2</sub>O<sub>3</sub>; calculated 247.10882, observed 247.1087.

#### **4-bromotryptophan**

4-bromotryptophan was isolated as a white powder (66.9 mg) in 59% yield. <sup>1</sup>H NMR (500 MHz, MeOD) δ 7.38 (d, 1H), 7.28 (s, 1H), 7.23 (d, *J* = 7.4 Hz, 1H), 7.00 (t, *J* = 7.9 Hz, 1H), 4.07 (dd, *J* = 10.3, 4.6 Hz, 1H), 3.98 (dd, *J* = 15.1, 4.6 Hz, 1H), 3.13 (dd, *J* = 15.1, 10.3 Hz, 1H). Spectrum matched previously reported spectra.<sup>21</sup>

#### **5-acetyltryptophan**

5-acetyltryptophan was isolated as a white powder (162 mg) in 42% yield. <sup>1</sup>H NMR (500 MHz, MeOD) δ 8.54 (d, *J* = 1.6 Hz, 1H), 7.85 (dd, *J* = 8.6, 1.7 Hz, 1H), 7.44 (d, *J* = 8.6 Hz, 1H), 7.32 (s, 1H), 3.87 (dd, *J* = 8.7, 4.3 Hz, 1H), 3.54 (dd, *J* = 15.1, 4.3 Hz, 1H), 3.24 (dd, *J* = 15.2, 8.7 Hz, 1H), 2.71 (s, 3H). <sup>13</sup>C NMR (126 MHz, D<sub>2</sub>O) δ 204.10, 174.67, 139.52, 128.34, 126.68, 126.36, 121.99, 121.84, 111.81, 109.80, 55.11, 26.35, 26.09.

**MS/ESI** m/z for [M-H]<sup>-</sup>; C<sub>13</sub>H<sub>14</sub>N<sub>2</sub>O<sub>3</sub>; calculated 245.0932, observed 245.0930.

#### **5-carboxamidotryptophan**

5-carboxamidotryptophan was isolated as a white powder (163 mg) in 52% yield. <sup>1</sup>H NMR (500 MHz, MeOD) δ 8.32 (dd, 1H), 7.74 (dd, *J* = 8.6, 1.7 Hz, 1H), 7.44 (dd, *J* = 8.6, 0.7 Hz, 1H), 7.31 (s, 1H), 3.88 (dd, *J* = 9.1, 4.0 Hz, 1H), 3.55 (ddd, *J* = 15.1, 4.1, 1.0 Hz, 1H), 3.19 (dd, *J* = 15.3, 9.1 Hz, 1H). Spectrum matched previously reported spectra.<sup>21</sup>

#### **5-ethoxytryptophan**

5-ethoxytryptophan was isolated as a white powder (82.7 mg) in 59% yield. <sup>1</sup>H NMR (500 MHz, MeOD) δ 7.26 (d, *J* = 5.3 Hz, 1H), 7.25 (s, 1H), 7.17 (s, 1H), 6.79 (dd, *J* = 8.9, 2.2 Hz, 1H), 4.15 – 4.06 (m, 2H), 3.84 (dd, *J* = 9.3, 4.1 Hz, 1H), 3.14 – 3.05 (m, 1H), 1.42 (t, *J* = 6.9 Hz, 4H). <sup>13</sup>C NMR (126 MHz, D<sub>2</sub>O) δ 151.88, 131.88, 127.20, 125.80, 112.78, 112.57, 108.23, 102.41, 65.51, 55.32, 27.44, 14.11.

**MS/ESI** m/z for [M-H]<sup>-</sup>; C<sub>13</sub>H<sub>16</sub>N<sub>2</sub>O<sub>3</sub>; calculated 247.10882, observed 247.1087.

#### **5-methoxytryptophan**

5-methoxytryptophan was isolated as a brown powder (556 mg) in 48% yield. <sup>1</sup>H NMR (500 MHz, MeOD) δ 7.27 (d, *J* = 3.3 Hz, 1H), 7.25 (d, *J* = 2.8 Hz, 1H), 7.17 (s, 1H), 6.79 (dd, *J* = 8.8, 2.4 Hz, 1H), 3.87 (s, 3H), 3.85 (ddd, *J* = 9.5, 3.9, 1.9 Hz, 1H), 3.52 – 3.46 (m, 1H), 3.11 (dd, *J* = 15.2, 9.6 Hz, 1H). Spectrum matched previously reported spectra.<sup>22</sup>

#### **6-chlorotryptophan**

6-chlorotryptophan was isolated as a white powder (63.8 mg) in 67% yield. <sup>1</sup>H NMR (500 MHz, MeOD) δ 7.68 (d, *J* = 8.5 Hz, 1H), 7.38 (d, *J* = 1.9 Hz, 1H), 7.23 (s, 1H), 7.04 (dd,

1H), 3.83 (ddd,  $J = 9.4, 5.6, 4.2$  Hz, 1H), 3.47 (dd,  $J = 15.2, 4.2$  Hz, 1H), 3.15 (dd, 1H). Spectrum matched previously reported spectra.<sup>21</sup>

### 6-nitrotryptophan

6-nitrotryptophan was isolated as a yellow powder (245 mg) in 98% yield. <sup>1</sup>H NMR (500 MHz, MeOD)  $\delta$  8.36 (d,  $J = 2.0$  Hz, 1H), 7.98 (dd,  $J = 8.8, 2.1$  Hz, 1H), 7.86 (d,  $J = 8.8$  Hz, 1H), 7.57 (s, 1H), 3.79 (dd,  $J = 8.2, 4.6$  Hz, 1H), 3.47 – 3.41 (m, 1H), 3.26 – 3.19 (m, 1H). Spectrum matched previously reported spectra.<sup>21</sup>

### 7-iodotryptophan

7-iodotryptophan was isolated as a white powder (94.3 mg) in 79% yield. <sup>1</sup>H NMR (500 MHz, MeOD)  $\delta$  7.75 (dd,  $J = 7.9, 0.9$  Hz, 1H), 7.54 (d,  $J = 7.4$  Hz, 1H), 7.30 (s, 1H), 6.88 (t,  $J = 7.7$  Hz, 1H), 3.86 (dd,  $J = 9.1, 4.2$  Hz, 1H), 3.50 (dd, 1H), 3.16 (dd, 1H). Spectrum matched previously reported spectra.<sup>21</sup>

## Cascade synthesis and isolation of tryptamines

4-6 mmol (1.4 mmol for 6-chloroindole) of the corresponding indole analog was added to a 1 L Erlenmeyer flask and dissolved in 20 mL MeOH. 12 mmol serine was added, and the resulting solution was diluted up to just under 500 mL with 50 mM potassium phosphate buffer pH = 8.0. PLP was added such that the final concentration was 300  $\mu$ M. Then, H275E was added at 0.05% mol catalyst relative to the indole analog. The solution was incubated at 75 °C for 16 h. (H275E was found to be activating at 75 °C, Fig S33). Following UPLC-MS analysis of conversion, the solution was cooled to 37 °C, upon which *RgnTDC* was added at 0.02 – 0.2% mol catalyst relative to the indole. The solutions were incubated at 37 °C for 24 h. Solutions were then evaporated down to 50 – 100 mL. To break emulsions, the solutions were acidified with 6 M HCl until pH < 1, 100 mL ethyl acetate (EtOAc) was added, and the resulting mixtures were centrifuged at 4000 x g for 10 min. These solutions were added to a separatory funnel, the aqueous layer was drained, and the organic layer removed. This was repeated twice more, with 2 mL 6 M HCl added in between extractions. Then, the aqueous layer was alkalized with 6 M NaOH until pH > 12.\* Tryptamine products were then extracted 3x with 150 mL EtOAc, with 2 mL 6 M NaOH added in between extractions to the aqueous layer. Organic layers were pooled, dried with sodium sulfate, filtered, and evaporated down to 5-10 mL. Solutions were transferred to 20 mL scintillation vials, evaporated to near dryness (tryptamines were observed as liquids at 50 °C), and dried under vacuum overnight. Dried samples were weighed and submitted for <sup>1</sup>H and <sup>13</sup>C NMR analysis.

### **\*6-nitrotryptamine purification**

Purification was carried out as described above until the solution was basified. The bright yellow solution was turned bright red upon addition of NaOH, and a yellow precipitate was observed. The precipitate was found to be insoluble in both diethyl ether and EtOAc and was filtered from both the aqueous and organic layers. Upon washing with cold water and diethyl ether, a yellow solid was obtained. The remaining aqueous solution was extracted 3x with diethyl ether, resulting in a pale-yellow organic layer. The organic extraction was evaporated dry, and the resulting yellow solid was combined with the filtered solid via resuspension in water. The resuspension was flash frozen and lyophilization was carried out to remove water. Over the freeze-drying process, the bright yellow powder turned a brownish color, which after two weeks reverted to the yellow color.

### **2-methyltryptamine**

F98V *RgnTDC* was used as 0.2% mol catalyst for the reaction with 2-methylindole. 2-methyltryptamine was isolated as a reddish oil (166 mg) in 19% yield. <sup>1</sup>H NMR (500 MHz, DMSO) δ 7.40 (dd, *J* = 7.6, 1.1 Hz, 1H), 7.22 (dt, *J* = 8.0, 1.0 Hz, 1H), 7.00 – 6.86 (m, 2H), 2.75 – 2.67 (m, 4H), 2.33 (s, 3H), 2.00 (s, 1H). Spectrum matched previously reported spectra.<sup>1</sup>

### **4-bromotryptamine**

L355M *RgnTDC* was used as 0.02% mol catalyst for the reaction with 4-bromoindole. 4-bromotryptamine was isolated as a light pink solid (995 mg) in 79% yield. <sup>1</sup>H NMR (500 MHz, DMSO) δ 11.16 (s, 1H), 7.36 (dd, *J* = 8.1, 0.9 Hz, 1H), 7.23 (s, 1H), 7.15 (dd, *J* = 7.5, 0.9 Hz, 1H), 6.95 (t, *J* = 7.8 Hz, 1H), 2.97 (dd, 2H), 2.84 (dd, *J* = 7.9, 6.5 Hz, 2H), 1.42 (s, 2H). Spectrum matched previously reported spectra.<sup>1</sup>

### **5-ethoxytryptamine**

W349K *RgnTDC* was used as 0.02% mol catalyst for the reaction with 5-ethoxyindole. 5-ethoxytryptamine was isolated as a tan solid (353 mg) in 27% yield. <sup>1</sup>H NMR (500 MHz, DMSO) δ 10.59 (s, 1H), 7.21 (d, *J* = 8.7 Hz, 1H), 7.07 (d, *J* = 2.3 Hz, 1H), 6.98 (d, *J* = 2.4 Hz, 1H), 6.70 (dd, *J* = 8.7, 2.4 Hz, 1H), 4.01 (q, *J* = 6.9 Hz, 2H), 2.80 (t, *J* = 6.9 Hz, 2H), 2.71 (t, *J* = 7.1 Hz, 2H), 1.42 (s, 2H), 1.34 (t, *J* = 7.0 Hz, 3H). <sup>13</sup>C NMR (126 MHz, DMSO) δ 152.49, 131.92, 128.15, 123.71, 112.81, 112.34, 111.86, 101.75, 63.84, 43.16, 30.08, 15.42.

**MS/ESI** m/z for [M+H]<sup>+</sup>; C<sub>12</sub>H<sub>16</sub>N<sub>2</sub>O; calculated 205.1335, observed 205.1333.

### **5-methoxytryptamine**

W349K *RgnTDC* was used as 0.02% mol catalyst for the reaction with 5-methoxyindole. 5-methoxytryptamine was isolated as a dark brown solid (387 mg) in 30% yield, which co-purified with 70 mg 5-methoxytryptophan. <sup>1</sup>H NMR (500 MHz, DMSO) δ 10.60 (s, 1H), 7.22 (d, *J* = 8.7 Hz, 1H), 7.08 (d, *J* = 2.4 Hz, 1H), 6.99 (d, *J* = 2.4 Hz, 1H), 6.71 (dd, *J* =

8.7, 2.5 Hz, 1H), 3.76 (s, 3H), 2.81 (t,  $J = 7.2$  Hz, 2H), 2.72 (t,  $J = 7.1$  Hz, 2H), 1.68 (s, 2H). Spectrum matched previously reported spectra.<sup>1</sup>

### **6-chlorotryptamine**

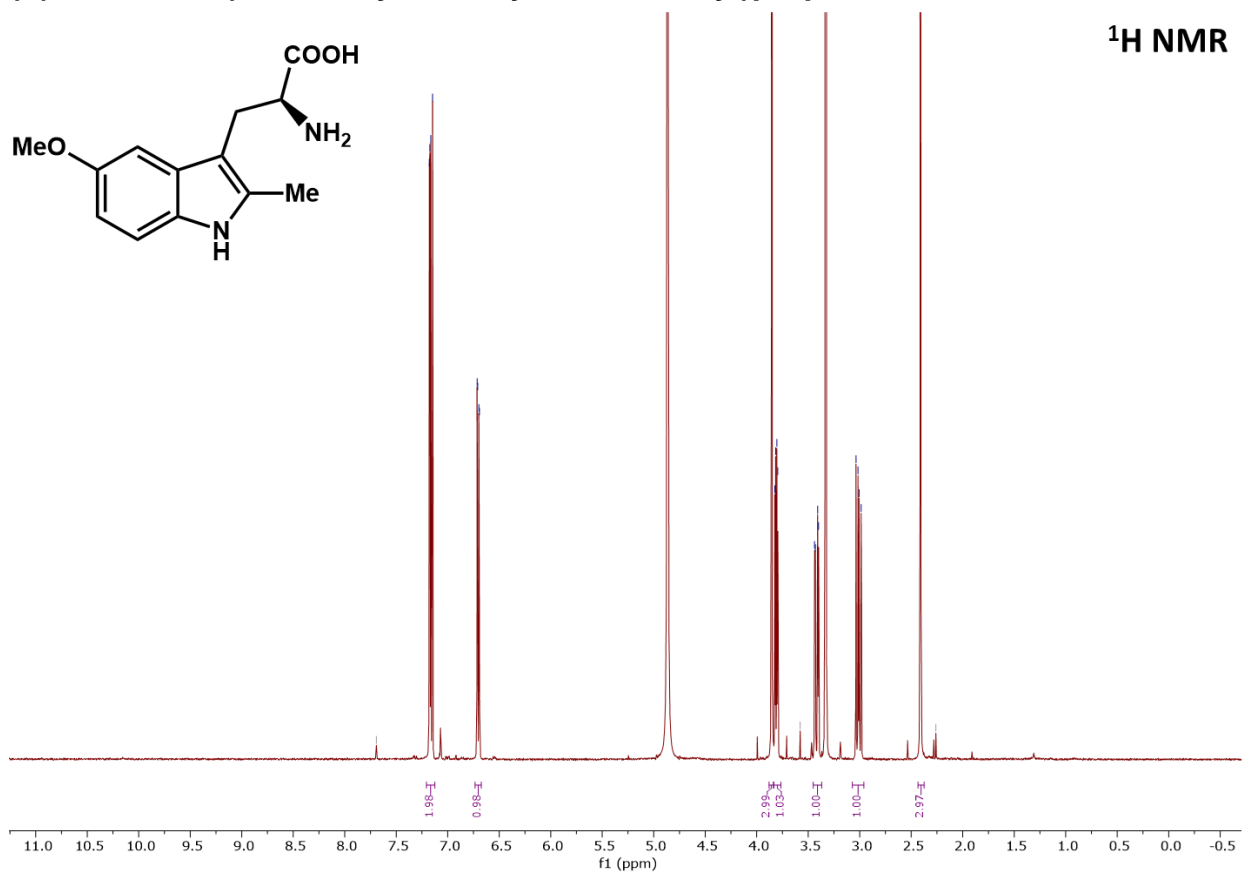
F98V *RgnTDC* was used as 0.02% mol catalyst for the reaction with 6-chloroindole. 6-chlorotryptamine was isolated as an off-white solid (144 mg) in 50% yield. <sup>1</sup>H NMR (500 MHz, DMSO)  $\delta$  10.97 (s, 1H), 7.52 (d,  $J = 8.4$  Hz, 1H), 7.37 (d,  $J = 1.9$  Hz, 1H), 7.19 (d,  $J = 2.2$  Hz, 1H), 6.98 (dd,  $J = 8.4, 1.9$  Hz, 1H), 2.84 (t,  $J = 14.5$  Hz, 2H), 2.77 (t,  $J = 7.1$  Hz, 2H), 1.85 (s, 3H). Spectrum matched previously reported spectra.<sup>1</sup>

### **6-nitrotryptamine**

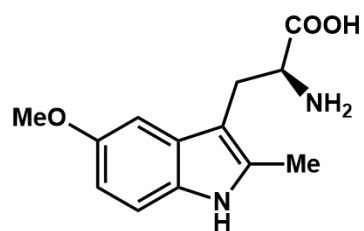
F98V *RgnTDC* was used as 0.02% mol catalyst for the reaction with 6-nitroindole. 6-nitrotryptamine was isolated as an initially brown powder (after 2 weeks became yellow) (495.5 mg) in 47% yield. Interestingly, this product produces a deep red color when dissolved in solution, which seems to be indicative of the amine group being deprotonated. <sup>1</sup>H NMR (500 MHz, ACN)  $\delta$  8.32 (d,  $J = 2.2$  Hz, 1H), 7.81 (dd,  $J = 8.8, 2.1$  Hz, 1H), 7.57 (d,  $J = 8.8$  Hz, 1H), 7.52 (s, 1H), 2.90 – 2.82 (m, 4H). Spectrum matched previously reported spectra.<sup>1</sup>

## NMR spectra

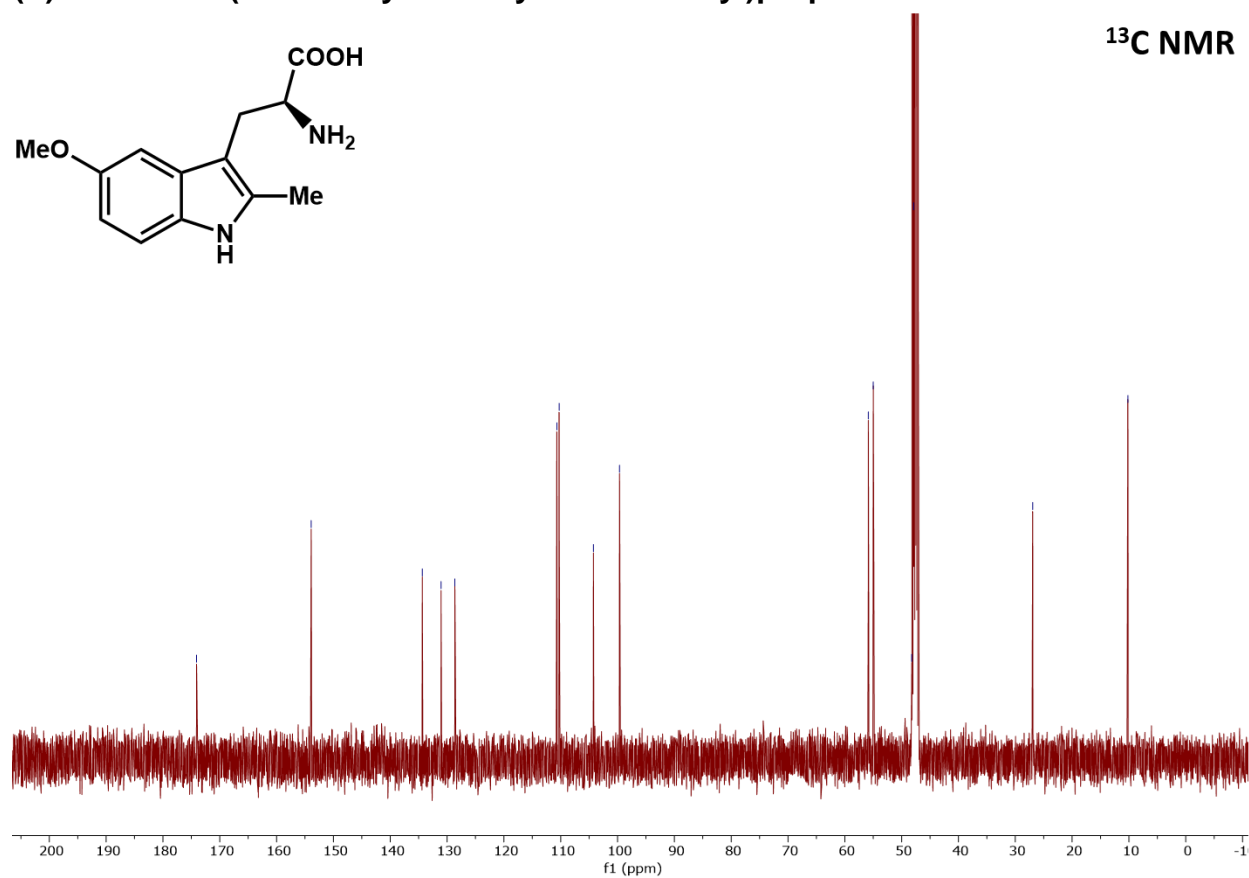
### (S)-2-amino-3-(5-methoxy-2-methyl-1H-indol-3-yl)propanoic acid



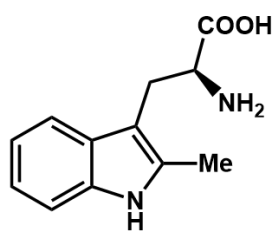
**(S)-2-amino-3-(5-methoxy-2-methyl-1H-indol-3-yl)propanoic acid**



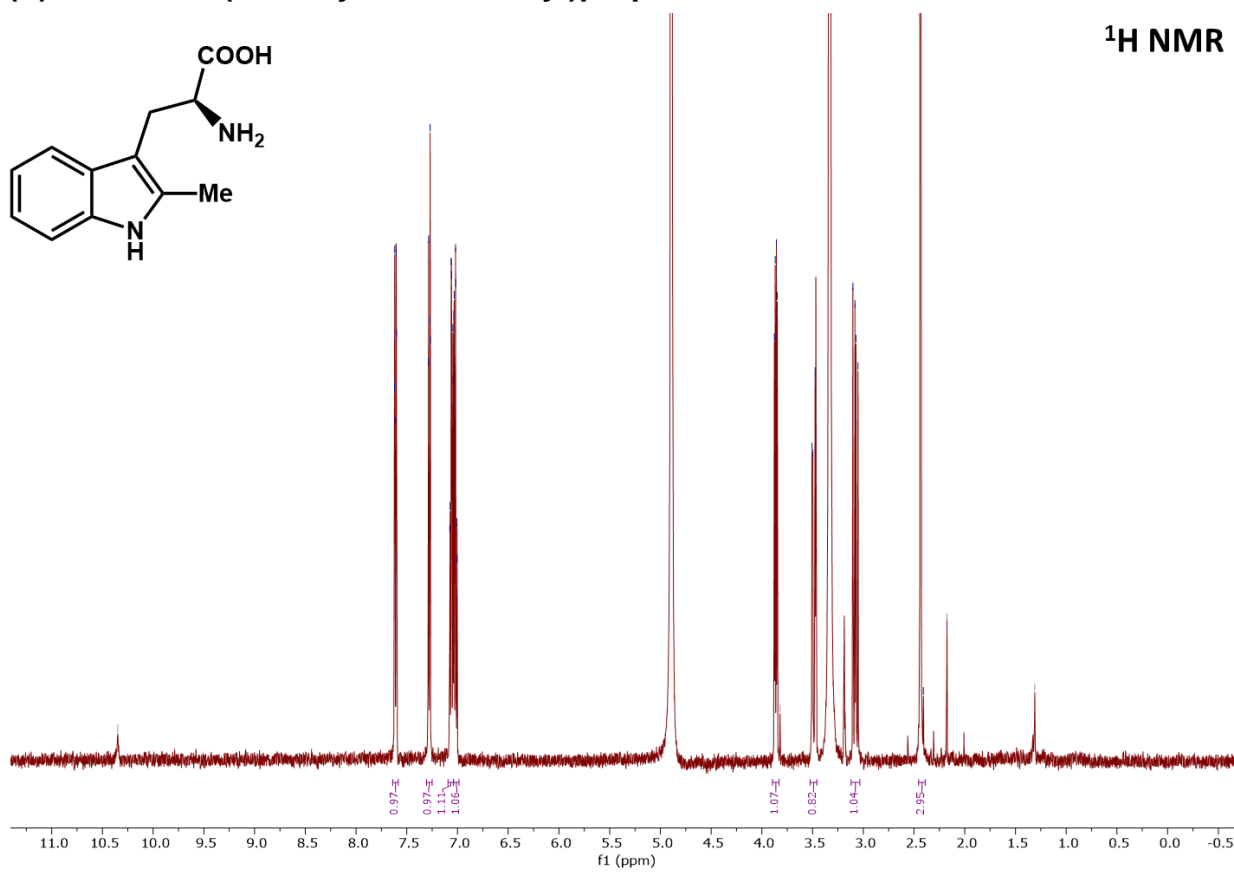
**<sup>13</sup>C NMR**



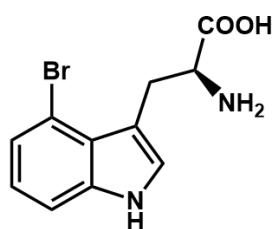
**(S)-2-amino-3-(2-methyl-1H-indol-3-yl)propanoic acid**



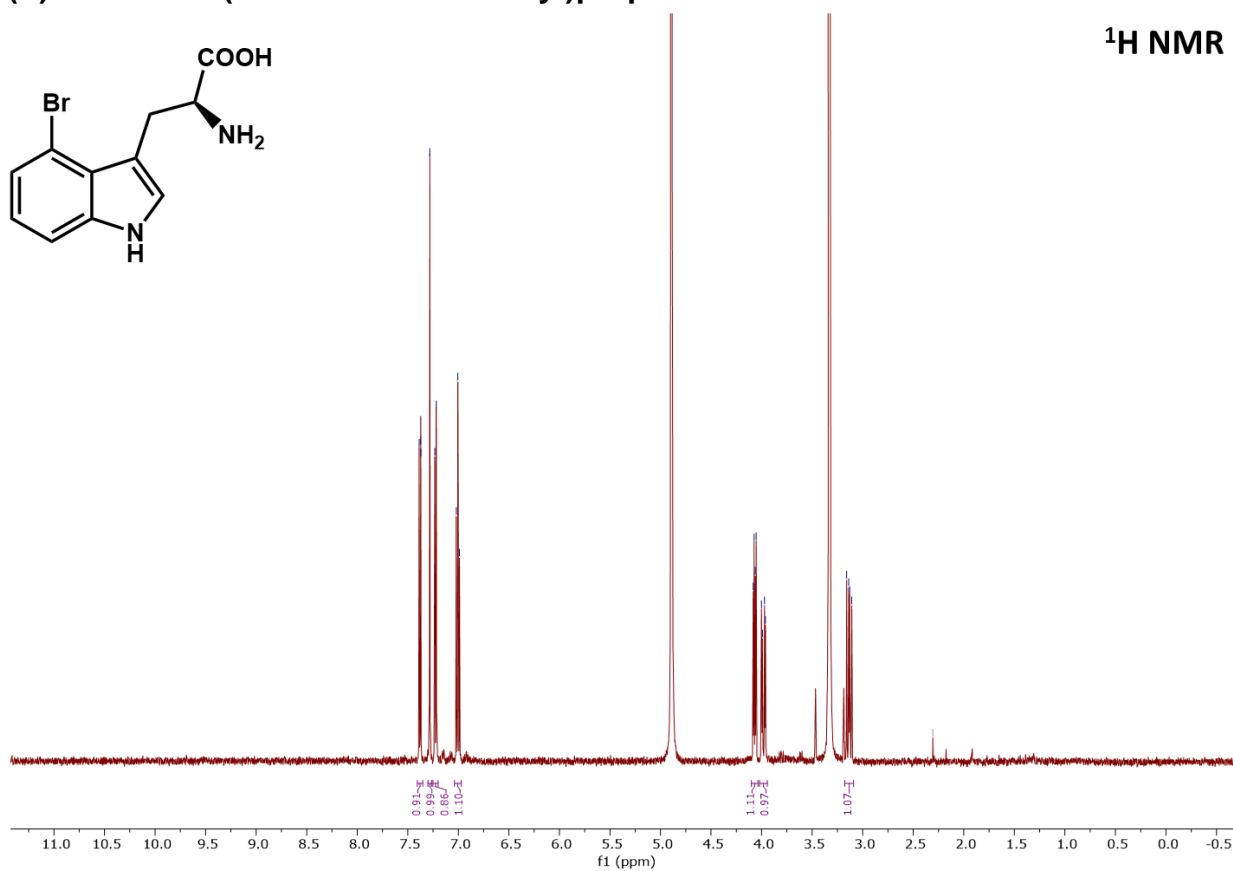
**<sup>1</sup>H NMR**



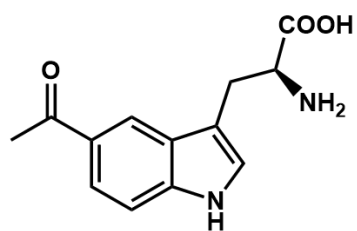
**(S)-2-amino-3-(4-bromo-1H-indol-3-yl)propanoic acid**



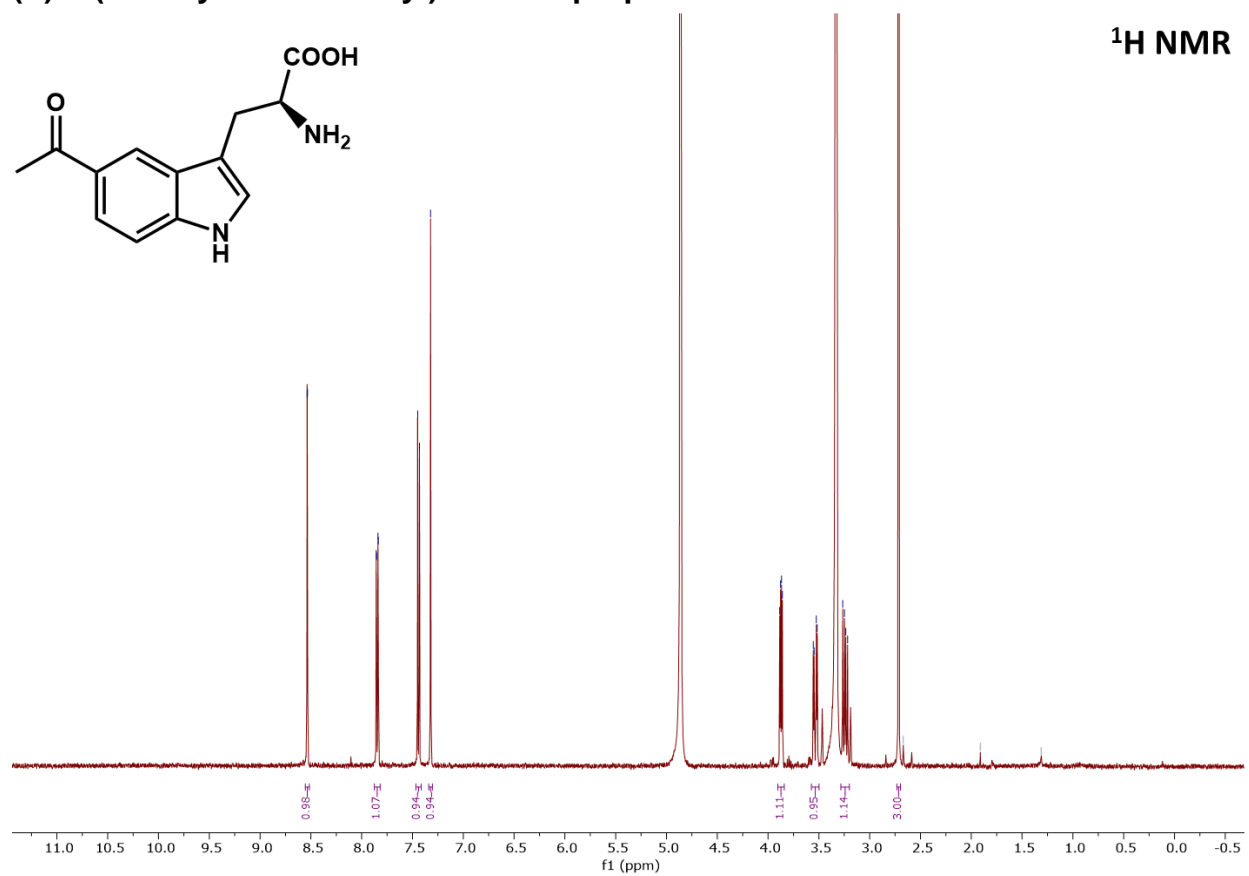
**<sup>1</sup>H NMR**



**(S)-3-(5-acetyl-1H-indol-3-yl)-2-aminopropanoic acid**

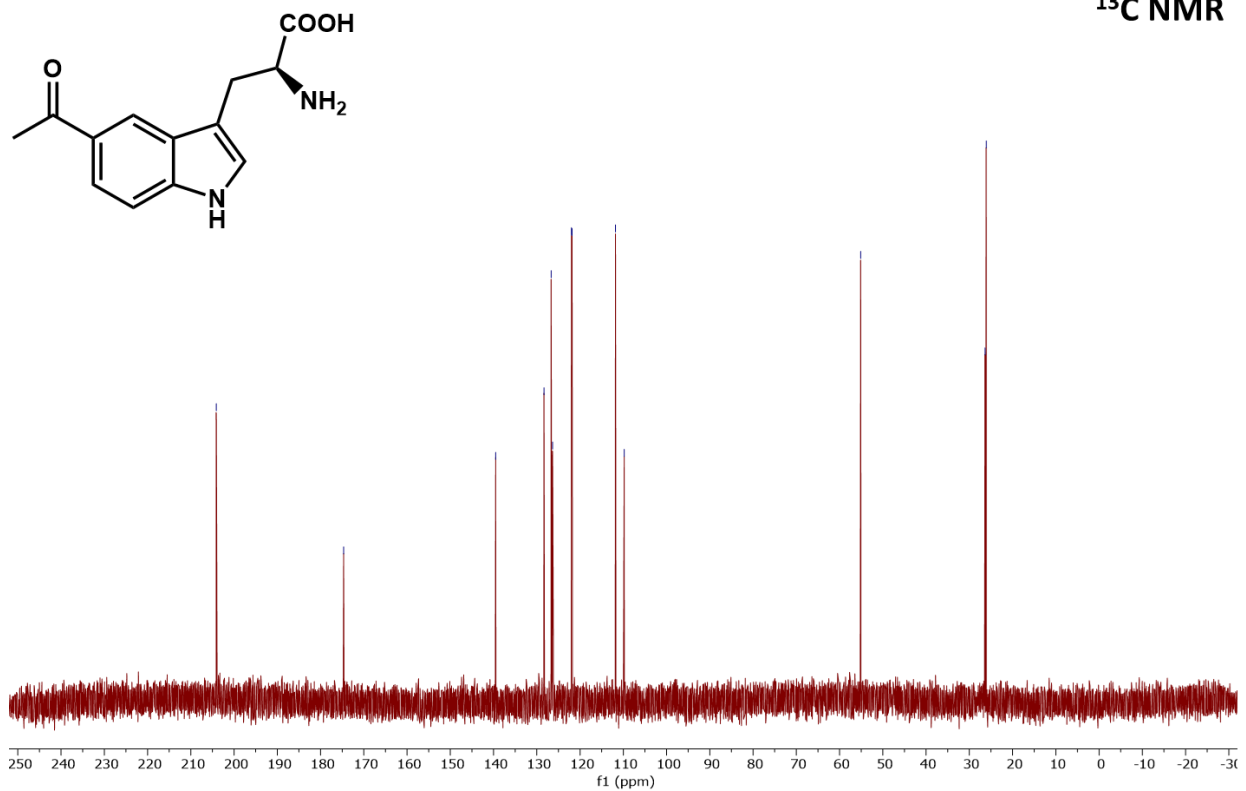


**<sup>1</sup>H NMR**



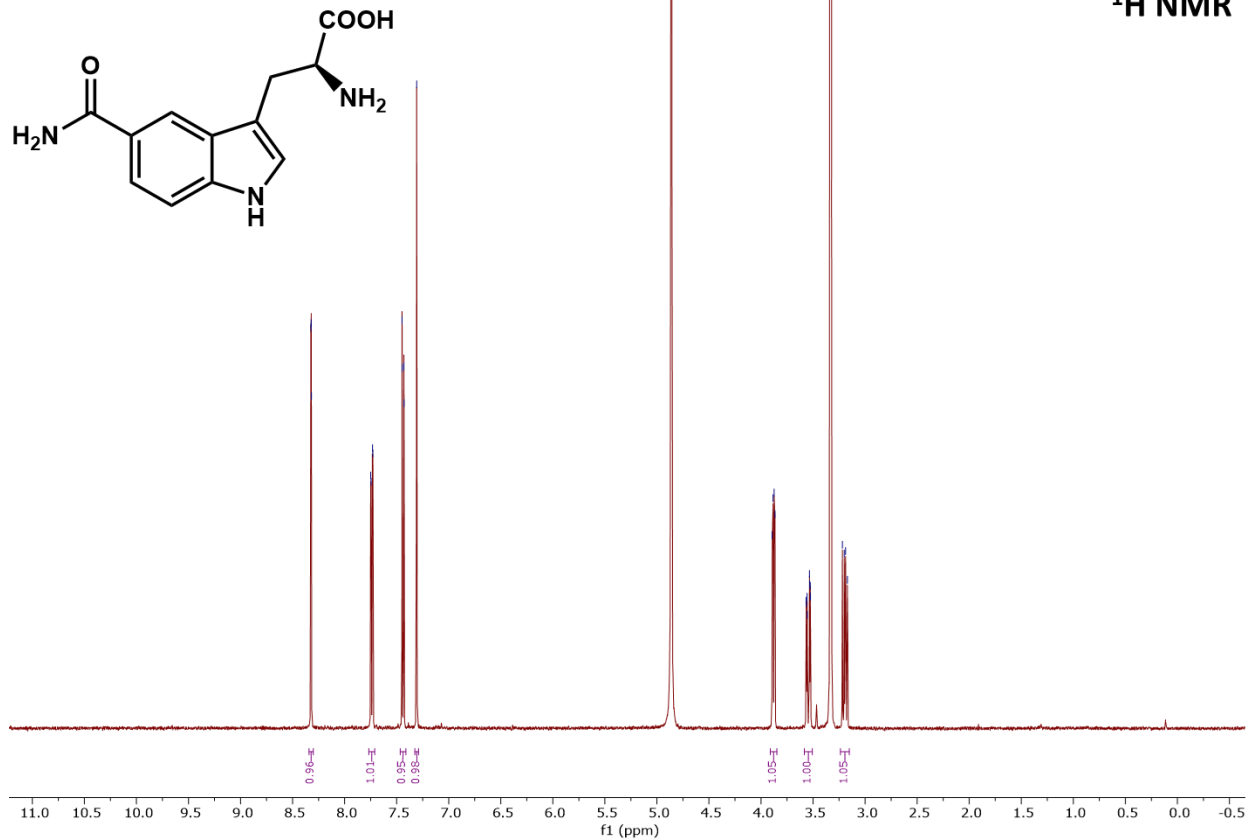
**(S)-3-(5-acetyl-1H-indol-3-yl)-2-aminopropanoic acid**

**<sup>13</sup>C NMR**

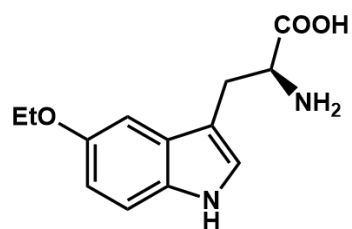


**(S)-2-amino-3-(5-carbamoyl-1H-indol-3-yl)propanoic acid**

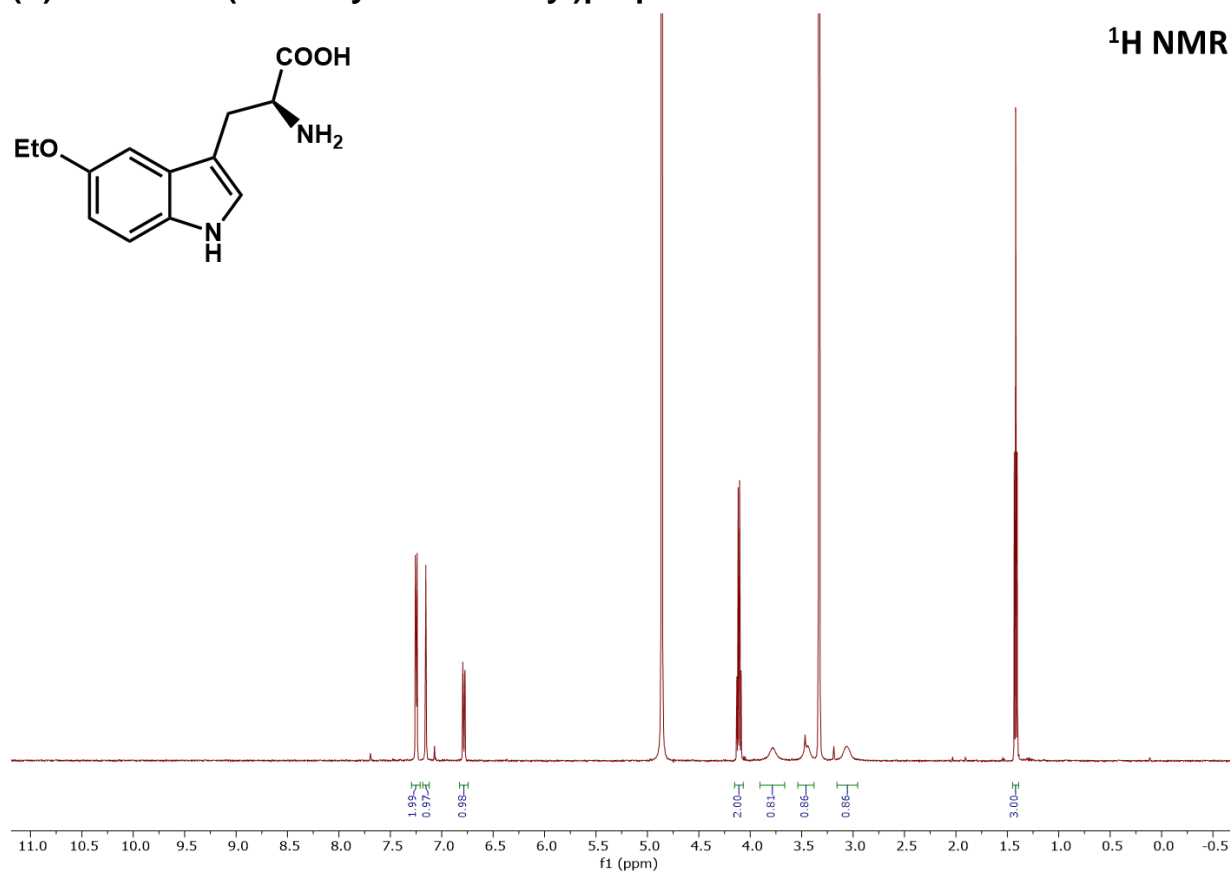
**<sup>1</sup>H NMR**



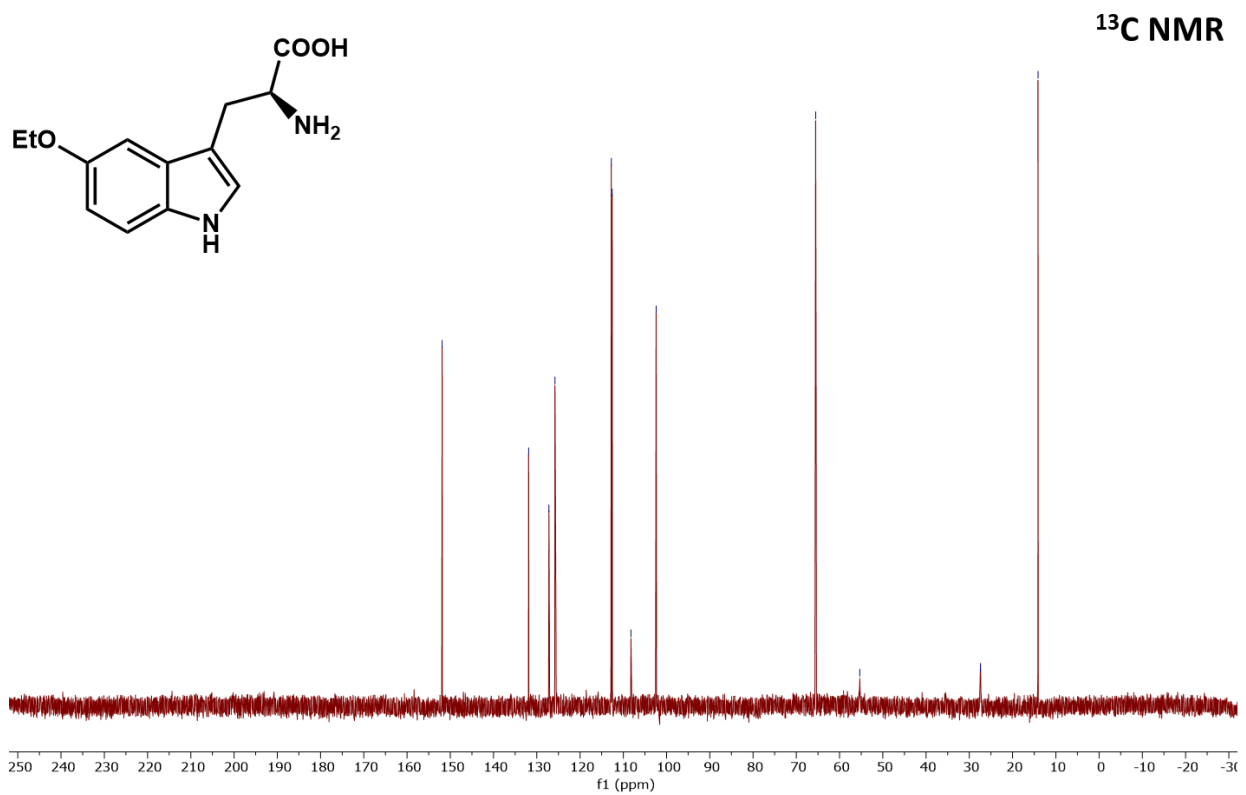
**(S)-2-amino-3-(5-ethoxy-1H-indol-3-yl)propanoic acid**



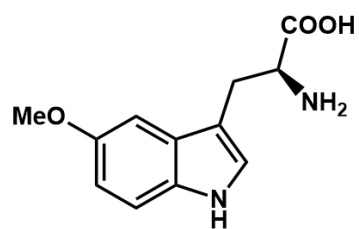
**<sup>1</sup>H NMR**



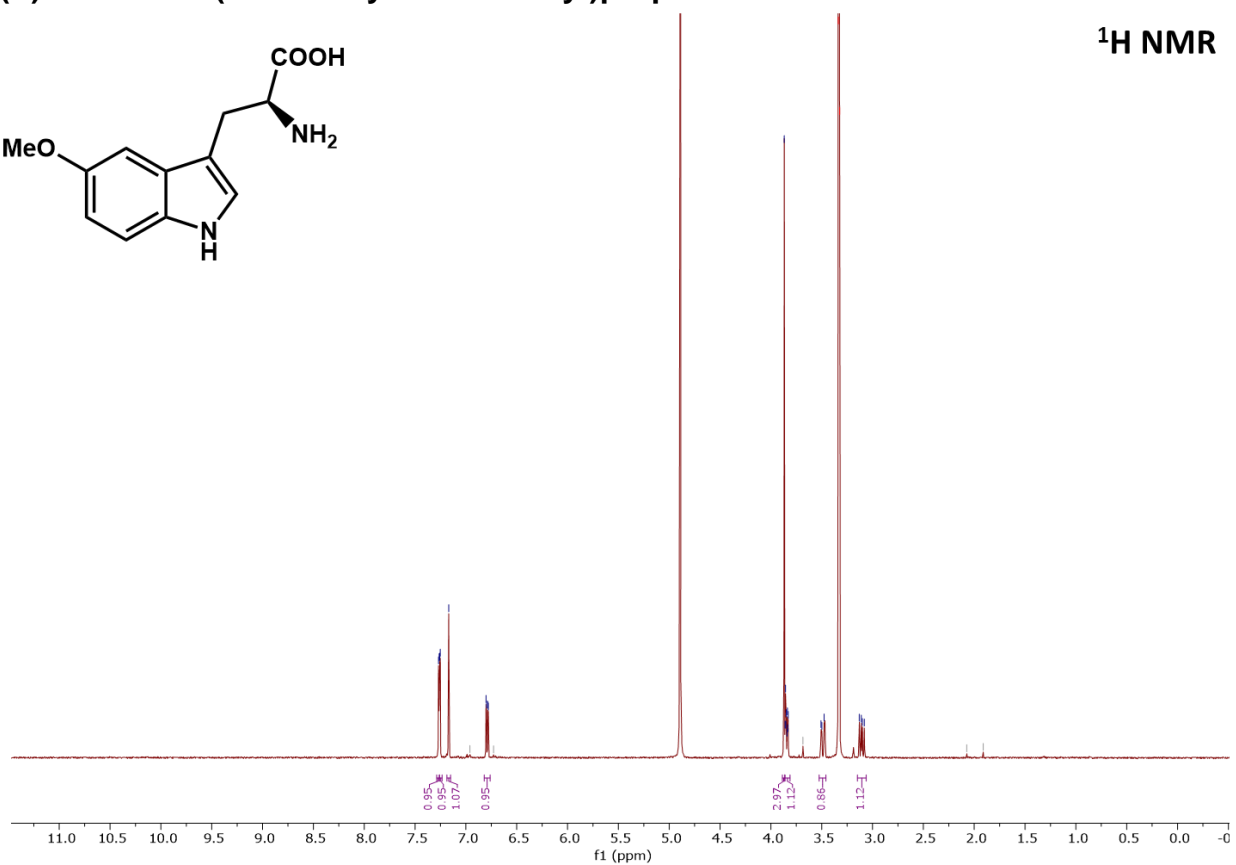
**(S)-2-amino-3-(5-carbamoyl-1H-indol-3-yl)propanoic acid**



**(S)-2-amino-3-(5-methoxy-1H-indol-3-yl)propanoic acid**

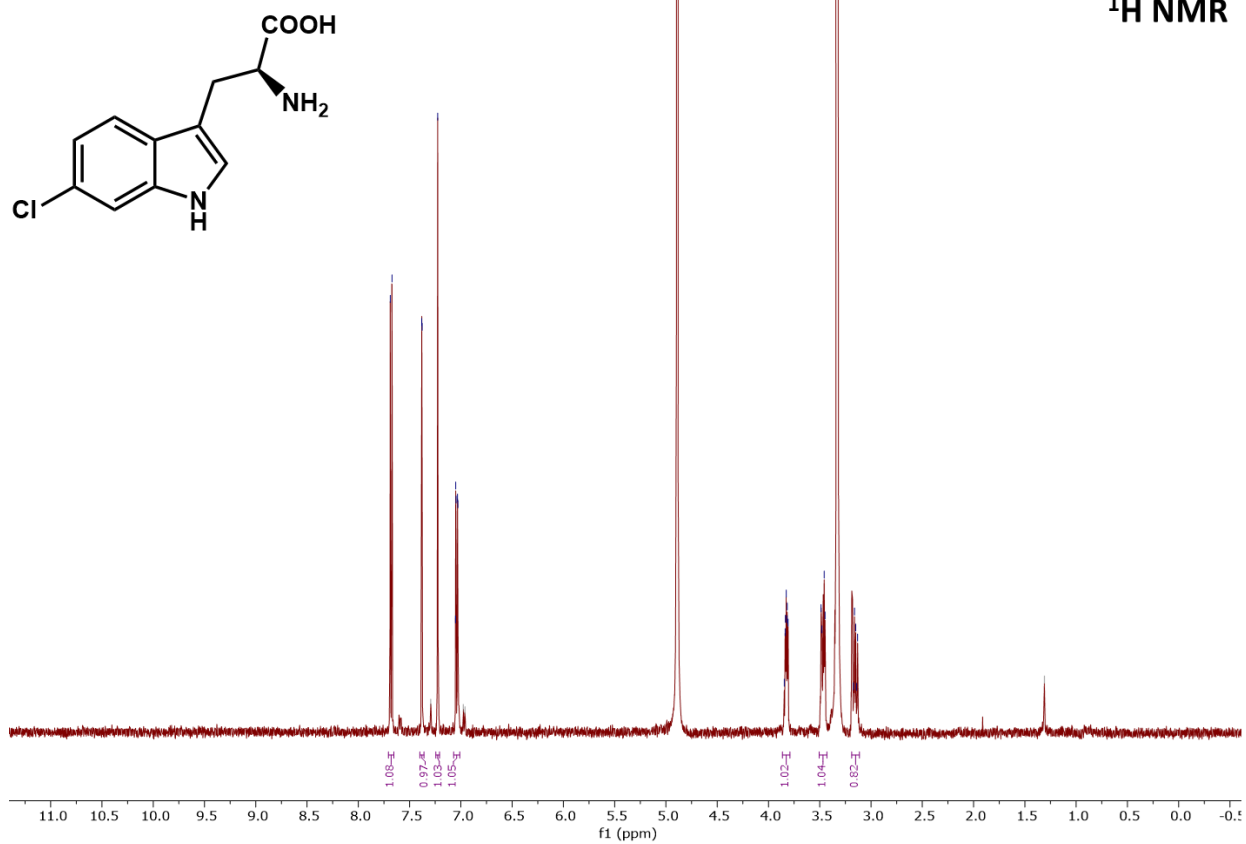


**<sup>1</sup>H NMR**



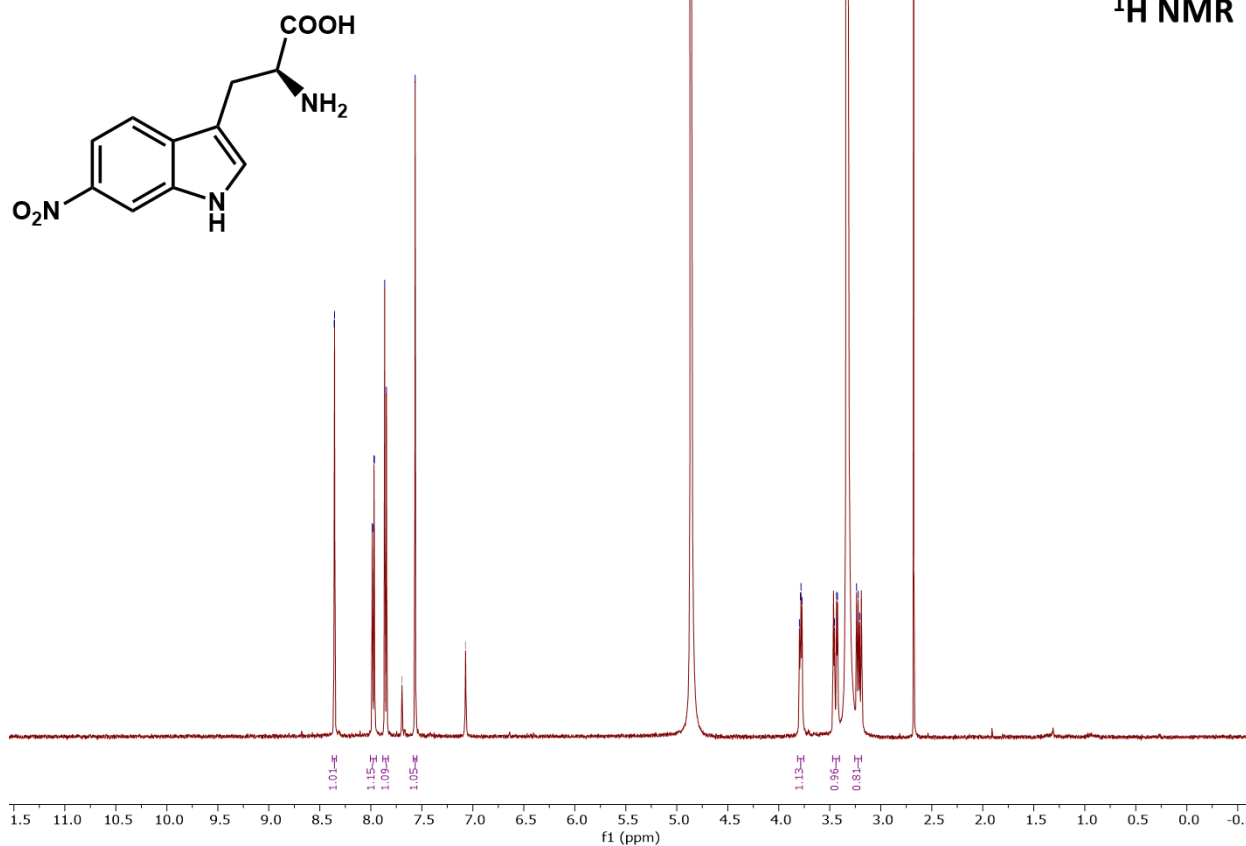
**(S)-2-amino-3-(6-chloro-1H-indol-3-yl)propanoic acid**

**<sup>1</sup>H NMR**

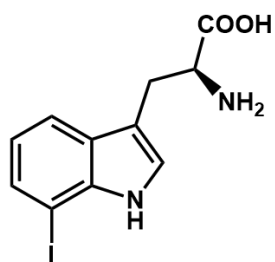


**(S)-2-amino-3-(6-nitro-1H-indol-3-yl)propanoic acid**

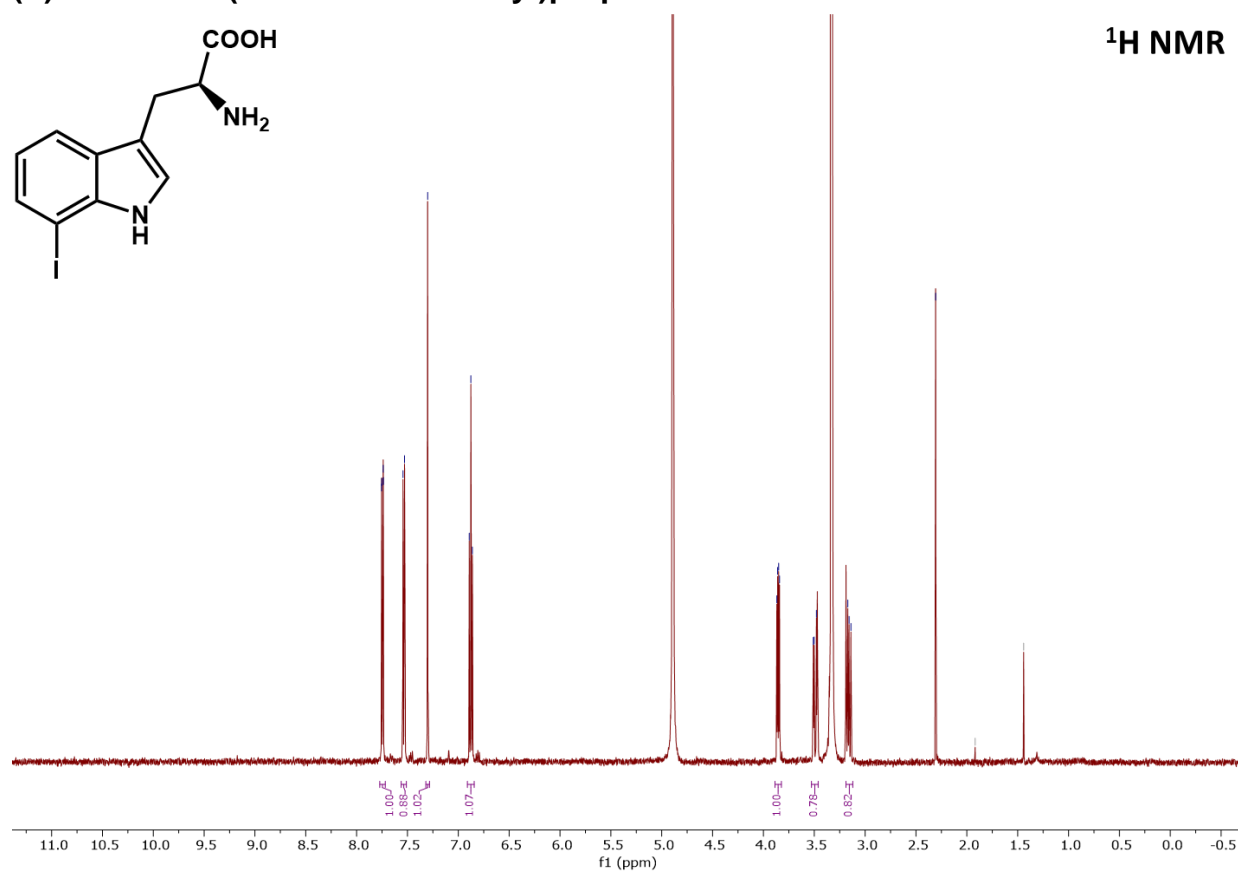
**<sup>1</sup>H NMR**



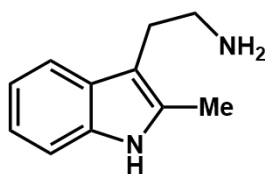
**(S)-2-amino-3-(7-iodo-1H-indol-3-yl)propanoic acid**



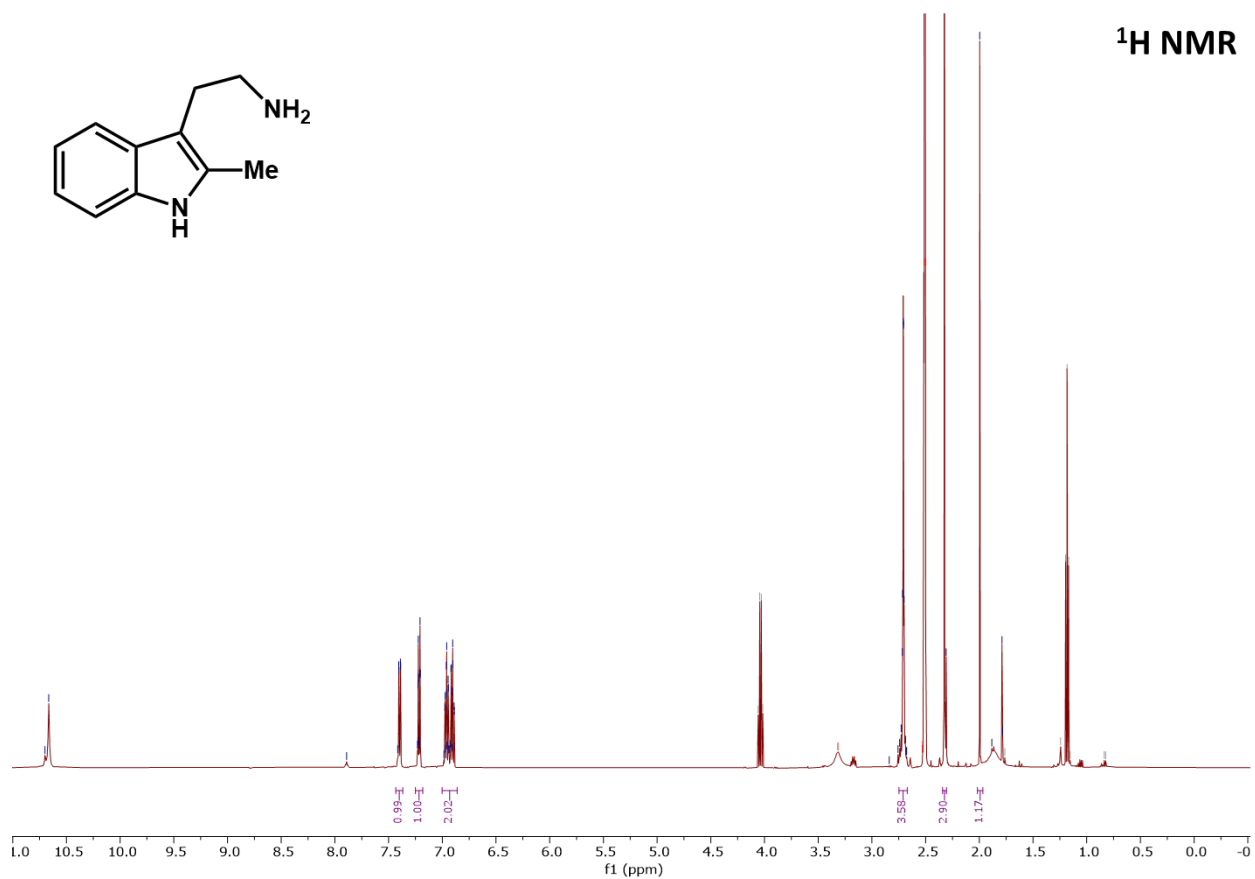
**<sup>1</sup>H NMR**



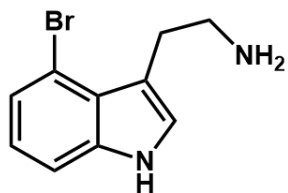
## 2-(2-methyl-1H-indol-3-yl)ethan-1-amine



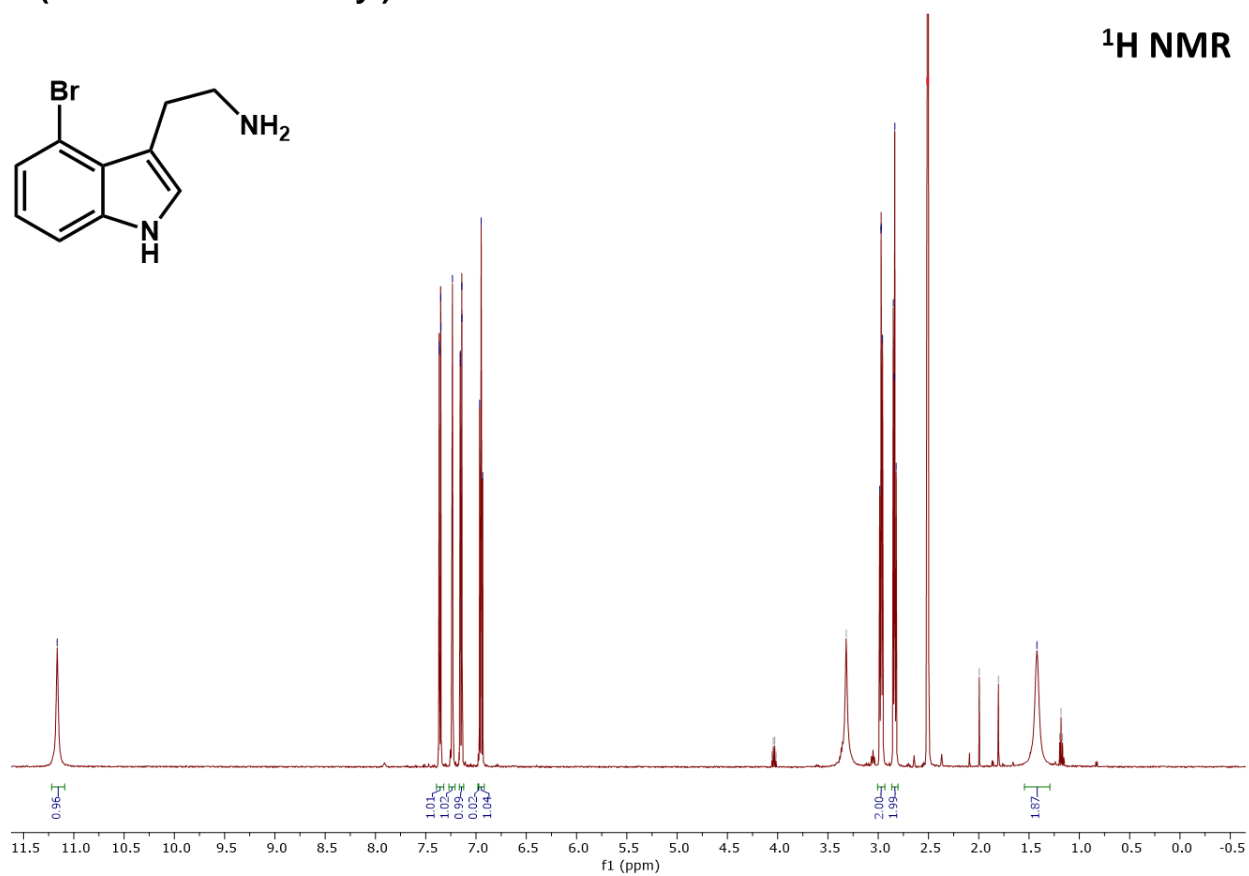
<sup>1</sup>H NMR



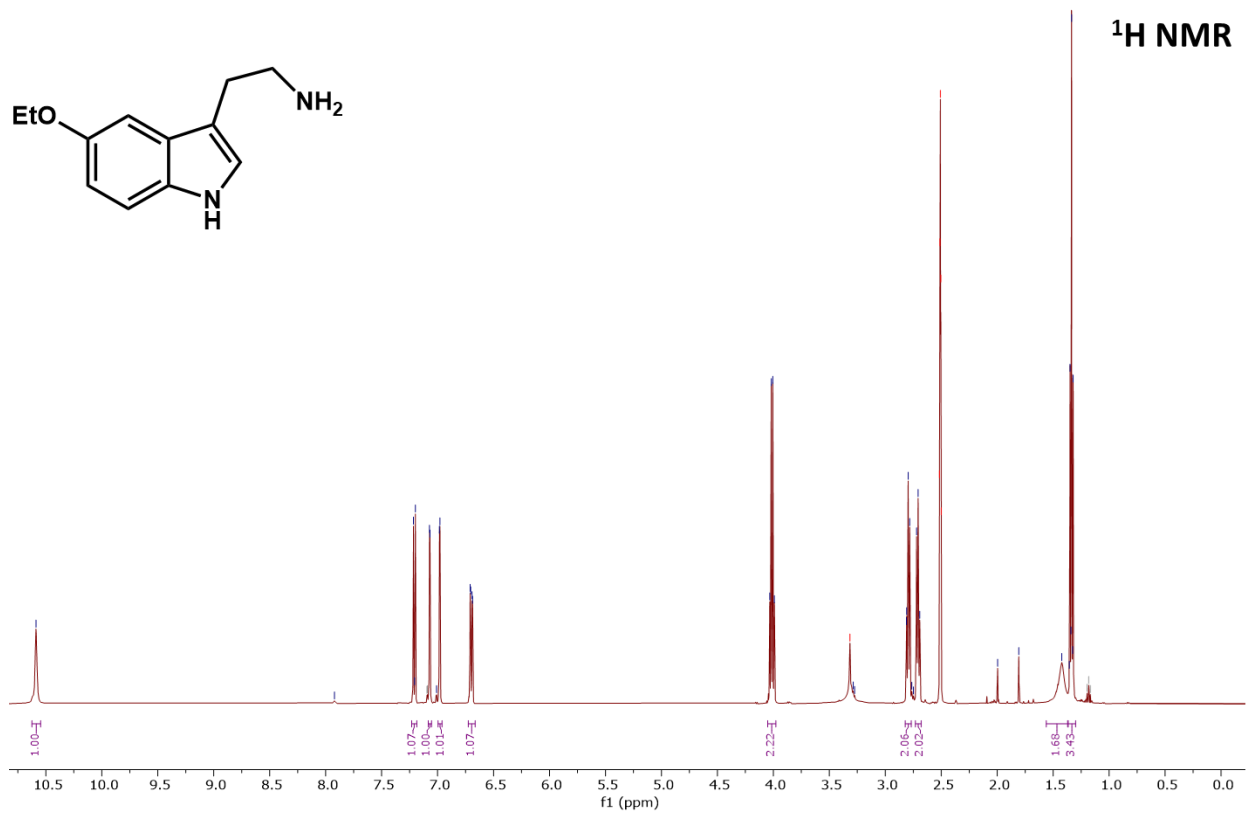
2-(4-bromo-1H-indol-3-yl)ethanamine:



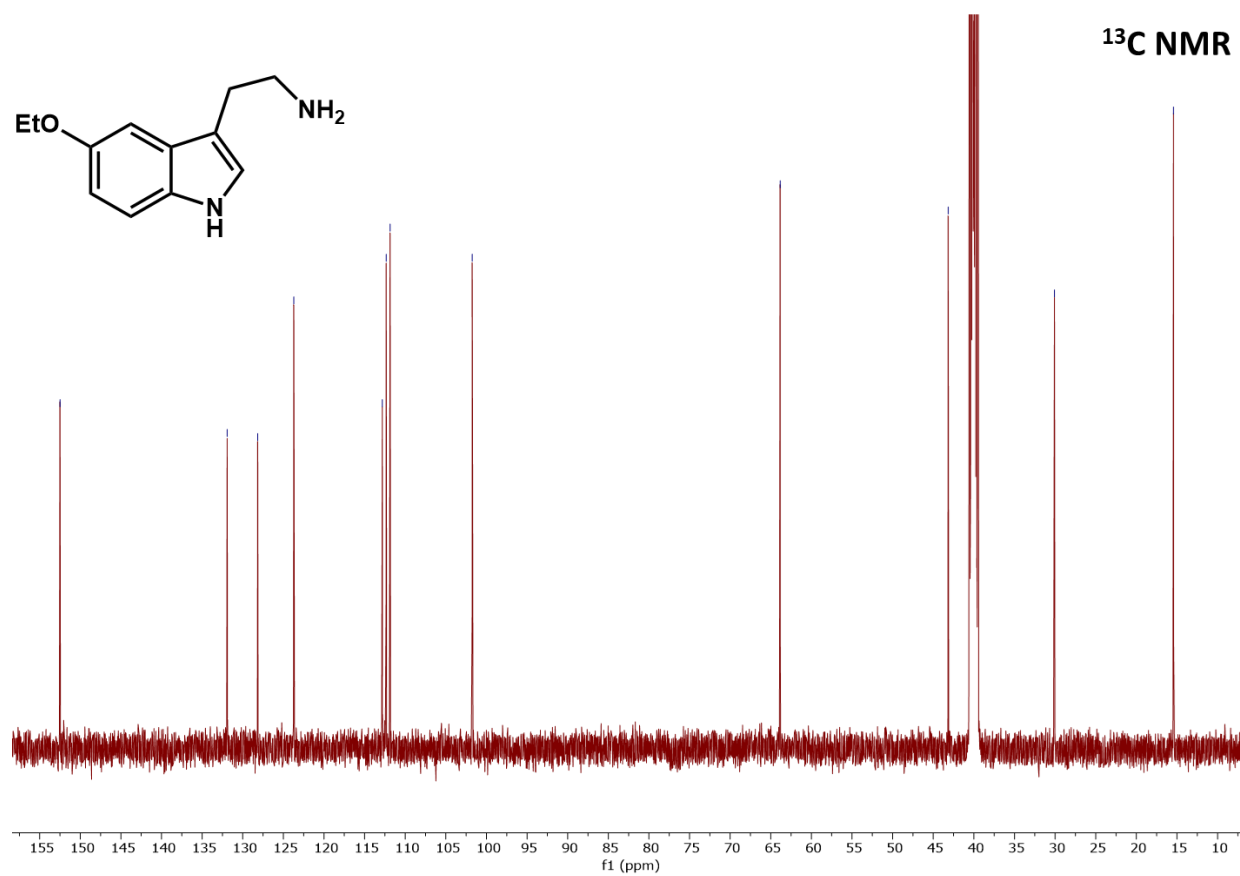
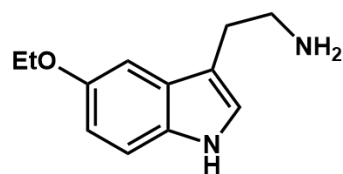
<sup>1</sup>H NMR



# 2-(5-ethoxy-1H-indol-3-yl)ethanamine



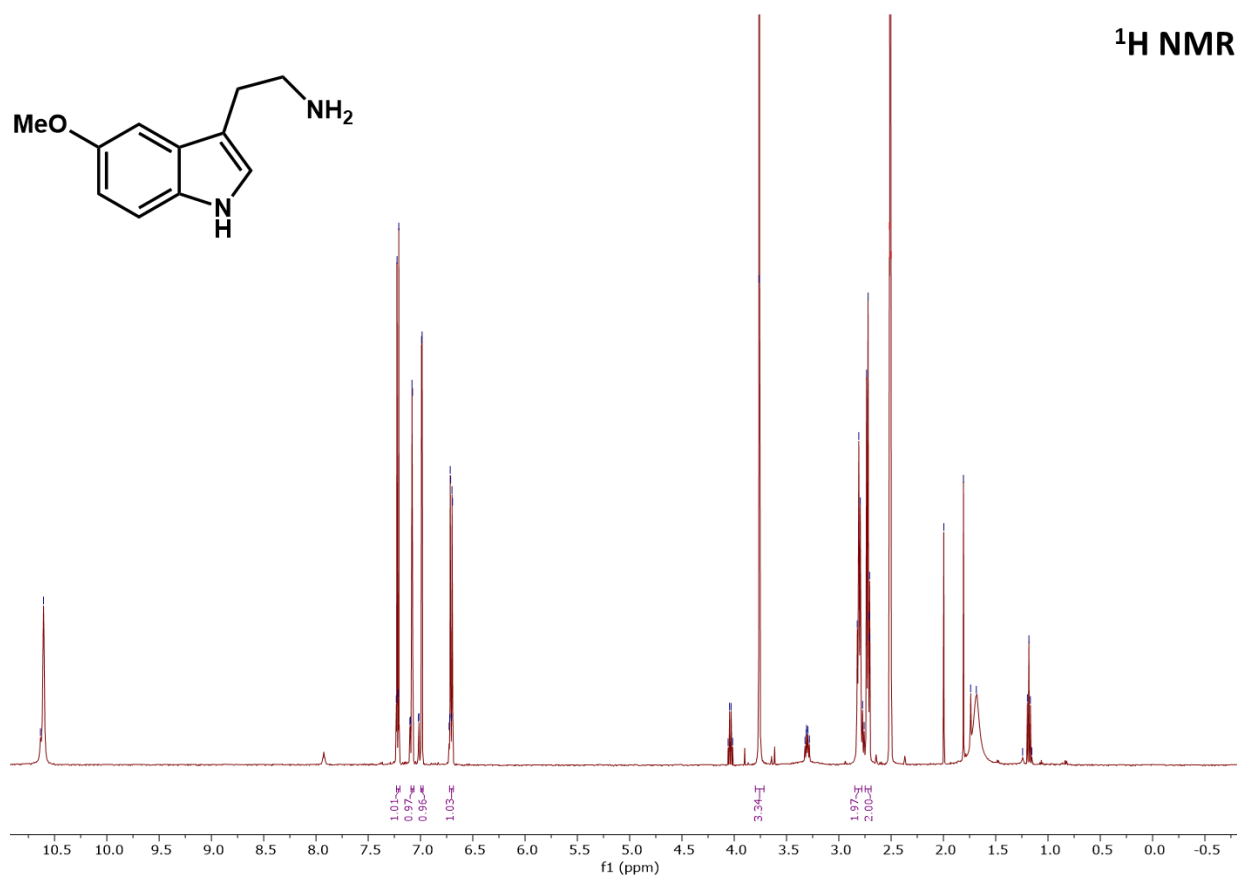
# 2-(5-ethoxy-1H-indol-3-yl)ethanamine



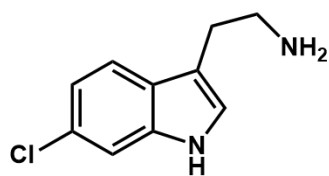
# 2-(5-methoxy-1H-indol-3-yl)ethanamine



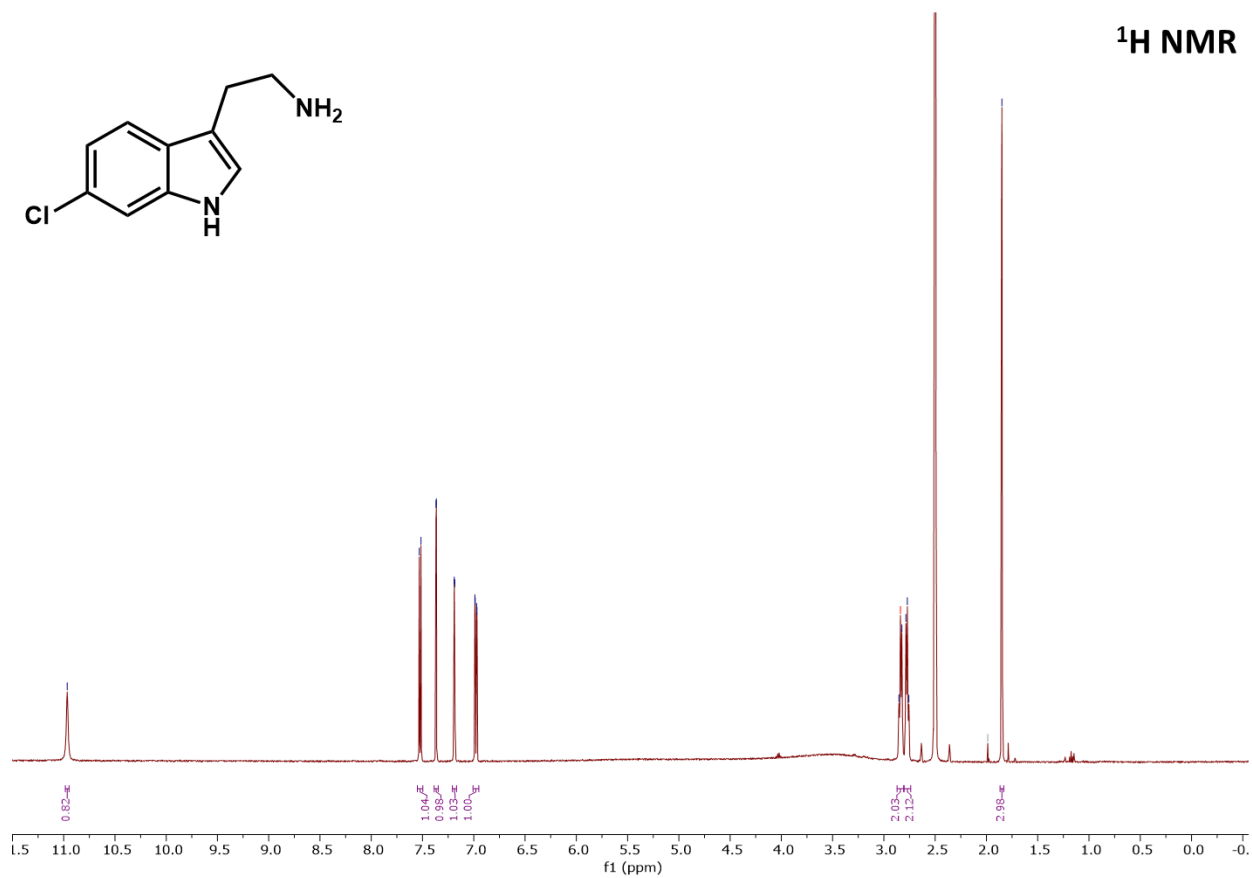
<sup>1</sup>H NMR



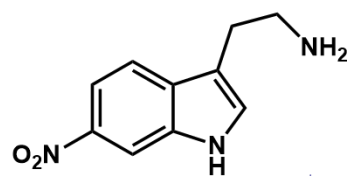
# 2-(6-chloro-1H-indol-3-yl)ethan-1-amine



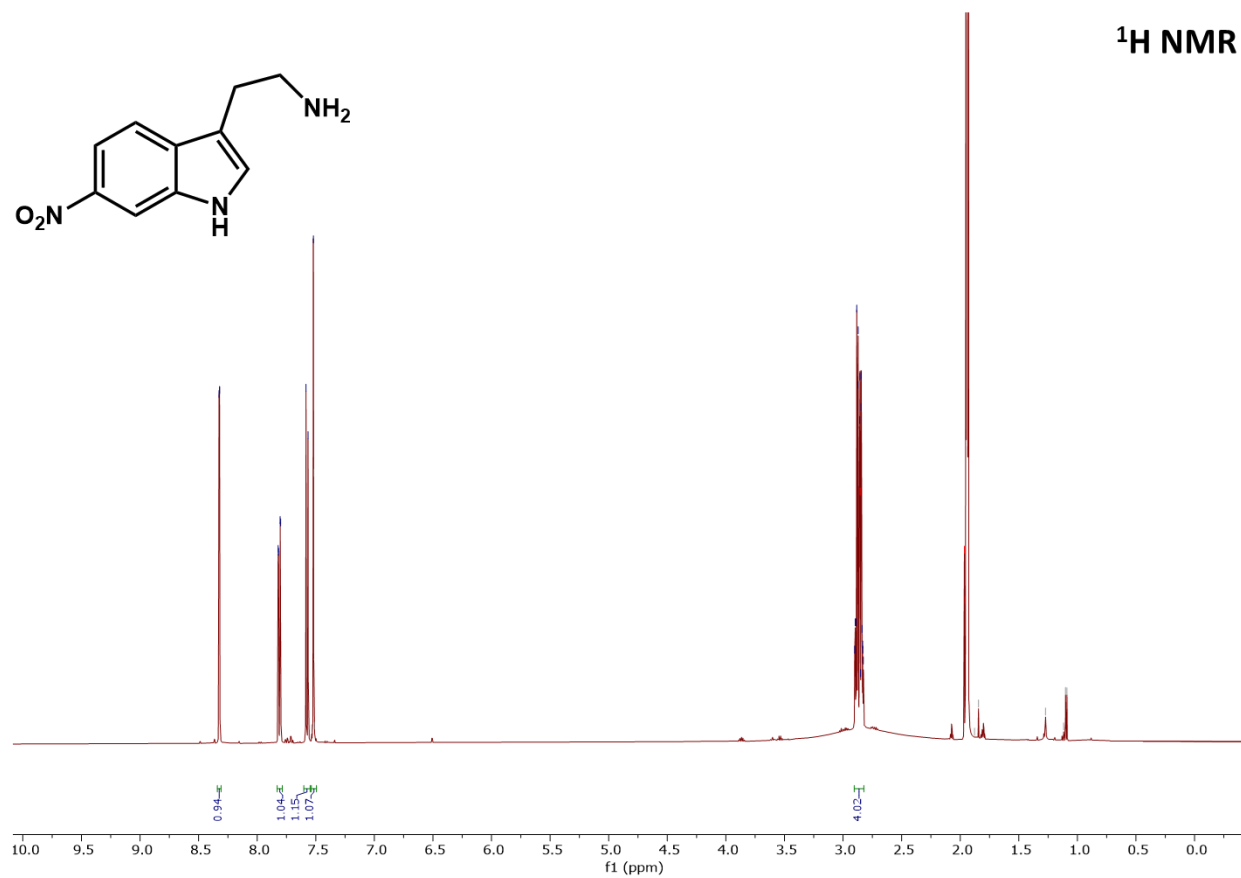
<sup>1</sup>H NMR



2-(6-nitro-1H-indol-3-yl)ethan-1-amine



<sup>1</sup>H NMR



## Supporting References

1. McDonald, A. D., Perkins, L. J. & Buller, A. R. Facile in Vitro Biocatalytic Production of Diverse Tryptamines. *ChemBioChem* **20**, 1939–1944 (2019).
2. Gibson, D. G. *et al.* Enzymatic assembly of DNA molecules up to several hundred kilobases. *Nat. Methods* **6**, 343–345 (2009).
3. Williams, B. B. *et al.* Discovery and characterization of gut microbiota decarboxylases that can produce the neurotransmitter tryptamine. *Cell Host Microbe* **16**, 495–503 (2014).
4. Kille, S. *et al.* Reducing codon redundancy and screening effort of combinatorial protein libraries created by saturation mutagenesis. *ACS Synth. Biol.* **2**, 83–92 (2013).
5. TerMaat, J. R., Pienaar, E., Whitney, S. E., Mamedov, T. G. & Subramanian, A. Gene synthesis by integrated polymerase chain assembly and PCR amplification using a high-speed thermocycler. *J. Microbiol. Methods* **79**, 295–300 (2009).
6. Herger, M. *et al.* Synthesis of  $\beta$ -Branched Tryptophan Analogues Using an Engineered Subunit of Tryptophan Synthase. *J. Am. Chem. Soc.* **138**, 8388–8391 (2016).
7. Buller, A. R. *et al.* Directed evolution mimics allosteric activation by stepwise tuning of the conformational ensemble. *J. Am. Chem. Soc.* **140**, 7256–7266 (2018).
8. Johnson, K. A. New standards for collecting and fitting steady state kinetic data. *Beilstein J. Org. Chem.* **15**, 16–29 (2019).
9. Buller, A. R. *et al.* Directed evolution of the tryptophan synthase  $\beta$ -subunit for stand-alone function recapitulates allosteric activation. *Proc. Natl. Acad. Sci.* **112**, 14599–14604 (2015).
10. Kabsch, W. XDS. *Acta Crystallogr. Sect. D Biol. Crystallogr.* **66**, 125 (2010).
11. Evans, P. R. & Murshudov, G. N. How good are my data and what is the resolution? *urn:issn:0907-4449* **69**, 1204–1214 (2013).
12. McCoy, A. J. *et al.* Phaser crystallographic software. *urn:issn:0021-8898* **40**, 658–674 (2007).
13. Winn, M. D. *et al.* Overview of the CCP4 suite and current developments. *urn:issn:0907-4449* **67**, 235–242 (2011).
14. Winn, M. D., Isupov, M. N. & Murshudov, G. N. Use of TLS parameters to model anisotropic displacements in macromolecular refinement. *Acta Crystallogr. Sect. D Biol. Crystallogr.* **57**, 122–133 (2001).
15. Chen, V. B. *et al.* MolProbity: all-atom structure validation for macromolecular crystallography. *Acta Crystallogr. Sect. D Biol. Crystallogr.* **66**, 12 (2010).
16. Stanišić, A., Hüsken, A. & Kries, H. HAMA: A multiplexed LC-MS/MS assay for specificity profiling of adenylate-forming enzymes. *Chem. Sci.* **10**, 10395–10399 (2019).
17. Chou, T. C. & Talalay, P. A simple generalized equation for the analysis of multiple inhibitions of Michaelis-Menten kinetic systems. *J. Biol. Chem.* **252**, 6438–6442 (1977).
18. Cornish-Bowden, A. Enzyme Specificity : Its Meaning in the General Case. *J. theor. Biol.* **108**, 451–457 (1984).
19. Kuo, Y. M., Henry, R. A. & Andrews, A. J. Measuring specificity in multi-

- substrate/product systems as a tool to investigate selectivity in vivo. *Biochim. Biophys. Acta - Proteins Proteomics* **1864**, 70–76 (2016).
20. Knorrscheidt, A. *et al.* Simultaneous screening of multiple substrates with an unspecific peroxygenase enabled modified alkane and alkene oxyfunctionalisations. *Catal. Sci. Technol.* 6058–6064 (2021) doi:10.1039/d0cy02457k.
  21. Romney, D. K., Murciano-Calles, J., Wehrmüller, J. E. & Arnold, F. H. Unlocking Reactivity of TrpB: A General Biocatalytic Platform for Synthesis of Tryptophan Analogues. *J. Am. Chem. Soc.* **139**, 10769–10776 (2017).
  22. Murciano-Calles, J., Romney, D. K., Brinkmann-Chen, S., Buller, A. R. & Arnold, F. H. A Panel of TrpB Biocatalysts Derived from Tryptophan Synthase through the Transfer of Mutations that Mimic Allosteric Activation. *Angew. Chemie - Int. Ed.* **55**, 11577–11581 (2016).